ABSTRACT

Title of Document: PREDICTIVE ANALYTICS LEAD TO SMARTER SELF-ORGANIZING DIRECTIONAL WIRELESS BACKBONE NETWORKS

David M. Coleman, Doctor of Philosophy, 2013

Directed By: Professor Christopher C. Davis, Department of Electrical and Computer Engineering

Directional wireless systems are becoming a cost-effective approach towards providing a high-speed, reliable, broadband connection for the ubiquitous mobile wireless devices in use today. The most common of these systems consists of narrow-beam radio frequency (RF) and free-space-optical (FSO) links, which offer speeds between 100Mbps and 100Gbps while offering bit-error-rates comparable to fixed fiber optic installations. In addition, spatial and spectral efficiencies are accessible with directional wireless systems that cannot be matched with broadcast systems. The added benefits of compact designs permit the installation of directional antennas on-board unmanned autonomous systems (UAS) to provide network availability to regions prone to natural disasters, in maritime situations, and in war-torn countries that lack infrastructure security. In addition, through the use of intelligent network-centric algorithms, a flexible airborne backbone network can be established to dodge the scalability limitations of traditional omnidirectional wireless networks.

Assuring end-to-end connectivity and coverage is the main challenge in the design of directional wireless backbone (DWB) networks. Conflating the duality of these objectives with the dynamical nature of the environment in which DWB networks are deployed, in addition to the standardized network metrics such as latency-minimization and throughput maximization, demands a rigorous control process that encompasses all aspects of the system. This includes the mechanical steering of the directional point-to-point link and the monitoring of aggregate network performance (e.g. dropped packets). The inclusion of processes for topology control, mobility management, pointing, acquisition, and tracking of the directional antennas, alongside traditional protocols (e.g. IPv6) provides a rigorous framework for next-generation mobile directional communication networks.

This dissertation provides a novel approach to increase reliability in reconfigurable beam-steered directional wireless backbone networks by predicating optimal network reconfigurations wherein the network is modeled as a giant molecule in which the point-to-point links between two UASs are able to grow and retract analogously to the bonds between atoms in a molecule. This cross-disciplinary methodology explores the application of potential energy surfaces and normal mode analysis as an extension to the topology control optimization. Each of these methodologies provides a new and unique ability for predicting unstable configurations of DWB networks through an understanding of second-order principle dynamics inherent within the aggregate configuration of the system. This insight is not available through monitoring individual link performance. Together, the techniques used to model the DWB network through molecular dynamics are referred to as predictive

analytics and provide reliable results that lead to smarter self-organizing reconfigurable beam-steered DWB networks.

Furthermore, a comprehensive control architecture is proposed that complements traditional network science (e.g. Internet protocol) and the unique design aspects of DWB networks. The distinct ability of a beam-steered DWB network to adjust the direction of its antennas (i.e. reconfigure) in response to degraded effects within the atmosphere or due to an increased separation of nodes, is not incorporated in traditional network processes such re-routing mechanism, and therefore, processes for reconfiguration can be abstracted which both optimize the physical interconnections while maintaining interoperability with existing protocols. This control framework is validated using network metrics for latency and throughput and compared to existing architectures which use only standard re-routing mechanisms.

Results are shown that validate both the analogous molecular modeling of a reconfigurable beam-steered directional wireless backbone network and a comprehensive control architecture which coalesces the unique capabilities of reconfiguration and mobility of mobile wireless backbone networks with existing protocols for networks such as IPv6.

PREDICTIVE ANALYTICS LEAD TO SMARTER SELF-ORGANIZING DIRECTIONAL WIRELESS BACKBONE NETWORKS

By

David M. Coleman

Dissertation submitted to the Faculty of the Graduate School of the
University of Maryland, College Park, in partial fulfillment
of the requirements for the degree of
Doctor of Philosophy
2013

Advisory Committee:
Professor Christopher C. Davis, Chair
Professor Julius Goldhar
Professor Shuvra S. Bhattacharyya
Professor Sennur Ulukus
Professor Subramanian Raghavan, Dean's Representative
Faculty Research Professor Stuart D. Milner

Dedication

To my family

for all their unconditional love and support.

Acknowledgements

I would like to thank my advisors, Dr. Stuart Milner and Dr. Christopher Davis, for their support throughout my graduate studies at the University of Maryland and friendship in my personal life. I would also like to thank the members of my committee for their time and service.

I am thankful to Dr. Kira Armacost (Auburn University) for her insight into molecular dynamics, assistance in adapting molecular principles to wireless networks, and constructive discussion throughout my graduate studies.

I would also like to thank Dr. Joseph Wunderlich (Elizabethtown College) for his friendship and never-ending support for my academic and personal success providing me with endless opportunities for each. Additionally, Dr. Jia Di (University of Arkansas) and Dr. Susan Gauch (University of Arkansas) have provided support both as technical advisors and friends.

Finally, I am forever grateful for my parents, grandparents, siblings, and friends for their unconditional support throughout my life.

Table of Contents

List of Publications

Coleman, D., Milner, S.D.; Davis, C.C., "A novel prediction methodology for detecting failures and instabilities in directional wireless networks", Proc. SPIE 8517, Laser Communication and Propagation through the Atmosphere and Oceans, 851705 (October 24, 2012)

Coleman, D.; Armacost, K.; Davis, C.C.; Milner, S.D.; , "A molecular-inspired approach for predicting topology change in directional mobile wireless networks," Intelligent Sensors, Sensor Networks and Information Processing (ISSNIP), 2011 Seventh International Conference on , vol., no., pp.562-567, 6-9 Dec. 2011

List of Tables

List of Figures

Chapter 1: Motivations and Objectives

1.1 Reconfigurable Directional Wireless Backbone Networks

Over the past 20 years, the US military has invested in research for a reduced-cost, highly adaptable secure communications network that is able to be deployed rapidly in unsecure regions to support operations as an alternative to existing satellite networks. This tactical intranet would support command, control, communication, computers, intelligence, surveillance and reconnaissance (C^4ISR) directives. Furthermore, the network would have specifications with respect to mobility, assuring end-to-end connectivity, maximizing coverage of the users, adapting to changing battlefield/environmental parameters, and maintaining the security of the communications against interception and detection. Additionally, modern network protocols and metrics for reliability, bandwidth, and scalability ought to be incorporated to provide applications and services similar to hard-wired installations.

An example of a rapidly deployable, reconfigurable architecture for directional mobile ad hoc wireless networks consists of two tiers and is illustrated in fig. 1-1. This network architecture was proposed in 1997 by Milner, et al. [19]. The bottom tier includes mobile wireless end-users (individual people and vehicles) that require broadband connectivity. The top tier includes high-capacity routers installed on-board aerial platforms such as unmanned autonomous systems (UAS) and is referred to as the backbone (or backhaul) of the wireless network since it routes traffic between two end-users separated by distance, terrain, or power constraints. For clarity, it is assumed that

Figure 1-1.A two-tier directional wireless backbone network architecture consists of 1) airborne, maritime, and ground units using directional point-to-point links acting as the backhaul entities and 2) numerous terrestrial end-users using RF subnets. This serves as the network framework for this dissertation.

two end-users within a given radius have the ability to communicate using peer-to-peer links and do not require routing on the higher tier. However, the majority of the end-user traffic is routed using the access points on the base-stations and the backbone network.

The effectiveness of this architecture is evident by the ability to immediately deploy UASs to support end-user activity within a region. Additionally, the same technology used to achieve high-data rates in the airborne backhaul network (directional RF and FSO) also improves the physical security of the network since the signal is a narrow beam. A narrow beam can be power limited to exclusively engage the desired users, is extremely hard to intercept/detect since the signal is only between two UASs (not in all directions like omnidirectional radios), and reduces interference from adjacent nodes [24, 27]. No additional hardware requirements are placed on the mobile end-users at the lower layer since the "hotspot" for which they reside utilizes existing omni-directional Wi-Fi technology on the base-station to establish a network access point for the end-users.

Though much effort has been invested in omni-directional mobile ad hoc networks (O-MANETs), it has been shown these systems do not scale efficiently [22, 23] and therefore, communications systems utilizing directional antennas are now preferred for the backbone units in directional wireless backbone networks. In addition to scalability, directional antennas are less prone to detection and interference since their transmission paths are narrow-beams and point-to-point [24]. The most common systems are either ultra-high frequency (e.g. 60-100GHz) radios (RF) or free-space optics (FSO). The trade-off between employed technologies is dependent upon the

atmospheric conditions, available power, throughput, and distance. However, recent advancements in RF systems lessen the differences between the two technologies and are expected to offer near 100Gb/s throughputs at distances greater than 200km [6]. This dissertation focuses on the reliability of the network, which is critical for assuring end-to-end connectivity, regardless of the employed technology.

1.2 Mechanical Beam-Steering in Networks

In general, two approaches are employed to steer the narrow beam point-to-point communication links in reconfigurable directional wireless backbone networks: mechanical and electrical. Mechanical steering utilizes low-weight, highly precise motorized gimbals to control the angle of the transceiver. Electrical steering, on the other hand, uses complex digital signal processing to integrate interference signals with the data to focus the narrow-beam in the desired direction. Complex MAC layer algorithms are required to schedule data transmissions [75]. Mechanical steering is more versatile, precise, less complex, and is available at a reduced cost compared to electrical steering processes. For these reasons, mechanical steering is used in this dissertation to establish all links in the backbone.

A mechanical beam-steered directional network utilizes a smaller number of antennas but possess capabilities to steer the signal in the direction of the receiver, as shown in fig. 1-2. Steerable gimbals are positioned behind the antenna and are controlled locally to provide accuracy down to the micro-radian of a degree. In this type of network, a link is established between two nodes by selecting a gimbal on node-A (pointing in the coarse direction of node B) and turning the antenna to satisfy the fine-grained angles. In this diagram, each gimbal is shown to have an exclusive 90°

field-of-regard (FOR), but in practice the FORs often overlap to provide redundant coverage. Mechanical beam-steered networks have advantages over electrical beam-steered networks in the reduction of the digital signal processing required to distinguish the received signal since the transmission signal is much narrower and is often exclusive to one antenna pairing [18]. This advantage reduces the need for MAC layer mitigation protocols and thus the controls for establishing a link in a mechanical beam-steered network can be removed from the Internet protocols.

The work in this dissertation is exclusively concerned with reconfigurable mechanical beam-steered directional wireless networks. The work in Chapter 2 which discusses link degradation in directional network can be abstracted for studies of electrical beam-formed networks. However, the work in Chapter 3 proposes the control architecture which assumes no MAC layer protocols for mitigating multiple accesses within a link between two nodes and thus pertains to mechanical beam-steered networks more directly.

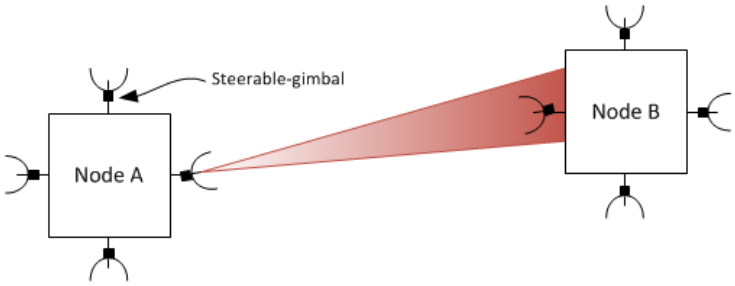

Figure 1-2. A beam-steered network uses controllable gimbals to steer the directional antenna in the direction of the receiving node. In this setup, less work is required by the receiving node since an exclusive pairing of transmitter/receiver has been established as compared to the electrical beam-steering approach.

1.3 Main Challenges in DWB Networks

The main challenges in reconfigurable directional wireless (DWB) networks are two-fold: 1) maintaining backbone connectivity in adverse environment conditions; and 2) maximizing the coverage of the end-users. The first challenge is referred to as topology control, uses a centralized algorithm and includes pointing, acquisition, and tracking (PAT), link assignments, and traffic routing. Topology control reacts to adverse conditions (e.g. link outages/degradations) by dynamically redirecting the directional antennas.

This dissertation establishes a framework towards the prediction of topological changes (in a proactive manner) within a connected network by modeling the network as a giant molecule. Similarities are drawn between the point-to-point links within DWB network and the chemical bonds within a molecule to first, better understand the inherent conformational change, and subsequently, to provide a basis for predicting when and where the configuration is most vulnerable (likely to occur).

The second challenge for DWB is referred to as mobility management and includes many facets of design such as platform dynamics/navigation. The dynamics exhibited by each node in the DWB network impacts the aggregate performance of the network and thus, incorporating such aspects unique to modern DWB networks, produces robust control architecture. In the second part of this dissertation, a control architecture integrates the platform dynamics/navigation, gimbal parameters, mobility control for DWB networks. In addition, an assessment of current radio paradigms will be investigated and evaluated.

1.4 Previous Efforts

Previous Work in DWB Networks

The initiative for mobile directional wireless backbone (DWB) networks has been spearheaded by the Defense Advanced Research Project Agency (DARPA). Even though extensive resources have been spent related to DWBs, the research and development appears to have been more focused on single link performance, dating back to the 1960s [4]. In other words, a plurality of nodes utilizing directional antennas with requirements of real-time reconfiguration (topology control), mobility, and network specifications to enhance C[4]ISR[1] operations have not been fully investigated.

A selected number of DARPA sponsored programs since 1980 have been indicated on the timeline illustrated in fig. 1-3. DARPA began introducing network-centric objectives in 1983 within the "HAVE LACE"[2] program and included bit-error-rates (BER) of 10^{-6} (similar to hard-wired systems) [1]. This also marked the first time commercial off-the-shelf (COTS) components were targeted to ensure technological reliability. Objective data rates >1Gbps were established in late 1995 within the "RILC"[3] program [2]. In 2003, a full-duplex 2.5Gbps link was used to transmit ISR[4] data over an ultra-wideband laser communication system at 40,000 feet [3]. Additional optical link tests include a 5.5Gbps, 142km experiment between mountain tops in Spain in 2006 [4]. Directional RF links were first included in 2007 to cooperate with FSO links increasing overall reliable of the system within the project, "ORCLE[5]" [77].

[1] C[4]ISR refers to Command, Control, Communications, Computers Intelligence, Surveillance, and Reconnaissance for military applications.
[2] HAVE LACE stands for Laser Airborne Communication Experiment
[3] RILC stands for Recce/Intel Laser Crosslink.
[4] ISR stands for Intelligence, Surveillance, and Reconnaissance
[5] ORCLE stands for Optical RF Communications Link Experiment

Similar programs have existed since 2007 with objectives now approaching 100Gbps links at distances in the backbone up to 200km [6].

Even though performance of individual links has improved by order of magnitudes, BERs are similar to wired lines, and transmission ranges extend beyond 200km, a network of these links has not been fully developed – albeit that it was specifically identified as a primary problem in 1997 [19]. Twelve years later in 2009, project "ORCA[6]" specifically outlined the networking challenges such as addressing airborne link outages (due to scintillations, obscuration, and aircraft performance), quality of service (QoS) constraints for applications, and the Internet Protocol (IP) stack [77]. Most recently, project "FOENEX[7]" demonstrated packet-error-rates around 10^{-6} for air-to-air and air-to-ground links. Even though this project also identified network-centric parameters, none were fabricated in the experiment and the demonstration was limited to a relay in the sky for two disjoint end-users. Current work by DARPA includes two projects which have similar *link-only* objectives as previous projects: "Mobile Hotspots" [5] and "100G" [6]. Other research outside of DARPA in DWB networks seem to focus primarily on the performance of single-links with varying levels of atmospheric attenuations [63-67].

Recently, the term "predictive routing" is appearing in research efforts of DWB networks and is offered through various techniques [15]. However, these efforts are at the network layer regarding traffic patterns and routing tables or node flight pattern prediction based off known route characteristics. Other "prediction" vocabulary is

[6] ORCA stands for Optical RF Communications Adjunct
[7] FOENEX stands for Free Space Optical Experimental Network Experiment

included in reference to the examination of terrain databases and vector extrapolations to "predict" link-blockages within a known environment. None of this work examines the complete network, optimizes the link assignments for a specified aggregate BER, or truly foreshadow issues arising in a connected network to yield improvements in reliability. That is, the "prediction" schemas beginning to appear in literature remain reactive to degradations in the aggregate network (or from known databases such as terrain), and do not provide a proactive approach for reliability, as is in this dissertation.

In this dissertation, the term prediction is operationally defined as a pro-active process which examines a connected network in an effort to identify a subset of links that are either degraded (from a configuration viewpoint), or unstable in the future of the network ahead of a reactive reconfiguration trigger. The prediction period will provide time to develop strategies to mitigate information loss while transitioning between the current and future network configurations such as buffering, computing routing tables, and rerouting traffic on stable links.

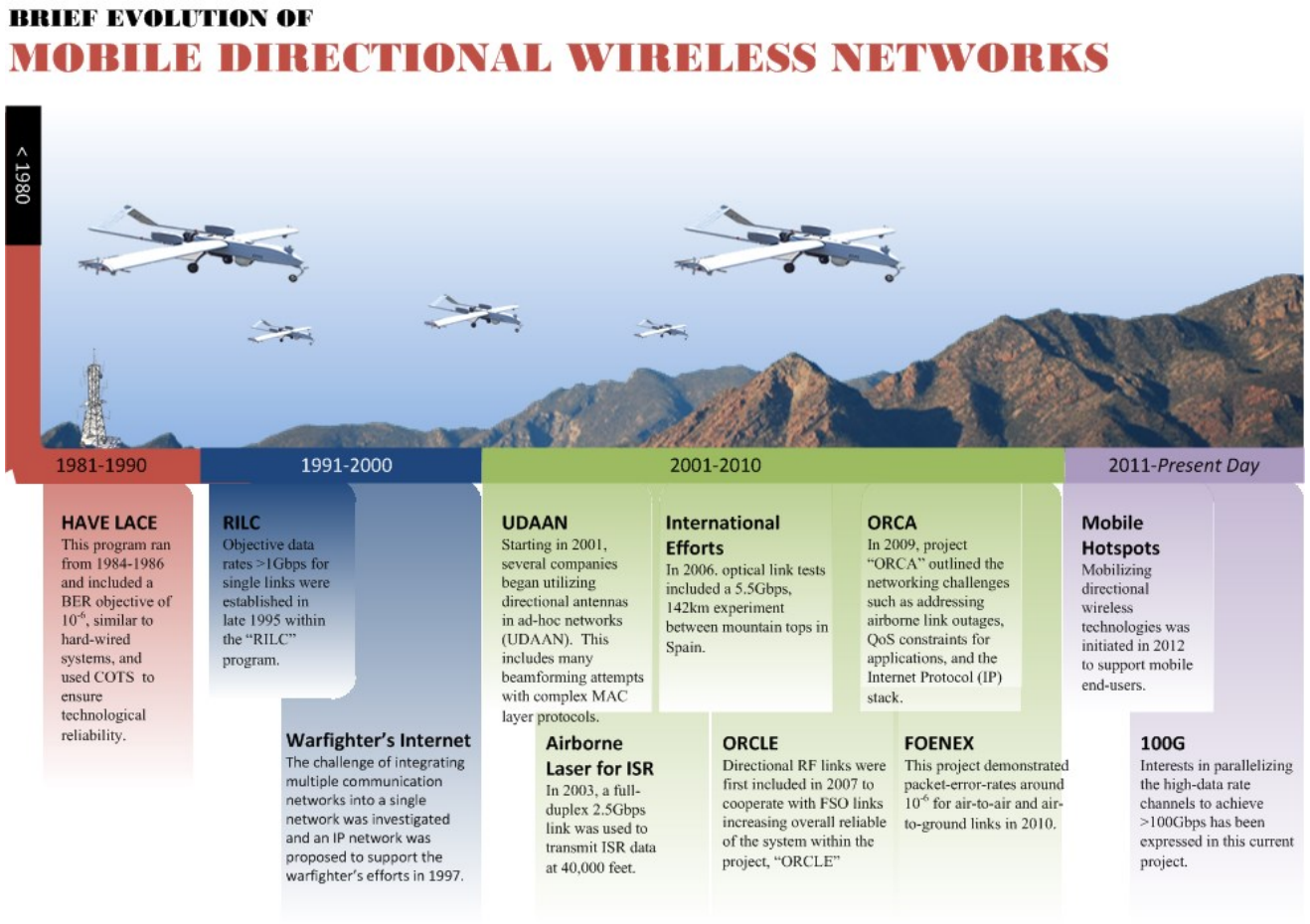

Figure 1-3. A brief evolution of mobile directional wireless networks sponsored by DARPA from 1980-2013. The majority of these projects have isolated link performance over network-centric objectives, such as assuring end-to-end connectivity.

Previous Work by Maryland Researchers in DWB Networks

Over the past 13 years, it has been the aim of the Center for Networking of Infrastructure Sensors (CNIS) and the Maryland Optics Group (MOG)[8] to develop modeling and simulation software aimed at providing better insight into the challenges within mobile DWB networks. These efforts have led to improved aggregate throughput by the re-pointing of directional links, increased coverage of end-users through mobility management techniques, and scalability studies to include 20+ backbone nodes and over 200 end-users [16, 17]. Additionally, CNIS/MOG has demonstrated these DWB network techniques on a fixed infrastructure [18].

CNIS/MOG's design of a mobile DWB includes two features that are not explicitly shown in fig. 1-1: 1) a background omnidirectional, low-bandwidth, control radio and 2) the designation of one node among the backbones for centralized origination of control decisions. First, the omnidirectional control radio has a range >200km and can be cascaded to increase the diameter of the DWB network, as well as intermittently turned on/off to hide the location of DWB nodes. This radio is not a limiting factor for DWB networks and has been common practice in previous link experiments [3-6, 77]. Second, one node (among the backbone nodes) is designated as the designated topology control node (DTCN) for the network and maintains responsibility for any centralized decision making process and algorithms (including backbone topology selection). This approach is necessary to mitigate oscillations in the directional link topology. However, this centralized control mechanism does not impact the scalability or fragility of the network as *any* node in the network can assume

[8] University of Maryland at College Park

DTCN responsibilities in the event of failure by the current DTCN, since the DTCN code is omnipresent among the backbone nodes kernel software [7].

Previous efforts by CNIS/MOG researchers [8-10] have established optimal backbone topology and terminal node assignment using a traditional algorithmic approach alongside nature-inspired distributed algorithms [11-13]. Topology control is defined as the assignment of links in the backbone and is a fundamental process in the network architecture due to the use of directional links. The work done by Llorca, et al. [7] developed a scalable mobility management process that minimized the aggregate energy necessary to maintain a network at a specified bit-error-rate. Fig. 1-4 illustrates this work. In fig. 1-4(a) the backbone (shown as blue nodes in the sky) is given an initial boot-strap topology and end-users (shown as red nodes on the ground) are connected to their nearest base-station. As a function of random end-user mobility, the base-stations shift their positions in an effort to optimize coverage and connectivity of end-users as shown in Fig. 1-4(b). In Fig. 1-4(c), the DTCN computes a new topology for the backbone and disseminates it among the other backbone nodes in an

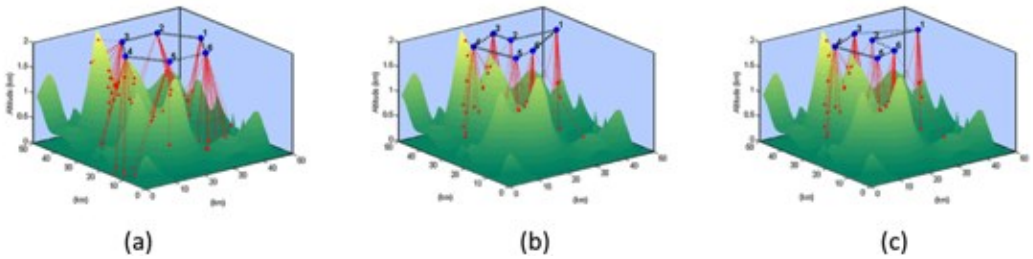

Figure 1-4. The topology control process and mobility management for a two-tier platform was first described by Llorca, et.al. a) The initial network is established using a boot-strapping technique. b) The network morphs over time as a function of end-user mobility.

effort to minimize transmit energy in the aggregate of the network while satisfying coverage and connectivity constraints.

In addition, the unrestricted mobility of the end-user nodes requires intelligent algorithms to adapt network connectivity while the obscuration rate (e.g. weather) must not hinder the network coverage. Inclusion of real-world dynamics has offered improved results to this joint-optimization problem for coverage and connectivity over traditional approaches. Zhang et al. [13] offered a nature-inspired methodology using flocking algorithms and particle swarm optimization. The mobility of each backbone node was governed by steering rules such that the communication energy was minimized. By referencing the terminal or end-user nodes as "leaders" and the backbone nodes as "followers", Zhang et al. [13] developed a distributed heuristic algorithm, based on a biology-inspired analogy to flocking behaviors, for improved end-to-end connectivity and assured coverage.

Llorca et al. [7, 12], in a similar manner, provided a physical-system analogy for solving this joint-optimization problem of coverage and connectivity. Thus, the minimization of the potential energy of the system (communication cost) will yield a balance between the two objectives. The mobility of the backbone nodes is governed by the local "forces" applied in the direction of the terminal or end-user node movements, and the interaction of neighboring backbone nodes in the network topology provides optimal coverage. This physical system analogy provides a framework for the work done within this dissertation.

1.5 Dissertation Contributions

This dissertation offers unique proposals in two aspects within reconfigurable beam-steered directional wireless backbone network research: 1) prediction of link degradation and network reconfigurations and 2) robust control architecture acknowledging the complexity of realistic platform and technology constraints.

1. **Predicting topological changes in DWB networks** – First, an analogous molecular conformation is developed using the dynamics and topology of a reconfigurable mechanically beam-steered DWB network. In this analogy, a DWB network is modeled as a giant molecule with the point-to-point links modeled as chemical bonds that can grow/retract as a function of potential energy within the structure. From this work, a normal mode analysis (NMA) is performed using only the convex potential energy function. Then, the potential energy function is extended to include disjoint energies between non-connected elements within the DWB network to derive the network's potential energy surface. This surface is a novel illustration of the network dynamics and identifies energy maxima, minima, and points of transition from one configuration to the next. Together, the NMA and PES approach have been validated to identify instabilities in the DWB network with respect to reconfigurations on the order of minutes prior to a reconfiguration.
2. **Validity of control architecture for DWB networks** – The control architecture for DWB networks differs greatly from the traditional Internet protocols of hard-wired networks. On first principles, managing topology

assignments to assure connectivity and mobility of individual nodes to maximize coverage is challenging in adverse environments. Additionally, the heterogeneous nature of the platforms and technology introduce new levels of complexity and has not been included in control decisions previously. As such, a robust control architecture is first outlined (including platform navigation/dynamics and an assessment of radio constraints) and is then validated with standard network metrics (e.g. throughput, latency). The conclusion of this work provides a framework for solving future DWB network challenges and a reference towards adapting the Internet protocol for such networks.

1.6 Dissertation Innovation

The novelty of the work in this dissertation is in the investigation and prediction of reconfigurations towards network optimality versus survivability. Outside the work done by UMD researchers, topology management processes reside at the network layer of the Internet protocol with solutions for re-routing traffic away from degraded links within the network. In addition, the objective of said topology management processes is maintaining a connected network versus the optimization of the topology control algorithms employed within UMD research. Furthermore, the "prediction" efforts of other research (which has only been shown recently) is a reactive process which re-routes traffic according to known flight patterns of the UASs, known terrain data, or extrapolations of previous measurements. In that regard, the "prediction" schemes only offer insight into the UP-DOWN connectivity decision of the individual links. On the other hand, the work in this dissertation goes beyond monitoring link parameters at any

layer in the Internet protocol (e.g. physical or network) and offers an innovative framework using a molecular analogy to identify the transition points between optimal topologies of the connected network. Correspondingly to the extension of the potential energy model for mobility management, the work herein, offers extension in the second-order for prediction of optimal reconfigurations in DWB networks.

Similar innovations exist for the control architecture proposed in this dissertation. Once again, the work done outside of UMD research, resides either at the network layer (latency) or the physical layer (received power). As such, it is argued herein, the Internet protocol does not sufficiently provide the controls necessary for reconfigurable DWB networks. Mainly, the information available to the physical layer is not passed up through the stack for intelligent evaluation. And any attempt to introduce the controls at the MAC layer of the Internet protocol will decrease the throughput of the network. Therefore, this dissertation validates the control architecture for DWB networks and includes topology control (i.e. link assignments). In this manner, the physical interconnections between the nodes can be redirected to provide an optimal network which subsequent traffic can be routed. This incorporates the unique aspect of reconfigurable DWB networks not available to hard-wired installation from which the Internet protocol was derived. Furthermore, other aspects of DWB networks such as platform heterogeneity and efforts in link pointing, acquisition, and tracking (PAT) are included to provide realistic expectation for throughput and latency.

Chapter 2: Predicting Topological Changes in DWB Networks

2.1 Problem Statement

The aggregate network performance of a reconfigurable beam-steered directional wireless backbone network (DWB) is directly related to the ability of the individual transceivers to rapidly reconfigure the network topology in the face of adverse environmental affects, increased separations, or a reduction in line-of-sight. Moreover, to achieve optimal network performance, reconfigurations may also occur to reduce transmit power, increase bandwidth, or increase connectivity. Each of these reconfiguration triggers may lead to temporary loss of data due to re-pointing and acquisition between stable nodes. Therefore, being able to predict such reconfiguration triggers, is helpful in reducing the amount of data lost by providing a sufficient amount of warning for processes such as re-routing, buffering, or transmission halts to occur before a link is severed.

For example, a network of 5 backbone nodes is shown in fig. 2-1(a). As the nodes shift in position to satisfy end-user demand at the lower tier (not shown) and random environmental effects are placed on the individual links, the operational energy[9] associated with the network will increase (fig. 2-1(b)). In this work, an optimization algorithm is being used to minimize the network energy as it relates to transmission power. As such, the transmit power is constantly being monitored and there will exist a point in time such that a reconfiguration is requested by the centralized

[9] The network energy is defined as the minimum aggregate transmit power necessary to communicate between all nodes at a guaranteed bit-error-rate (e.g. BER < 10^{-6}).

topology control node. This request is due to the operational network energy exceeding the pre-determined threshold over the optimized network energy in order to invoke a reconfiguration. This threshold is used to reduce the amount of reconfigurations executed and prevents oscillations between optimization outputs. During the reconfiguration period, the topology of the network is unstable, which results in a temporary period of reduced throughput in the aggregate (fig. 2-1(c)). After this period, the network is now in an optimal configuration and operates at an optimal aggregate energy (fig. 2-1(d)). Each of these events has been identified on the energy graph shown in fig. 2-1(e).

In order to develop proactive processes, a methodology to study and predict reconfiguration is necessary. The amount of time between the transition trigger and prediction will be referred to as $T_{predict}$, and is the execution time available for such proactive processes. Thus, proactive processes can be developed that permit for *soft* breaks in the network when resources are available versus *hard* breaks when links become fully obstructed (or exist at too high a cost).

One limitation on the quality of the prediction is with respect to the lifespan of a topology. The lifespan of a topology, T_{life}, is defined as the amount of time a topology is stable. Therefore, any prediction methodology must provide a warning ahead of the reconfiguration request and is bounded by T_{life}. The specific amount of time will vary with the number of nodes since the lifespan of any topology will decrease as the number of possible configurations increases. Furthermore, while the magnitude of $T_{predict}$ is important to invoke processes for re-routing, buffering, or halting transmissions, the

specific amount of time is hard to quantify since the mobility and environmental effects are random[10]. Each of these variables has been identified in fig. 2-1(e).

This section is divided up into four parts. First, a molecular-inspired framework is investigated as an extension of the physical previously explored by University of Maryland researchers. That is, a DWB network is analogously modeled as a giant molecule whose links are modeled as bonds that can grow/retract as a function of potential energy. The second part will extend the potential energy of the DWB network to include disjoint node energies to define regions of instabilities within the environment with respect to backbone node positions, and will define the DWB network potential energy surface (PES). A common technique employed in molecular studies, the PES illustrates the transition points within a reaction; or in this case, will aide in the warning of an impending network reconfiguration due to one node transitioning between minimum energy-wells on its PES. The third section offers a second-order harmonic approximation of the nodal dynamics (i.e. mobility) as a function of the network topology. This is known as a normal mode analysis (NMA) and is frequently performed in molecular science to understand the bonding of molecules. In a similar way, the NMA is used in this work to identify instable network configurations (i.e. topologies). Lastly, results are offered in the last section that validates the molecular-inspired methodology. Collectively, the molecular model will predict the reconfiguration triggered in Fig. 2-1(e).

[10] Received power is dependent on separation (i.e. mobility) and environmental effects.

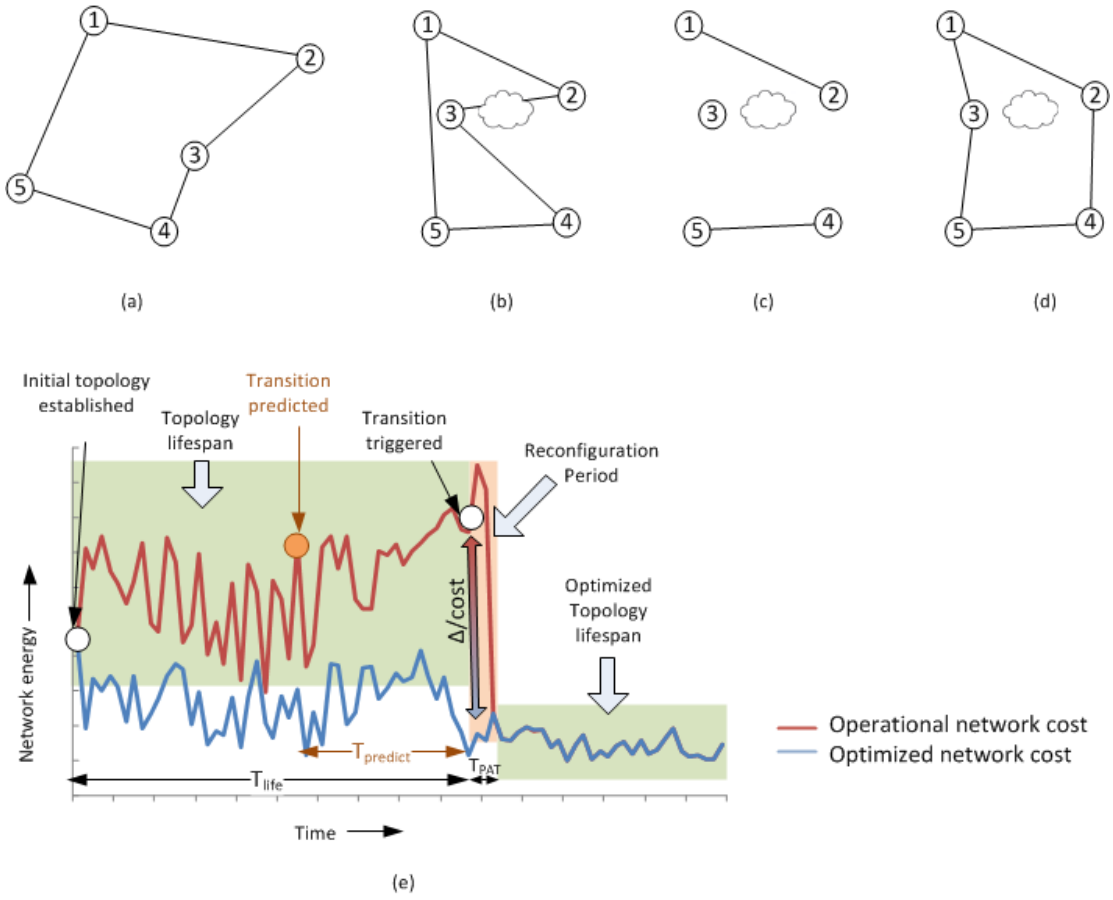

Figure 2-1. The backbone of a DWB network is shown in (a) with a bi-connected configuration. (b) The backbone shifts its position to satisfy the end-user demand at the lower tier. (c) Due to node separation and the inclusion of obscuration between nodes 2 and 3, the network undergoes a reconfiguration. (d) The network reconfigures to a stable topology. (e) The network is optimized based on the aggregate network energy when it exceeds a threshold value with respect to the optimal network energy. This change can be predicted using molecular modeling.

2.2 A Molecular-Inspired Model for DWB Networks

The dynamics of a reconfigurable directional wireless backbone network (DWB) can analogously be modeled as a molecule whose potential energy is a function of the growth and retraction of its bonds (i.e. links). Using an energy-constrained optimization function, both systems (molecule and network), invoke reconfigurations in their conformations (i.e. topology) to reduce the aggregate potential energies. As such, the work is this dissertation will use an analogous approach to mimicking the behavior of molecular systems to predict reconfigurations and the assessment of node movements within the network as they relate to and can be used to predict the overall network strength (i.e. network energy). This strategy involves the use of electronic structure theories such that the network entity is modeled as a giant molecule and the communication links are thought of as chemical bonds. Through this analogy, the specific configuration (i.e. topology) available to the network is a combination of the potential energy of each link and the environment. In addition, new tools are available to predict the formation of new bonds (i.e. reconfigurations) such as a normal mode analysis (NMA) and the potential energy surface (PES). This is an extension to potential energy function for the topology control process; in a similar manner as the gradient of the potential energy function provided energy minimization to the mobility control process (see Appendix A).

On first-principles, a molecular system is a combination of atoms and bonds and the interaction each establish both the configuration of the molecule and its potential energy. The total potential energy of a molecular system can be expressed as,

$$U_{total} = U_{stretch} + U_{angle} + U_{torsion} + U_{non-bond} \quad (1)$$

where $U_{stretch}$ and U_{angle} represent the harmonic potential energy associated with atomic pairs, $U_{torsion}$ represents the rotational energy associated with covalent bonds, and $U_{non-bond}$ represents the energies associated with non-bonded atomic interactions such as *van der Waals* and electrostatic interactions. The first two terms are relative to the atomic pair separation and include an equilibrium variable, similar to the potential energy associated with a spring. The non-bonded interactions play an important role in the reactionary transitions exhibited in molecular reconfigurations. Additionally, each term in the potential energy function includes parameters for atomic weights and environmental effects.

Equivalently, at the backbone layer, a reconfigurable DWB network is a combination of base-stations and communications links. Therefore, similar to the molecular system, a potential energy function for a DWB network can be expressed as

$$U = U_{link} + U_{non-link} \quad (2)$$

where U_{link} represents the energy associated with a selected link in the network and $U_{non-link}$ represents a non-selected link. Though similar to the potential energy model offered by J. Llorca [7], the potential energy function used herein is restricted

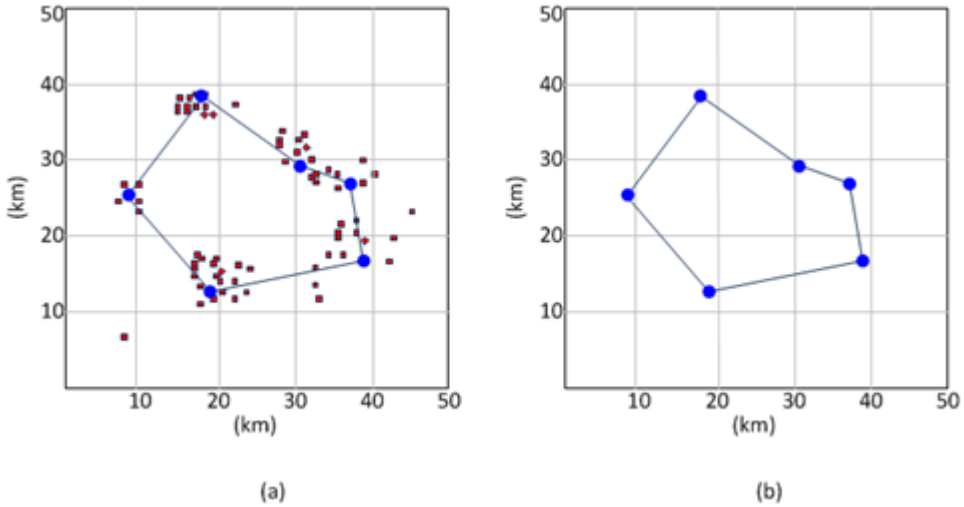

Figure 2-2. The predictive methodology only pertains to the control movements of the backbone UAS. The behavior of the end-users is still included to provoke mobility by the UASs, yet is not used for prediction since their movements are random.

to the backbone base-stations exclusively since the prediction scheme targets degradations and reconfigurations (i.e. connectivity) which have substantial impact on the aggregate network performance, as shown in fig. 2-2; whereas the topology control algorithms offered by Llorca [7] jointly optimized connectivity and coverage. Furthermore, since the mobility of the base-stations is controllable, a self-diagnosing capability can be achieved through focusing only on their information. Also note at this time, the potential energy function for a DWB network does not include relative angle contributions. Future implementations of this methodology may include terms for U_{angle} and $U_{torsion}$ to identify interference configurations among established links. However, the focus of this dissertation is on narrow-beam directional wireless systems and the interference is only present with extreme angles.

The components of the potential link energy for a DWB network are derived from the linked and potential link set as illustrated in fig. 2-3. The two sets are formally defined as

$$Linked = \{(i,j)|\,(i,j) \in T\} \tag{3}$$

$$Potential\_Link = \{(i,k)|\,(i,k) \notin T\}. \tag{4}$$

The link energy for communication in the directional wireless network from the source i to the destination node j is a function of distance $L_{i,j} = \|R_i - R_j\|$, minimum transmit power to guarantee a specified bit-error rate P_{R0}^j, the atmospheric attenuation coefficient α_{ij}, directivityof the transmitter D_T^i, and the effective receiver area A_R^j[27]:

$$\begin{aligned} U_{link} &= \sum_i^n \sum_{j\neq i}^n b_{ij} \left(P_{R0}^j \frac{4\pi}{D_T^i A_R^j}\right) {L_{i,j}}^2 e^{\alpha_{ij} L_{i,j}} \\ where\ b_{ij} &= \begin{cases} 1 & if\,(i,j) \in T \\ 0 & o.w. \end{cases} \end{aligned} \tag{5}$$

The additional energy for non-bonded nodes (*Van der Waals* interactions) shown in eq. (4) is used for prediction and mobility characterization and does not increase the overall required supply energy. In this system, these interactions are

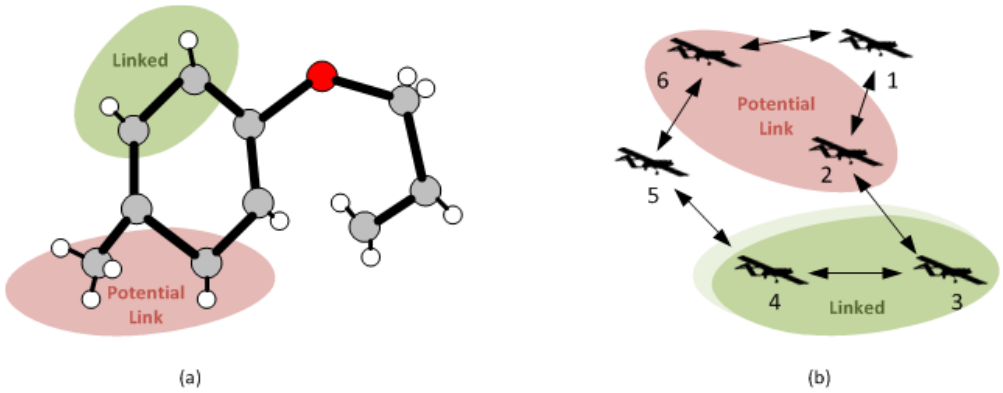

Figure 2-3. Two sets are necessary to derive the potential energy for the DWB network: linked and potential link. The link set includes L={(1,2), (2,3), (4,5), (5,6), (6,1)} and the potential link set includes PL={(1,3), (1,4), (1,5), (2,4), (2,5), (2,6), (3,5), (3,6), (4,6)}. Note the sets are reflexive because the links are bi-directional.

modeled as a Lennard-Jones potential for its computational simplicity compared to a traditional Morse potential [61]:

$$U_{non-link} = \sum_i^n \sum_{m\neq i}^n -4\varepsilon \left[\left(\frac{\sigma}{\|R_i - R_m\|} \right)^{12} - \left(\frac{\sigma}{\|R_i - R_m\|} \right)^{6} \right] (1 - b_{im}) \\ where\ \varepsilon = \max\left(\left\| R_i - R_j \right\|, \|R_i - R_k\| \right) \tag{6}$$

where ε is the disassociation distance, σ is the width of the potential well, and b_{im} is defined in the same manner as b_{ij} from eq. (5); note that $(1 - b_{im})$inverts the value as to select unconnected nodes as opposed to eq. (5) where connected nodes were selected. The simplicity of the L-J potential lies in that the twelfth power is the square of the sixth and the even exponents remove the need for the square-root in vector distance calculations [61].Note the dissociation factor is purely a function of distance since obscuration between two disjoint nodes would have to be measured. A more detailed discussion of the dissociation distance is in section 2.4 in regards to the potential energy surface. The total energy surface is a summation of eq. (5) and eq. (6):

$$U_{total} = \underbrace{\sum_i^n \sum_{j\neq i}^n b_{ij} \left(P_{R0}^j \frac{4\pi}{D_T^i A_R^j} \right) \left\| R_i - R_j \right\|^2 e^{\alpha_{ij} \|R_i - R_j\|}}_{U_{link}} \\ + \underbrace{\sum_i^n \sum_{m\neq i}^n -4\varepsilon \left[\left(\frac{\sigma}{\|R_i - R_m\|} \right)^{12} - \left(\frac{\sigma}{\|R_i - R_m\|} \right)^{6} \right] (1 - b_{im})}_{U_{non-link}} \tag{7}$$

Further analogous parameters between a molecule and a directional backbone network are outlined in Table 2-1. One notable difference between the modeling of a molecule and the harmonic model used herein for a directional network is in link strength (i.e. link energy). In the network potential energy model, the energy of a link grows exponentially as the link is stretched or obscured until a pre-specified amount of energy is reached. On the other hand, in the molecule a similar bond weakens as it is stretched and will break when the force between two pair-wise atoms is zero. This is because the optimization function for which the methodology herein seeks to predict upon is a minimization of aggregate transmit power of the network verses the received power. Therefore, it is expected of the analysis that it will be inverted compared to the molecular counterpart.

The objective of this work is to promote the molecular-inspired approach as a viable option for predicting failures in the network with respect to link degradation, link breakage, and congestion. It should be noted that this work focuses on the connectivity of the network and maintains the self-organizing features previously offered by Llorca et al [7, 13]. On the other hand, a novel self-diagnosing capability is introduced with respect to the optimization. This work is a first-of-its kind and resides at the physical layer of the network stack (versus predictive-routing techniques [25], which reside at the network layer) and thus offers new methodologies for network science.

Table 2-1. Analogous parameters exist between a molecule and a directional wireless backbone network. In the simplest form, the point-to-point links between nodes in a DWB network can be modeled as the bonds between atoms in a molecule and are able to grow/retract to satisfy the applied (internal and external) forces.

Parameter	Directional Network	Equivalent Molecule Parameter [41,42]
Analysis Approximation	Our convex spring model approximation minimizes the potential energy of the network and the analysis is performed using only the base-stations.	The Born-Oppenheimer approximation neglects kinetic energy and focuses only on the heavier nuclei of a molecule.
Nodes	Each base-station can be weighted uniquely to identify its priority in the network.	The mass of each nucleus determines its ability to maintain bonds.
Links	The potential energy of a link is a function of distance and obscuration. The number of end-users per base-station is restricted by channel capacity.	The potential energy of a link is a function of distance, bond angle, dihedral angle, and Van der Waals interactions. The number of electrons per nucleus is restricted by availability in its valence shell.
Link Organization	The topology control process finds the minimum energy topology. A single network can exist in multiple states - topologies.	The structure (configuration, composition, etc.) of a molecule is a result of energy minimization. A single molecule may have multiple configurations known as isomers.
Environmental Effects	Link availability can change with weather patterns, turbulence, terrain, end-user demand, etc.	The specific isomer present is a function of environment parameters (e.g. water, air).

2.3 Understanding Nodal Dynamics on the Network Potential Energy Surface

Like the molecular dynamic counterpart, the analysis of the reconfigurable DWB network configuration can be evolutionary. That is, the motion of the aggregate energy for the DWB network will be tracked along the potential energy space/surface over time and approximated between two configuration spaces. This will aide in the identification of the minimum energy path with respect to the applied forces (e.g. end-user demand). However, unlike chemical systems, the specific motion demonstrated by the backbone of the DWB network will not strictly adhere to the energy surface since the demand for connectivity and coverage is counter to the minimum energy efforts of molecules – though useful information is still available for DWB network analysis.

This approach maintains the previous physical joint-optimizations for coverage and connectivity developed by Llorca et al. [7, 12] while providing parallel assessment of communication links as they relate to the network's potential energy. This ensures that the network continues to be self-organizing with the addition of being self-diagnosing with respect to impeding link failures and non-optimal configurations (i.e. topology).

2.3.1 Potential Energy Surfaces in the Studies of Molecular Dynamics

In chemical systems, molecules can exist in multiple bonding configurations known as isomers. The specific isomer a molecular resides in is a result of the external forces being applied, the environment of the reaction, and the specific bonds present [41]. Thus, energy minimization is the problem. The Born-Oppenheimer potential energy hypersurface (PES) [42] is a theoretical model used by chemists to aide in the understanding of the specific molecular structure present during a reaction. Specifically, three main elements are important to discern from the PES: energy minima, energy maxima, and the resulting reaction path connecting the two minimum energy states within a reaction - the product and the reactant states, respectively. The reaction pathway between a reactant and product state follows the path of greatest descent along the surface; thus, minimizing the reaction energy. The local minima and maxima encountered along the reaction path illustrate the intermediates and transition structures, respectively. Transition structures are the highest energy barriers that a molecule must overcome for the reaction to precede. Intermediates are a midpoint of a reaction, lower in energy than a transition structure that last a short period of time. By knowing the energy levels of each, chemists are able to fully understand the kinetics driving a reaction to completion.

As an example, the Claisen rearrangement (reconfiguration) of allyl-*p*-tolyl ether (structure) is illustrated along the internal coordinates, R_{12} and R_{45} between nodes (1,2) and (4,5), respectively, in fig. 2-4 [60]. The grey nodes are carbon atoms, the red node is an oxygen atom, and the white nodes are protons. The potential energy surface for this reaction is shown on the top right. The energy as a function of the reaction at

hand can be traced along this energy surface. Key energy states are identified by points A, B, C, and D. At the beginning of the reaction, nodes (1,2) are bonded and represent a minima energy on the potential energy surface (point A).The reaction is excited through externally applied forces which stretch the (1,2) bond and relax the (4,5) non-bond. This yields a transition structure in the center of the PES (point B) at which point the (1,2) bond is released and the (4,5) bond is formed. The molecule now resides in a new minimum energy state illustrated on the PES (point C). These unique molecular configurations are known isomers of ally-*p*-tolyl ether. Note the reaction pathway is from points A-B-C and goes from one energy minima, over a transition point, and into the next energy minima. Other dynamics of the rearrangement, such as simply stretching the (1,2) bond are also illustrated on the PES (point D), even though they are not included in the reaction pathway.

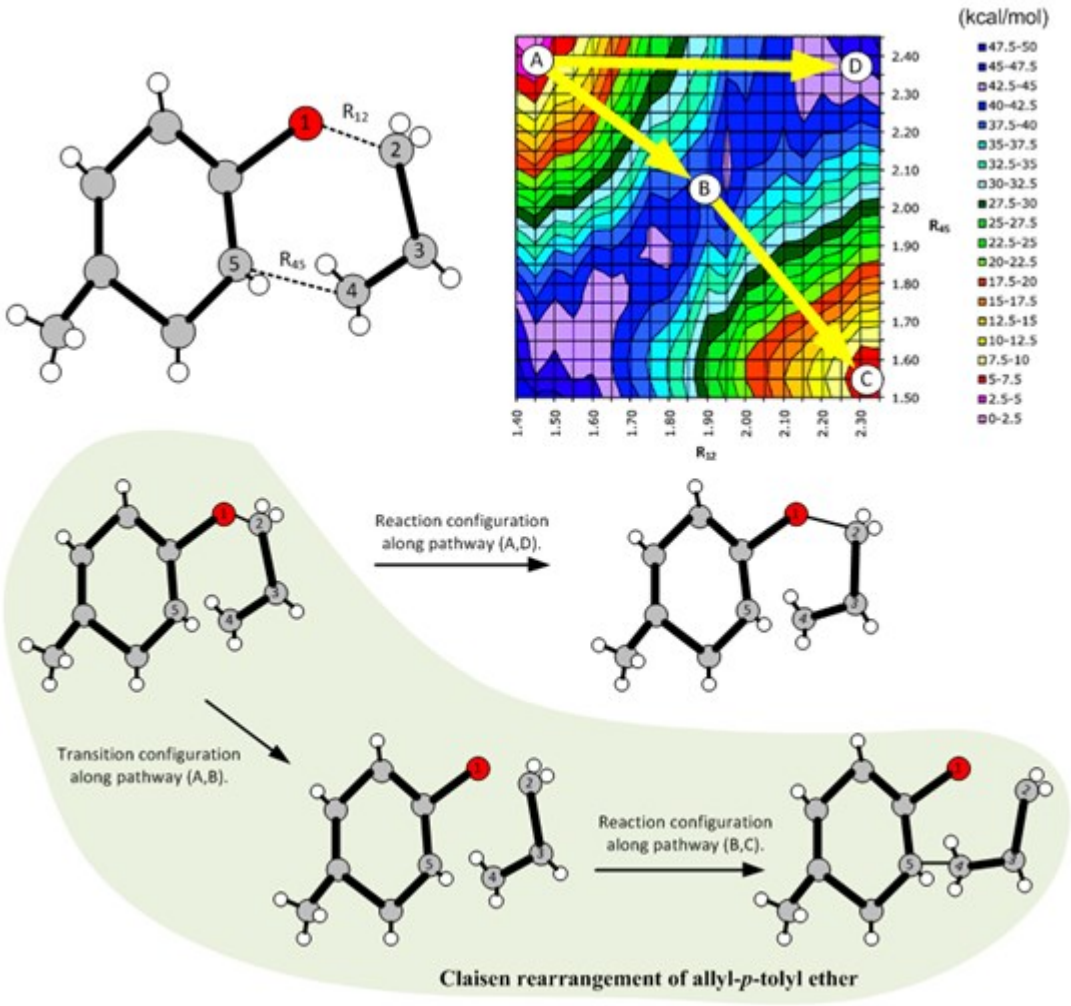

Figure 2-4. The Claisen rearrangement of allyl-*p*-tolyl ether occurs along the reaction coordinates R_{OC} and R_{CC} (top image). The potential energy surface illustrates the bonding decisions as a function of energy minimization (bottom image). The red areas represent a minimum and the dark blue area represents a maximum in molecular energy. Bond rearrangement is analogous to an imminent network reconfiguration.

2.3.2 Potential Energy Surface: DWB Network Evolution

This follows a similar approach that mimics the chemical analysis seen in the previous section is available by developing an energy surface for the DWB networks in which minima, maxima, and transition states can be discerned with respect to network configurations. In other words a network will reside in a minimum region when its links are relaxed and a maximum region when its links are stretched. The transition point between two minima regions will aide in the prediction of a potential network reconfiguration (similar to the previously seen rearrangement in the chemical reaction). By analogy, this methodology allows an understanding when bonding will occur through a naturally occurring process, which in turn permits application of that knowledge to network (re)configuration.

As shown in eq. (2), the potential energy of the network consists of two interactive components: links and non-links. The non-link interaction is a function of distance between two non-connected nodes. Furthermore, to account for reconfigurations, the dissociation distance used in the term $U_{non\text{-}link}$ is set uniquely at each node and is dependent on the current links as shown in fig. 2-5. In fig. 2-5(a) the dissociation distance is set by the maximum distance link established (e.g. R_i *to* R_j). In fig. 2-5(b) the dissociation distance is set by the maximum distance link established (e.g. R_k to R_l). As expected, $\varepsilon_{R(i)} \neq \varepsilon_{R(k)}$. This is significant because the dissociation factor determines when nodes from the potential link set are below energy within the link set. In other words, there exists a possible new connection that conserves energy. In fig. 2-5(a), node R_m is within $\varepsilon_{R(i)}$ and therefore, is a possible new connection evident on the DWB-PES.

Now that each term has been fully investigated in the potential energy function, an N-dimensional energy surface can be computed to illustrate the effects network dynamics has on the energy function. However, given the N-dimensions, the potential energy surface is best understood as a function of its established links. Further benefiting from the bi-connectivity of the DWB network, the PES can be illustrated as a contour map with regions of high energy in red and low energy regions in red. A distributed PES is offer for each of the individual nodes in the network in fig. 2-6.The coordinates of individual contour maps are absolute positions within the simulations.

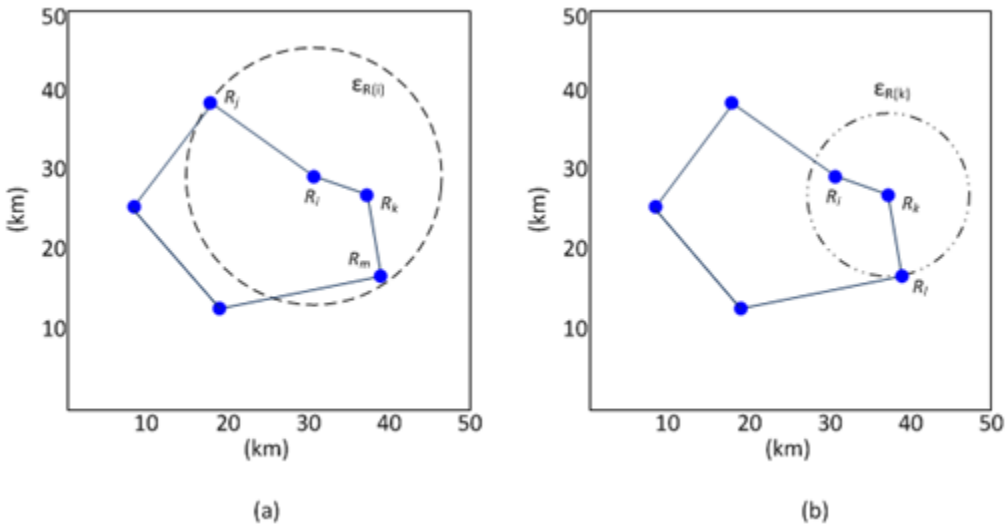

Figure 2-5. The disassociation distance $\varepsilon_{R(i)}$, is unique to each node R_i. In (a), this distance is defined by the maximum length between R_i and nodes (R_j, R_k). In (b), this distance $\varepsilon_{R(k)}$ is defined by the maximum length between R_k and nodes (R_j, R_l). Note a node R_m within the distance $\varepsilon_{R(i)}$, is a possible neighbor discernable on the DWB-PES.

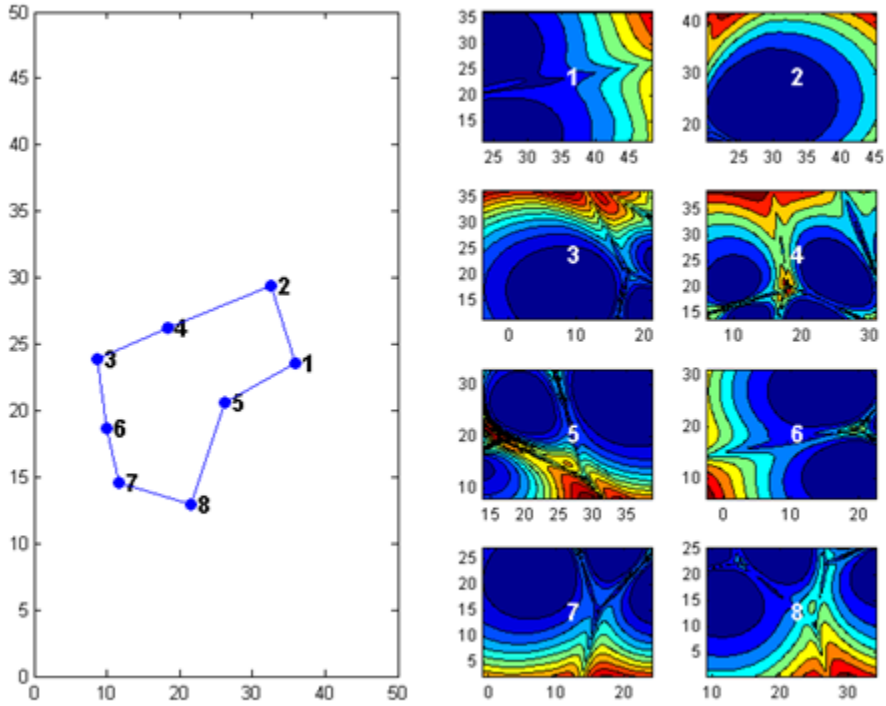

Figure 2-6. Potential energy surface simulation showing N=8 contour graphs. The dark blue represents a minimum and red represents a maximum. The node position in its respective graph is identified by its number.

2.3.3 Analysis of the DWB Potential Energy Surface

Just like the chemical reaction previously discussed, the dynamics of the DWB network can be traced along the DWB-PES. In this case, however, the DWB-PES slice is specific to each node giving the surface three dimensions. Focusing on UAS-5 in the initial positions indicated in fig. 2-7, the topology reconfigurations can be traced along the DWB-PES. For example, if UAS-5 moves in a north-western direction (from point-A to point-B), a reconfiguration will occur to establish links between UAS-5 and UAS-6, UAS-7. Similarly, if UAS-5 moves in the direction of points C or points D, a reconfiguration will occur which optimize the topology with respect to transmit power. In addition, negative consequences, such as stretching a link beyond the available transmit power (where no reconfiguration can satisfy optimality), is evident on the DWB-PES (point E). It should be noted that the direction exhibited by UAS-5 is not directly related to the minimum energy path between two energy-minima on the DWB-PES. This is due to the restrictions placed on the UAS backbone to satisfy end-user coverage/connectivity. Therefore, the DWB-PES identifies proximate regions of reconfigurations, versus expect path taken. Information from the DWB-PES is available to determine the transition points between two optimal configurations. By tracing the DWB-PES for the transition point an increase in the amount of time available between the current location of a UAS and the reconfiguration request by the topology control algorithm is seen.

Further information can be obtained from the DWB-PES, such as the flexibility with respect to a node movement within the current configuration. A node's classification is based on the range of motion available such that the overall communication cost is not noticeably impacted. These characterizations include:

- *Flexible node* – A node has a free range of motion within its current configuration without the need to reconfigure such as seen by UAS-2 and UAS-3 in fig. 2-6. Though it may not be sitting in the global minimum of its PES, the occupied well is very large in area and thus UAS-2 and UAS-3 have a high degree of flexibility and their mobility does not impact the overall cost of the network.
- *Rigid node* – A node has a confined region within its PES to move and a network reconfiguration may be required from small deviations. For example, UAS-5 in fig. 2-6 is currently sitting in a valley between multiple wells thus any large deviations from its current position will impact the topology cost (and may force a topology change as previously discussed).
- *Exiting node* – A node moves away from the network thus stretching its current communication links. At some point a decision will need to be made to drop the node from the network since its connectivity cost grows exponentially. An example of this movement can be seen by moving node UAS-1 away from the network away from the network cluster in fig. 2-6.

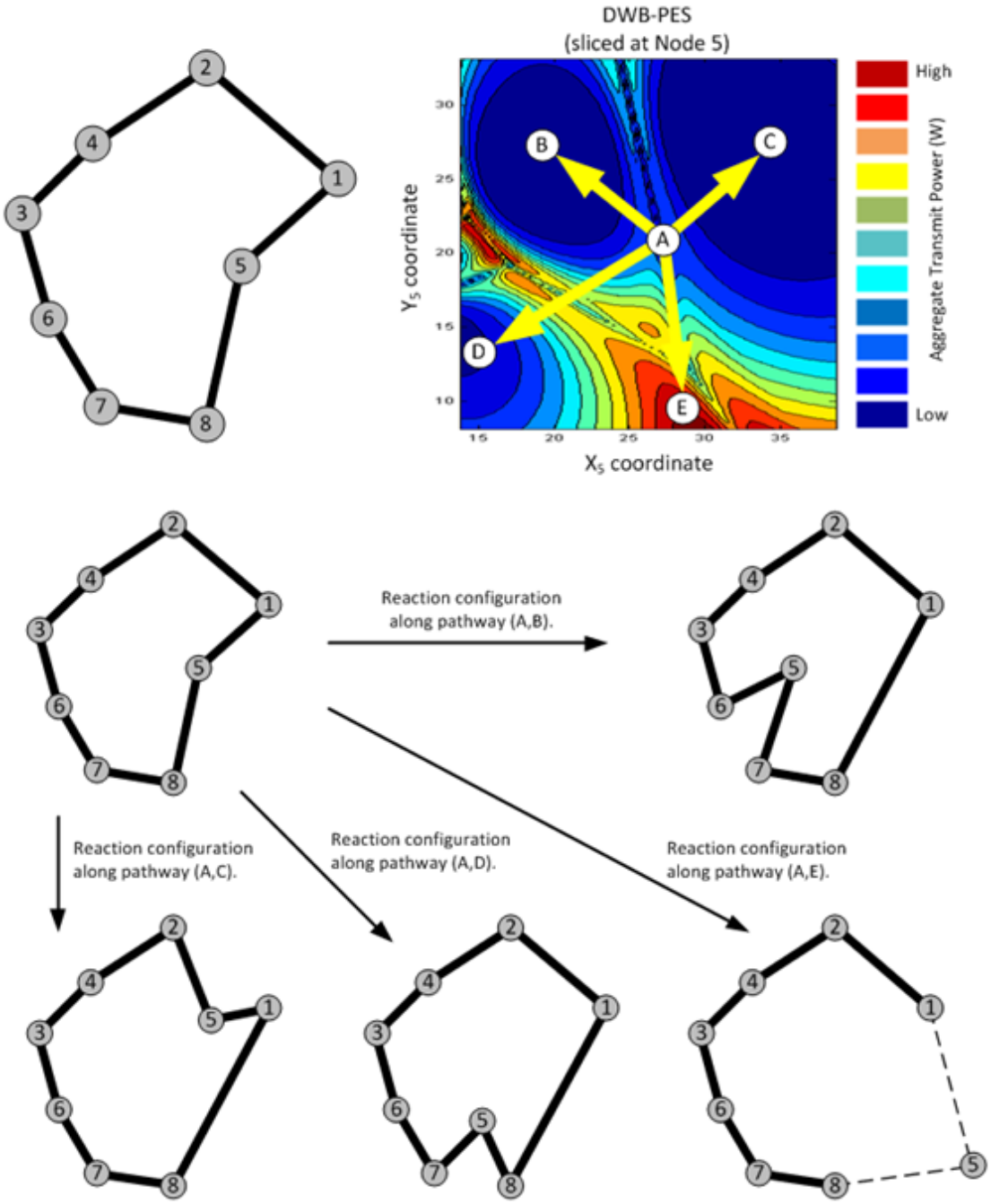

Figure 2-7. The reconfiguration of a DWB network can be identified on the distributed DWB-PES as a function of each node's movement. In this example, node 5's PES is shown on the top right and the reconfiguration topologies are illustrated below at points A, B, C, and D. Point E on the PES illustrates node 5's movement away from the network.

2.4 Normal Mode Analysis and Second-Order Dynamics of Potential Energy

A normal mode analysis is the study of an oscillating system wherein all parts exhibit sinusoidal motions with an equivalent frequency. In other words, it is a perturbation study of each node with respect to its connections to other nodes in the system. On first principles, a normal mode analysis (NMA) describes the inherent agility of each node with respect to its connections (i.e. links). It is theorized that a NMA on a DWB network will aide in the identification of unstable network configurations or impending network reconfigurations, in a similar manner that NMA is used in molecular dynamics to predict bonding reconfigurations.

Most notably and uniquely, NMA has only enjoyed recent success with the inclusion of modern computing powers and has never been applied to a directional wireless backbone network. For this reason, the methodology is broken up into five parts: a brief definition of normal modes and an example is provided in section 2.4.1; a background review of NMA in modern computational chemistry is offered in section 2.4.2; the mathematics with respect to DWB networks is offered in section 2.4.3; the last two sections outline the eigenvalues and eigenvectors as indicators of reconfiguration activity. The results are withheld for discussion in section 2.5.

2.4.1 Definition of Normal Modes

The definition of a normal mode pertains to an oscillating system wherein all parts exhibit sinusoidal motions with an equivalent frequency. The amplitude of motion is different and therefore complex motions of a system can be described by a linear combination of its normal modes [14]. Mathematically, a system with *N* nodes can be expressed as

$$q_i = \sum_{k=1}^{3N} l_{ik} K_k \cos\left(\lambda_k^{\frac{1}{2}} t + \varepsilon_k\right) \tag{8}$$

where q_i is the mass-weighted Cartesian displacement coordinate

$$\begin{array}{ccc} q_1 = \sqrt{m_1}\Delta x_1 & q_2 = \sqrt{m_1}\Delta y_1 & q_3 = \sqrt{m_1}\Delta z_1 \\ q_4 = \sqrt{m_2}\Delta x_2 & q_5 = \sqrt{m_2}\Delta y_2 & q_6 = \sqrt{m_2}\Delta z_2 \\ \vdots & \vdots & \vdots \\ q_{3i-2} = \sqrt{m_i}\Delta x_i & q_{3i-1} = \sqrt{m_i}\Delta y_i & q_{3i} = \sqrt{m_i}\Delta z_i \\ \vdots & \vdots & \vdots \\ q_{3N-2} = \sqrt{m_N}\Delta x_N & q_{3N-1} = \sqrt{m_N}\Delta y_N & q_{3N} = \sqrt{m_N}\Delta z_N \end{array} \tag{9}$$

K_k and ε_k is an arbitrary amplitude and phase for node *k*, respectively, and l_{ik} is a normalization factor such that$\sum_i l_{ik}^2 = 1$. The frequency associated with each normal mode *k* is λ_k and is equivalent for each node *j* (*j*=1…*N*). This means that a node which possesses larger amplitude K_k must also possess more energy in order to satisfy the normal mode frequency constraint.

A system with *N* nodes has *3N* normal modes because each node has three-degrees of freedom. However, there are only 3*N*-6 modes of vibration since six modes define the translation (x, y, z) and rotation (x/y, x/z, y/z) of the full system in three dimensions[11]. Illustration of the normal modes of vibration for $H_2O$is provided in fig.

[11] In a linear molecule with *N* atoms there are only 3*N*-5 normal modes

2-8. Since the water molecule includes three atoms (N=3), there will be three modes of vibration,

$$\#\ of\ modes = 3N - 6 = 3(3) - 6 = 3. \tag{10}$$

In addition, since the weight of the Oxygen atom is approximately 16 times heavier than the Hydrogen atoms, its amplitude of the motion is one-fourth that of the Hydrogen atoms.

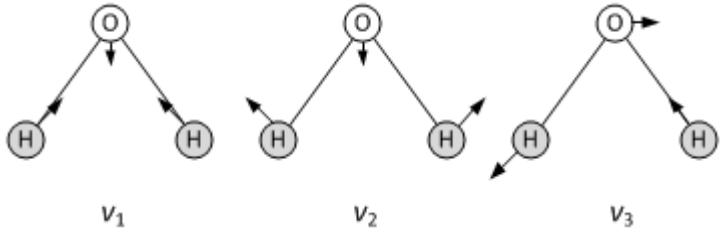

Figure 2-8. A water molecule, which includes three atoms, has 3(N)-6 = 3 modes of vibration. Each of these modes is illustrated. Note the Oxygen's mobility is ¼ that of the Hydrogen since its weight is 16x that of Hydrogen. Thus, the illustration is not to scale.

2.4.2 Related Work

The work within this section performs a normal mode analysis (NMA) on the DWB networks. This is the first-time an analysis of this kind has been included in the study of DWB networks and ties together the analogous molecular dynamics with a similar counterpart from modern research. Collectively, NMA has yielded results with the addition of modern computational resources and it is justified as a reliable framework for predicting instabilities in DWB networks.

A simplified spring model for a complex polymer was developed by Rohrig and Frank [45, 46] to study the first-principle molecular dynamics (MD) of a polymer under tensile stress. This work used numerous MD simulations to identify the influencing

factors that rupture a covalent bond. The spring model had parameters for external sources as well; including temperature, environmental features, and separation rate. This work is very similar to the approaches taken in [7] and serves as a comparison model for DWB and MD simulations.

Aktah and Frank [47] offered unique insight into the breaking of bonds in molecules including protein transfers and reaction pathways. One caveat to their work - which directly relates to the network topology reconfigurations for the reason of aggregate optimal transmission powers – details their modified interpretation in the identification of which bond will break during a reaction. Their work concludes with the most vulnerable bonds being those most easily attracted by the new molecular configuration versus weakest bond present. Specifically, [47] served as the first attempt to compare the results provided within this dissertation with the classical approach of monitoring power for predicting link failures. A correlation between the ionic and electronic motions in [47] found by NMA did provide comparative evidence that initial NMA results were onto a surprising conclusion within DWB networks [48]!

The output of a NMA is often complex and provides many directions of structural changes as identified by J. Ma [49]. Though DWB networks possess a finite number of backbone nodes (usually much less than 20), the number of directions available for reconfiguration is on the order of 60+. The scope of experiments, in addition to the most functionally important modes was discussed within [49] and is still debated today. Therefore, the work in this chapter attempts to investigate vast number of experimental setups and use random end-user trajectories to remove irregularities in the results.

Previous work by Milner, Davis, and Llorca [48] provides a basis for the validity of NMA on DWB networks concluding that a spike in the eigenvalues of the NMA indicate a favorable prediction towards a network reconfiguration, as shown in fig. 2-9. After said reconfiguration, the eigenvalues softens. This is similar to the work done by Bradley and Weaire [50], who identified a spike in the eigenvalues associated with instabilities of two liquids coming into contract. After contact, the eigenvalues spikes due to the instability of the classical symmetry. However, work in this chapter will refute this eigenvalues spike and show it is not prevalent in all cases.

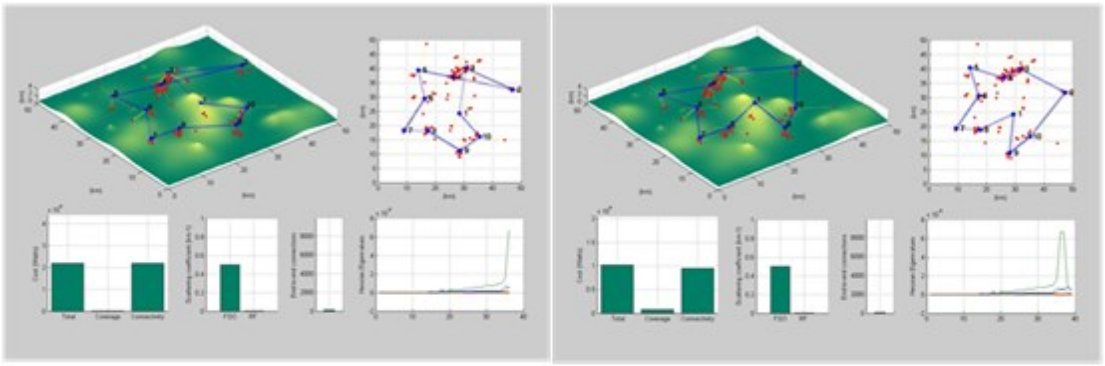

Figure 2-9. Previous work by Milner, Davis, and Llorca, correlated a spike in the eigenvalues of the Hessian with a reconfiguration in the network. This provided a framework for further investigation into the normal modes of a DWB network.

Ultimately, the most motivating factor for the investigation of NMA (and later potential energy surfaces) is by Karplus in the forward of [51]. In this book, he states, "the identification of a conformational transition with one or a few normal modes tells us something about the inherent flexibility of the molecule but does not provide an understanding of the dynamics of the conformational change, which requires knowledge of the free energy along the reaction coordinate." In the same manner, it is equally justified that the reconfiguration of a network's topology will not be justified by first-principles of an NMA, yet by the combination of several techniques alongside the understanding of the dynamics influencing the reconfiguration (e.g. mobility, optimization). That is, the topology and mobility of the backbone within the DWB network will include both inherently flexible and structurally rigid nodes (and links) that will either permit movement of the nodes or require a network reconfiguration – each predictable through NMA, environmental understanding (e.g. terrain), and potential energy surfaces.

Further studies of normal modes in other scientific fields has led to isolation of particular normal modes that contribute to favorable bonding coordinates in molecules (e.g. lower bonding energy barriers [52, 53, 69-74]), understating of complex dynamics of proteins[54, 55], and even exploitation of structural instabilities to separate DNA strands [56].

2.4.3 Normal Mode Analysis of DWB Networks

Degradation of the network at the backbone layer is dependent on the topology and mobility of the base-stations. Therefore, instabilities can be detected through tracking of the base-station normal modes which are expressed through a normal mode analysis (NMA). NMA utilizes a harmonic approximation of the potential energy around a global aggregate energy minimum. In other words, NMA is a perturbation analysis for a structure (e.g. network, molecule, spring network) where the pair-wise interconnections between connected nodes determine the structure's normal modes and respective resonance frequencies. The normal modes are orthogonal to one another such that any collective movement of the structure can be expressed by a linear combination of its normal modes.

Mathematically, the normal modes for a given bi-connected network are derived from the potential energy function associated with the *N*-mechanical convex "springs" in the network according to Hooke's Law. The potential energy of the network can be expressed as a power series in the displacement Cartesian coordinates (x_i, y_i, z_i)[14]:

$$\begin{aligned} 2U &= 2U_0 \\ &+ \underbrace{2\sum_{i=1}^{N}\left[\left(\frac{dU}{dx_i}\right)_0 x_i + \left(\frac{dU}{dy_i}\right)_0 y_i + \left(\frac{dU}{dz_i}\right)_0 z_i\right]}_{first-ordervariations} \\ &+ \underbrace{\sum_{i,j=1}^{N}\left[\left(\frac{d^2U}{dx_i dy_j}\right)_0 x_i y_j + \left(\frac{d^2U}{dx_i dz_j}\right)_0 x_i z_j + \left(\frac{d^2U}{dy_i dz_j}\right)_0 y_i z_j\right]}_{second-ordervariations} \\ &+ higherterms \end{aligned} \tag{11}$$

The first two terms can be dropped since the NMA will be performed around the minimum energy point; the higher order terms can also be neglected for sufficiently small amplitudes of vibration. Additionally, all non-connected pair-wise elements are set to zero. The potential energy of the convex mode [7] can be expanded for its higher-order variation energies,

$$U = \underbrace{ke^{\alpha L_{ij}}L_{ij} + 2ke^{\alpha L_{ij}} + \alpha L_{ij}ke^{\alpha L_{ij}}}_{=0\ @t_{reconfigure}} + ke^{\alpha L_{ij}}L_{ij}\left[\alpha^2 L_{ij}^2 + 4\alpha L_{ij} + 2\right] \quad (12)$$

where α is the obscuration, L is the distance between source i and destination j, and k is a technology constant. The output of the topology control process is an optimal minimum-energy topology and therefore, the first two terms can be neglected. In matrix notation, the final result is a 3Nx3N matrix (known as the Hessian),

$$H = \begin{bmatrix} h_{11} & h_{12} & h_{13} & \cdots & h_{1,N} \\ h_{21} & h_{22} & h_{23} & \cdots & h_{2,N} \\ \cdots & \cdots & \cdots & \cdots & \cdots \\ h_{N,1} & h_{N,2} & h_{N,3} & \cdots & h_{N,N} \end{bmatrix}$$

$$where h_{ij} = h_{ji} = \begin{bmatrix} \frac{d^2U}{dx_i dx_j} & \frac{d^2U}{dx_i dy_j} & \frac{d^2U}{dx_i dz_j} \\ \frac{d^2U}{dy_i dx_j} & \frac{d^2U}{dy_i dy_j} & \frac{d^2U}{dy_i dz_j} \\ \frac{d^2U}{dz_i dx_j} & \frac{d^2U}{dz_i dy_j} & \frac{d^2U}{dz_i dz_j} \end{bmatrix} \quad (13)$$

Note the dimensionality of the Hessian results from the N nodes in the backbone expressed in three-dimensional Cartesian coordinates. The normal modes and

associated natural frequencies are derived from the eigenvectors and eigenvalues of the Hessian, respectively, as expressed in eq. (14). For non-linear spring networks, there are 3*N*-6 non-zero eigenvalues – the six missing roots correspond to complete rotation and translation of the network as a whole in the coordinate space. The 3*N*-6 normal modes now form a basis for all movement of the network in three dimensions.

$$\boldsymbol{H} \cdot \boldsymbol{\xi^i} = \lambda_i \boldsymbol{\xi^i} \forall i = 1 \ldots (3N - 6) \tag{14}$$

2.4.4 Tracking the Eigenvalues of the Hessian Matrix

As an example, the normal modes for a 6-node DWB network configuration are offered in fig. 2-10 for two-dimensional coordinates (x, y). In two-dimensional Cartesian coordinates, there are 2*N*-3 normal modes – the two translational modes (x,y) have been removed from fig. 2-10; however, the rotational mode (x/y) remains since it is harder to identify. The arrows attached to each normal mode are the normalized displacement vectors.

The employment of more techniques from computational chemistry began first by looking into tracking the natural frequencies of the backbone Hessian matrix. The goal was to relate the depression of eigenvalues with instabilities in the network – similar to "normal mode softening" [56]. An example of this method is shown in fig. 2-11 as a function of lateral stretching of the 6-node hexagon configuration. In this case (as expected), the eigenvalues spike as the network is stretched laterally which is expected utilizing the convex exponential model. In addition, the contribution of the first few normal modes (ranked in descending order with respect to natural frequencies), was substantial compared to the remaining modes. This is also expected

and aligns with other research, which often illustrates molecular conformational changes using only a handful (<10) normal modes [57]. Yet, in the end, though, no correlation was fruitful between the complex motions of the backbone and the normal mode frequencies – even though previous efforts indicated promising conclusions [58]. This technical breakdown was contributed to the mobility of base-stations dependence upon end-user demand (coverage and connectivity).

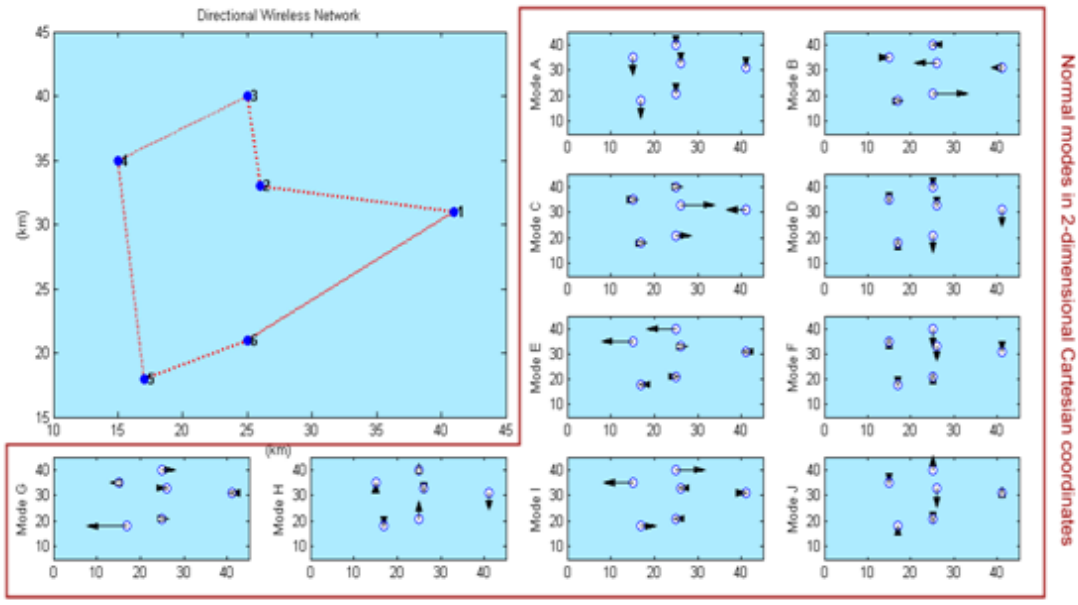

Figure 2-10. The normal modes for a bi-connected backbone are dependent on the topology. In 2D Cartesian coordinates, the system has 12 normal modes including rotational and translational modes. Identifying the two translational modes is trivial and therefore, these modes have been removed. Identification of the rotational mode is more complex. These normal modes form a basis for any movements of the system. The arrows attached to each mode reflect the normalize displacement vector.

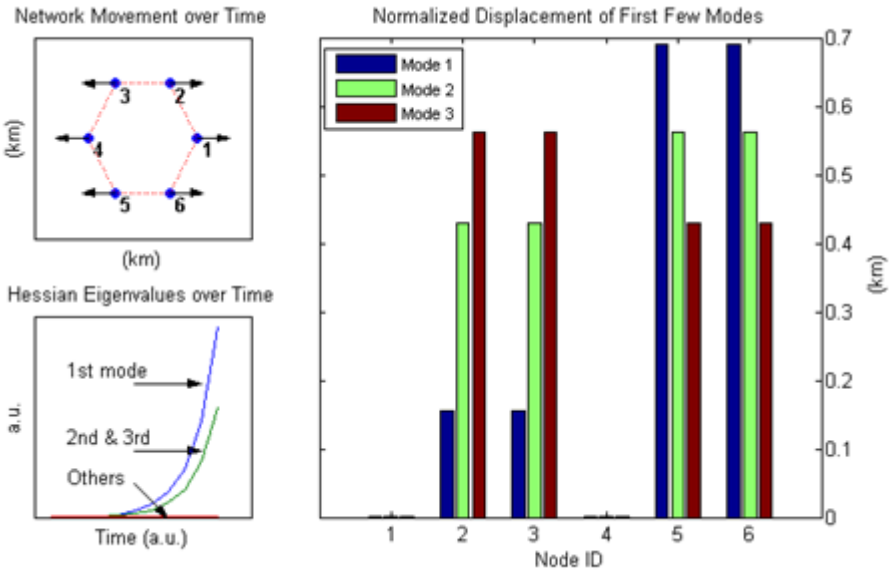

Figure 2-11. Normal mode tracking provides insight into nodal dynamics. (Top left) The network is stretched laterally by separating the farthest right nodes and the farthest left nodes. (Bottom left) The first three mode eigenvalues rapidly increase in value as a function of laterally stretching the network. The blue line is the largest eigenvalue and the green represents the degrenerate second and three values. The remaining eigenvalues are illustrated by the red line near zero. (Right) The first three modes, which are in the same lateral direction of the network movement are the dominant normal modes with the largest normalized magnitude of displacement.

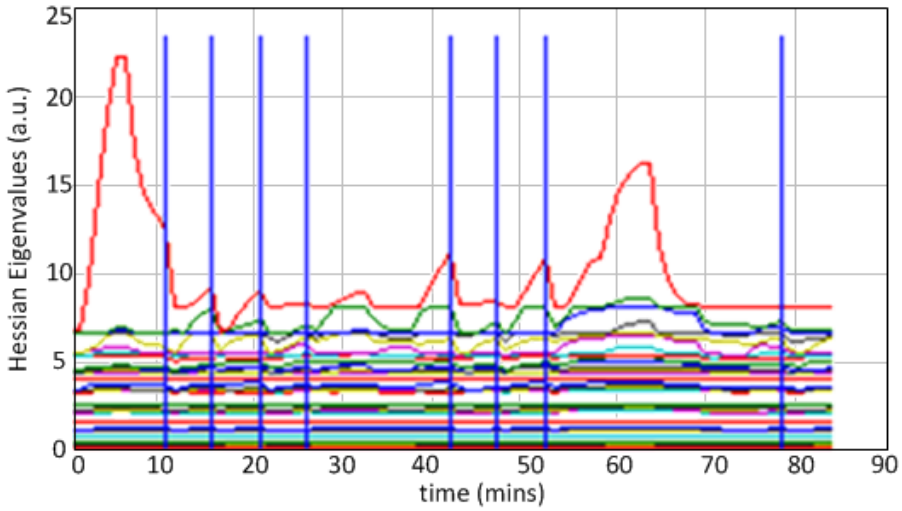

Figure 2-12. Tracking the Hessian eigenvalues revealed a spike was not always present as previously thought. The blue vertical lines represent when a network reconfiguration occurs. Over an 80+ minute simulation, 8 reconfigurations occurred. This provided first insights that the eigenvalues may not tell the whole story towards network reconfigurations.

Further difficulties in tracking the eigenvalues of the Hessian include reconfigurations which occurred with and without aforementioned "spikes" as shown in fig. 2-12. As a function of time, the network reconfigurations are marked on the graph with vertical blue lines. The correlation between the blues lines and the spikes in the eigenvalues – specifically the largest eigenvalues (red) – did not match in all cases. A spike is seen immediately at the start of the simulation (time < 5mins) and again at time ≈ 64mins; yet no reconfiguration of the network was performed. Additional reconfigurations at time = (11, 14, 27) were seen without significant changes in the eigenvalues. For this reason, a second investigation was performed with respect to the eigenvectors. Specifically, the amplitude and the behavior associated with stable and flexible nodes were explored.

2.4.5 Tracking the Eigenvectors of the Hessian Matrix

Progress has been made in the tracking of amplitude changes in the normal modes. The amplitude for each displacement vector is illustrated in fig. 2-10 in the form of arrow length. A longer arrow signifies greater displacement in the respective direction. Tracking the "flexibility" of each node has proven successful to detect instabilities in the network – instead of tracking the changes in natural frequencies. Similar success has been shown in the dynamics of bond breaking in molecules [53, 59]. The "flexibility" of a node is defined by the magnitude displacement across all modes j (j = 1…3N-6), for each base-station i,

$$\frac{d\xi_i}{dt} = \xi_{i_0} - \sqrt{\sum_{j=1}^{J}\left(\Delta x_{ij}^2 + \Delta y_{ij}^2 + \Delta z_{ij}^2\right)}\ foreach i = 1 \ldots N$$

$$where \quad \boldsymbol{\xi} = \begin{bmatrix} \Delta x_{1,1} & \Delta y_{1,1} & \Delta z_{1,1} & \ldots & \ldots & \Delta x_{N,1} & \Delta y_{N,1} & \Delta z_{N,1} \\ \Delta x_{1,2} & \Delta y_{1,2} & \Delta z_{1,2} & \ldots & \ldots & \Delta x_{N,2} & \Delta y_{N,2} & \Delta z_{N,2} \\ \vdots & \vdots & \vdots & \ldots & \ldots & \vdots & \vdots & \vdots \\ \Delta x_{1,J} & \Delta y_{1,J} & \Delta z_{1,J} & \ldots & \ldots & \Delta x_{N,J} & \Delta y_{N,J} & \Delta z_{N,J} \end{bmatrix}^T \quad (15)$$

where ξ_{i0} is established after a topology reconfiguration. An example is illustrated in fig. 2-13 where the network begins in its initial hexagon configuration at time equal to zero in fig. 2-13(a). Obscuration in the form of clouds has been added to this scenario to illustrate the simultaneous effects of distance and obscuration on the required energy of a link. Figure2-13(b) and fig. 2-13(c) illustrate the morphing network backbone configuration over time. Figure2-13(d) corresponds to the change in "flexibility" of each node. A positive slope in flexibility indicates a node having an increase in mobility; whereas a negative slope indicates a node becoming more rigid. The increase in flexibility of two connected nodes makes the links shared between them susceptible to failure. For example, notice the link between nodes 2 and 3 is dropped during the transition from topology state **A'** and **B**. This is consistent with the increased flexibility seen at nodes 2 and 3.

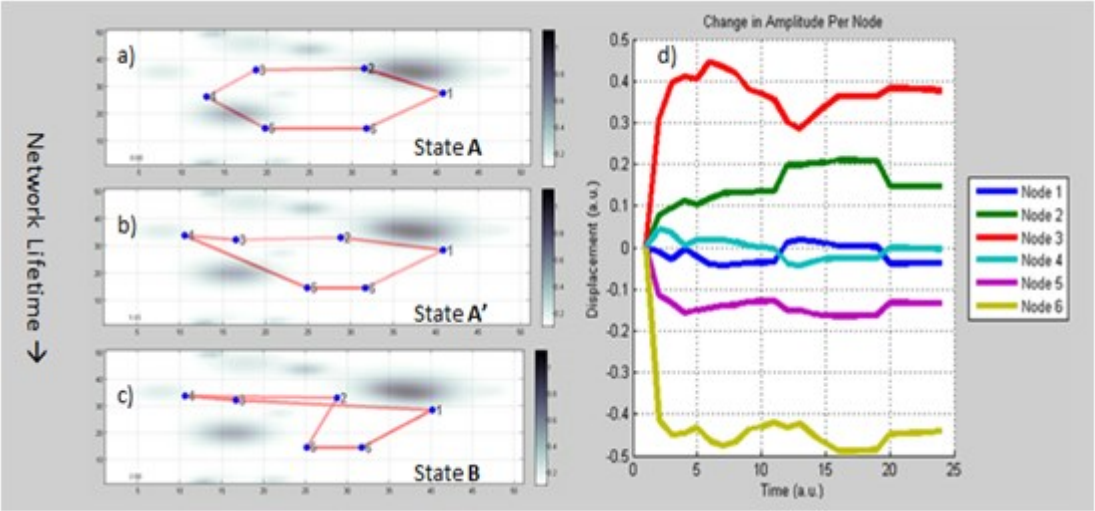

Figure 2-13. The change in node flexibility is a key indicator towards the detection of unstable links in the network. The link shared between two nodes possessing a positive slope in their flexibility provides a trend in a negative way for the network. a) Initial configuration of backbone network with obscurations depicted with grey areas from low to high levels. This configuration is state A. b) The network morphs as a function of servicing the end-user's demand. This configuration is state A'. c) The network after topology reconfiguration. This configuration is state B.

Tracking the slopes of the amplitudes of the eigenvectors should provide evidence for identifying instabilities in the network prior to a reconfiguration. In other words, understanding inherent flexibilities at each node is critical in determining instabilities in the network. For example, a node that possesses a high degree of flexibility (in magnitude) is more likely to be the catalyst for reconfiguration; whereas a rigid node will maintain its connections due to less mobility. From this observation, three methodologies will be tested using the same simulations and data points.

1. Most Flexible Node Theory (MFNT) – This theory hypothesizes a node which possess the most inherent flexibility (largest eigenvector amplitude) will become the catalyst for a reconfiguration decision.

2. Node with Increasing Flexibility Theory (NIFT) – Similar to the MFNT approach, this theory hypothesizes that a node whose flexibility is most rapidly increasing will be the catalyst for the network configuration change.
3. Link Tracking Theory (LTT) – Instead of tracking the individual nodes, a link shared by two flexible nodes is most vulnerable and is hypothesized to be dropped during a reconfiguration.

Of these three theories, the MFNT is the most easily satisfied and therefore it will be as the most rigorous methodology. Of course, any approach is valid since this research is novel and the only existing prediction methodology for comparison is a purely random guess.

2.5 Results& Discussion

To investigate the reliability of NMA eigenvector tracking methodology, test-bench software was written in MATLAB. The use of such software allowed scalability and reliability of the methodologies to be tested simultaneously. For instance, the number of end-users nodes scales with the number of backbone nodes to ensure each network under test is of moderate and applicable size. The number of backbone UASs will scale from $N = 6$ to 15, while the number of end-users, m, scales $m = 20 * N$. Each scenario will run for 30 minutes of simulation time with constant obscuration and random terrain in the environment generated at the start of the scenario.

A comparative analysis of the three methodologies offered in section 2.3.5 is shown in fig. 2-14, fig. 2-15, and fig. 2-16 as a function of the number of backbone UASs. The results are averaged over 400 simulations, each lasting 30 minutes for a total of 200 hours of network time. First, notice the number of reconfigurations increases with respect to the number of backbone UASs in fig. 2-14. This is expected since the size of the environment (50km x 50km) is constant and optimal link assignment will adjust more frequently since more connections are available to select. This insight will lead to additional rationales with respect to the prediction methodologies under test. For instance, since the number of reconfigurations with 15 UASs is on average close to 10 per 30 minute simulation (or one every 3 minutes), any prediction strategy is upper-bound at T_{life} = 3 minutes (the time between two reconfigurations) as hypothesized at the onset of this chapter and the accuracy should be fairly high to gain advantage in resource allocation and re-routing of traffic; on the

other hand, when the time between reconfigurations is greater (as in a network of only 6 UASs), the prediction time can be longer.

The accuracy of the three methodologies under test (LTT, NIFT, MFNT) has been measured (on average) to be 9.06%±6.36%, 54.92%±5.18%, and 65.12%±6.07%, respectively, across UAS backbone size. The MFNT provided the most accurate approach since its constraints were most easily satisfied tracking only the node possessing the highest eigenvector amplitude. The amount of time available is measured as the time difference between the node being introduced onto the most vulnerable node listing and the time of reconfiguration as dictated by the topology control algorithm. Once again, the MFNT proved to be the best approach providing 95.48±19.35 seconds ahead of the topology control algorithm. The other approaches yielded LTT = 67.87±36.31 and NIFT = 88.39±28.23 seconds. Once again, these values are upper-bound by the amount of time a network topology is active, T_{life}.

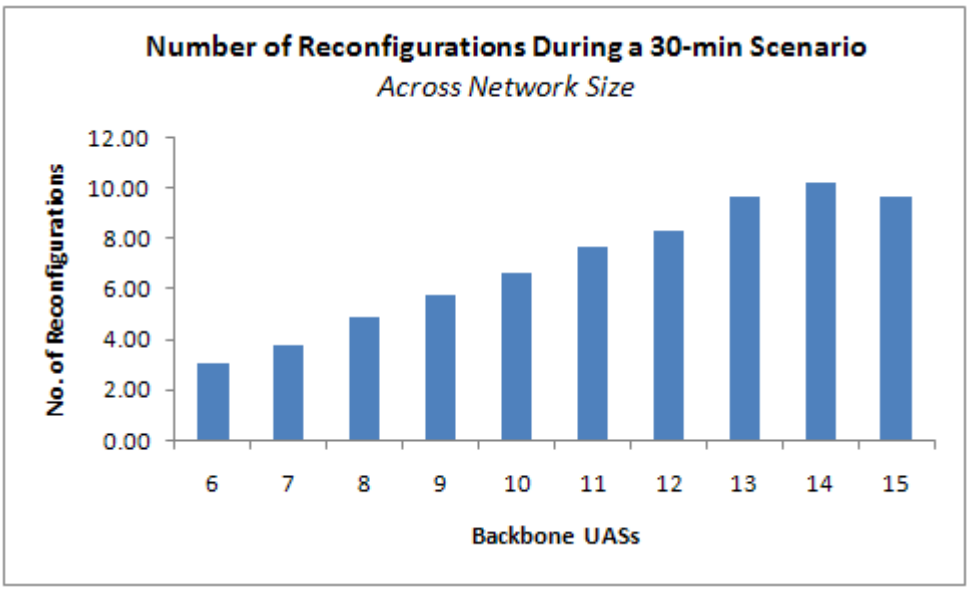

Figure 2-14. The number of reconfigurations during a 30-min scenario is a function of the number of backbone nodes. This is a direct result of the optimization algorithms employed in the topology control process wherein the increase in the plurality of backbone nodes provides additional opportunities to reconfigure toward achieving optimal aggregate network transmission power.

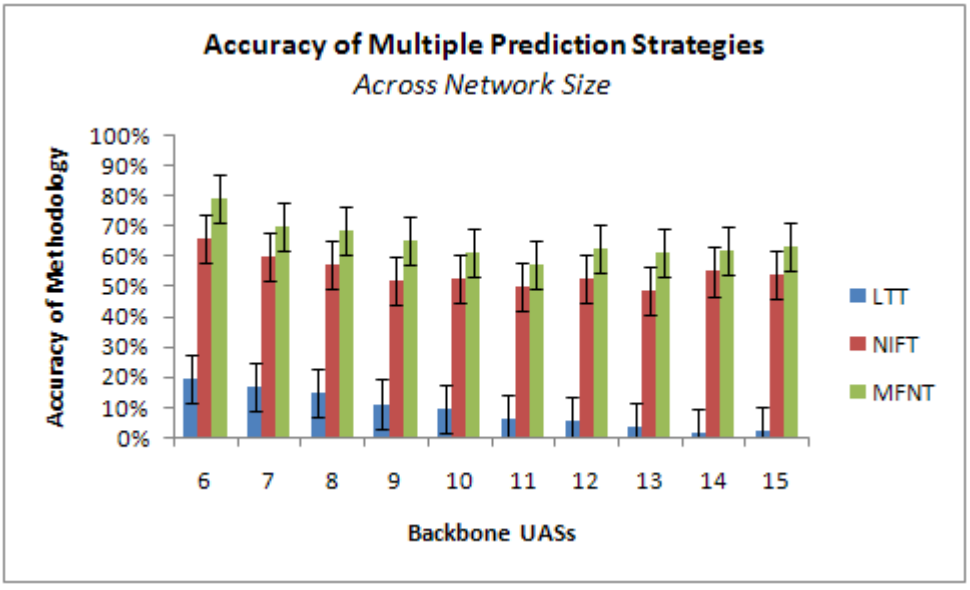

Figure 2-15. The three methodologies under test perform adequately as the network scales. Tracking the most flexible node yields over 65% accuracy in the prediction of a network reconfiguration.

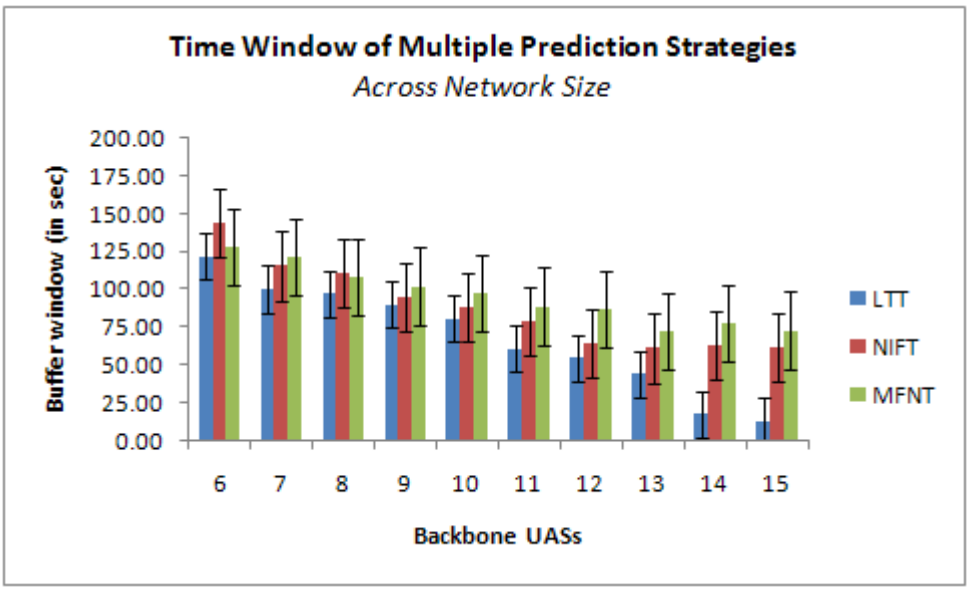

Figure 2-16. The time difference between the prediction warning and the actual network reconfiguration – as an output of the topology control algorithm – is fairly consistent as the network scales in size. The upper bound of this time is defined by the time for which a topology is active. In other words, if the number of reconfigurations increases with the size of the network, the amount of time to predict decreases since the topologies switch more frequent.

In order to verify the effectiveness of the PES approach, five 40-minute simulations were run for a variety of threshold values[12]. The network evolved as necessary to provide end-to-end connectivity and coverage to the end-users. However, focus was on the connectivity threshold in order to determine how well the methodology could predict a topology change. The potential energy surfaces were constructed after each topology reconfiguration throughout the network's evolution and for each 40-minute simulation. Each simulation included eight mobile base stations acting as the backbone layer at an altitude of 2 kilometers with constant obscuration. One-hundred end users are distributed in a 50km x 50km plane and they

[12]As discussed at the onset of this chapter, a threshold variable is used to reduce the number of reconfigurations triggered.

move according to the RPGM model [43]. The previously developed force-driven model is used to make backbone nodes adjust their locations until convergence to the optimal backbone configuration [12].

A topology reconfiguration was observed when a backbone node transitioned between two energy minima on its respective contour map. This movement allowed the definition of $T_{predict}$ as the difference between a node exiting its previous energy well or region and the reconfiguration event. As shown in Table 2-2 the $T_{predict}$ varies from an average of 3.42 minutes when there is 10% reduction aggregate network energy to an average of 2.53 minutes when there is 20% reduction in aggregate network energy. This suggests the greater the threshold or energy reduction objective, the less time available for the buffer or prediction period. This negative correlation means that degradation point on the PES is closer to the reconfiguration point. This is expected since a higher cost reduction requirement (e.g.$\tau = 20\%$) demands an equivalently large evolution of the network. In addition, the PES and NMA methodologies are perturbational, and as such do not include large deviations from energy minima. As seen in the second column of Table 2-2, the average number of reconfigurations decreases as the energy reduction threshold increase. This is intuitively obvious since a smaller threshold will result in a greater of reconfigurations.

Table 2-2. The molecular-inspired approach shows a negative correlation in the average number of reconfigurations and buffer period with respect to aggregate topology cost reduction. This is due to the potential energy surface being a perturbation analysis of the network configuration. A larger threshold requires a larger change in the network and therefore, extends beyond a vibration dynamic; resulting in a reduced prediction period.

Aggregate Topology Cost Reduction (τ)	Average Number of Reconfigurations	Average Buffer Time prior to reconfiguration
10%	3.80	3.42 minutes
15%	3.20	2.75 minutes
20%	3.00	2.53 minutes

2.6 Summary

A novel molecular-inspired methodology is introduced in this chapter as a way to predict link degradation and the assessment of node movements within a DWB network. It was shown that the molecular-inspired framework is a valid approach to predict the reconfiguration triggers in the optimization of aggregate network energy. The strategy involves the use of electronic structure theories (isomers) such that the network entity is modeled as a giant molecule and the communication links are thought of as chemical bonds.

Two techniques from modern molecular science were employed to validate the rigor of the approach: normal mode analysis and potential energy surfaces. The NMA provided insight into the second-order dynamics of the network while the PES offered understanding of the interactions between non-connected elements as it pertains to network reconfiguration events. Each of these methodologies was validated using MATLAB simulations and yielded a prediction time, $T_{predict}$ on the order of minutes ahead of a reconfiguration trigger. This work can aide in the future developments of re-routing, additional buffering, or other proactive processes ahead of a reconfiguration – versus the reactive [67, 68] methodologies currently employed in networking science to mitigate degradations in DWB networks.

Chapter 3: Comprehensive Control Architecture for Reconfigurable Beam-Steered DWB Networks

3.1 Problem Statement

The control decisions associated with reconfigurable beam-steered directional wireless backbone (DWB) networks are more complex than their hard-wired counterparts. These challenges are primarily associated with two unique aspects of DWB networks: a rapidly, reconfigurable network topology and a mobile platform (i.e. base-station) operating in an ever-changing environment. For these reasons, the control architecture must incorporate traditional networking aspects such as routing, addressing, and quality-of-service metrics with that of platform specific constraints such as navigation/dynamics (e.g. turbulence, turning radius, banking), technology availability (e.g. radio channel assignments), and network topology reconfigurations. The work in this chapter of the dissertation focuses on the inclusion of all aspects necessary to facilitate end-to-end connectivity for a DWB network operating in realistic conditions. Modeling and simulation software will be used to validate the control architecture and arguments will be made to support the inclusion of each facet as it relates to on-going research efforts.

The proposed control scheme will offer insight into the following:

1. A refined integrated approach for the topology control process and existing routing and addressing protocols (e.g. OSPF and IPv6);
2. Mitigation techniques for network partitions and link degradations in real-time with moderate to severe traffic volumes;

3. An autonomous tactical network including hybrid routing schemes that balance environmental parameters with link feasibilities to maximize bandwidth and minimize latencies;
4. Incorporation and analysis of modern directional radios to assess the efficiency of the dedicated channel paradigm;
5. Inclusion of additional parameters for realistic modeling of platform navigation/dynamics to highlight the impact such parameters uniquely impose on DWB networks.

Collectively, this chapter seeks to outline the complete control architecture for DWB networks and argues for an exclusive addition to the traditional Internet protocol, specific to DWB networks. The control framework is outlined in section 3.2 with specifics on each facet of the architecture. The control framework is incorporated into modeling and simulation software to validate its design and principles using standard IPv6 addressing and OSPF routing protocols in section 3.3. Finally, results are provided in section 3.4 and a summary in section 3.5.

3.2 Control Architecture for DWB Networks

The control architecture for a DWB network should include all facets of the system from collecting data from individual nodes to quality-of-service metrics. A complete system-level view of the control processes necessary for DWB network implementation is shown in fig. 3-1. The interweaving of the processes is shown with directed arrows with each sub-system color-coded for clarity. Below is a detailed description of each control process.

1. **Omnidirectional Control Radio** - Information such as Global Positioning System (GPS) and Inertial Navigation System (INS) originating at each mobile node should be shared globally, ideally using a long-range low-bandwidth omnidirectional control radio, periodically over the lifetime of the network. This requirement assists in the maintenance of a potential neighbor database necessary for the network connectivity control processes. Additionally, this control radio is used to alert node additions/deletions into and from the network and to distribute reconfiguration information. Link state updates (LSUs) are also disseminated on the control radio. The potential neighbor database can be masked with terrain information (either measured or from existing databases) to eliminate known obscurations and hidden neighbors.
2. **Topology (Network Physical Connectivity) Control Processes -** Real-time monitoring of node connectivity, aggregate network performance (e.g. bit-error-rate, signal-to-noise ratio), and environmental changes such as an approaching storm act as inputs to the topology control algorithms developed to provide instructions for the redirection of mechanically beam-steered links to yield a more

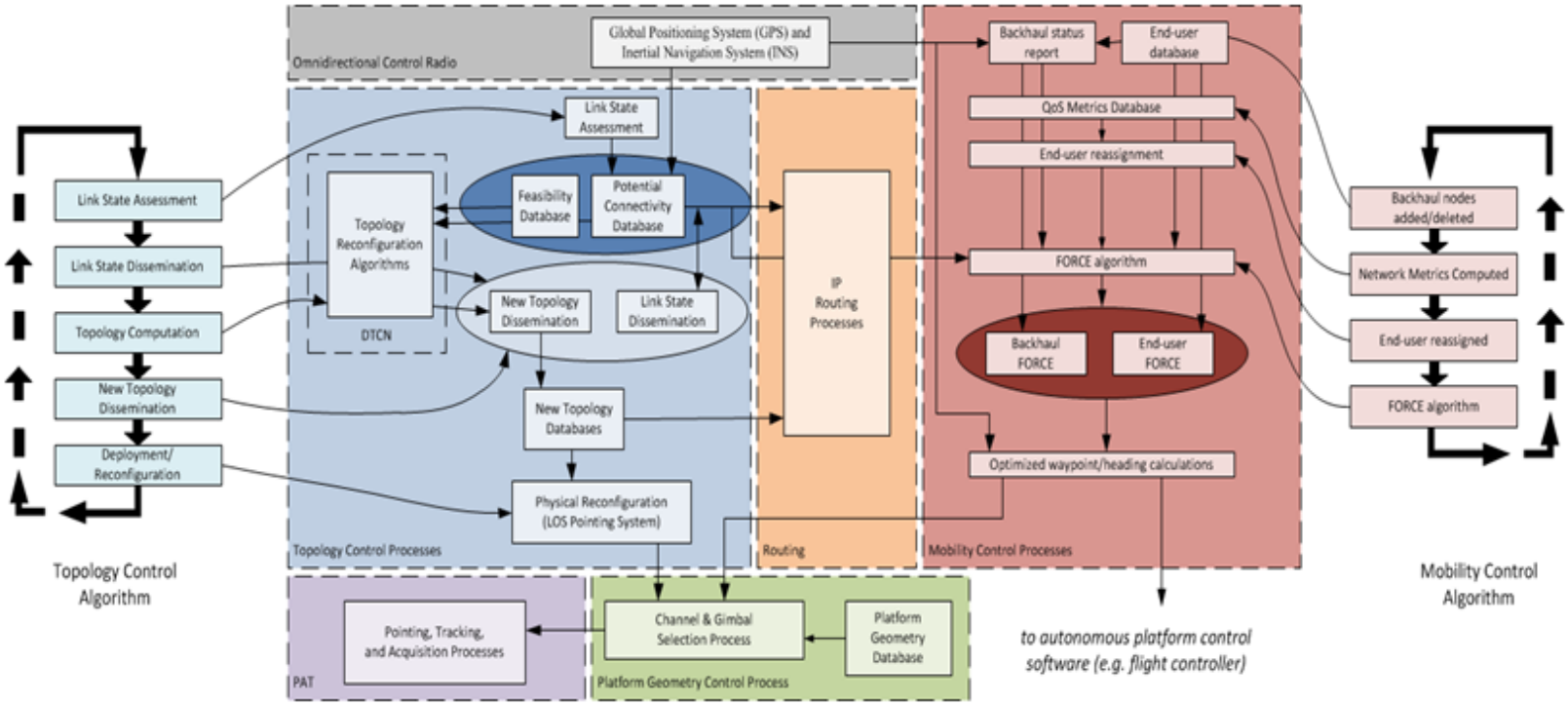

Figure 3-1. The considerations for platform geometry, PAT, and control radio can be integrated with the previously develop mobility management and topology control processes. Furthermore, all of these processes are seamlessly integrated with existing IP-protocols for routing such as IPv6 and OSPF.

stable and better performing network. This was the focus of the prediction work provided in the previous chapter.

3. **Platform Geometry Database** - The heterogeneous nature of mobile platforms means that establishing narrow beam point-to-point communication links between certain pair-wise nodes may be limited based off the mobility of the platform. For example, a mobile node may possess only one transmitter/receiver, whereas another may possess up to four units. Additional considerations for unique flight patterns, turning radii, and field endurance are all considered in this architecture.
4. **Link Adaptation**- The link capacity, ability to penetrate obscuration, and power efficiency are all parameters affected by the frequency of a radio. Additionally, the type of radio and channels available determine the connection availability and the capability of two nodes to communication. For example, a platform whose radio can only transmit on 71-75 GHz and receive on 76-81 GHz cannot communication with another platform that has the same channel specificity. This will be explored in more detail later in this section.
5. **Internet Protocol Routing Processes**–Existing protocols for addressing (IPv6), routing, and quality-of-service are incorporated within this control architecture to operate in a DWB network. Such interoperability provided generational scaling within DWB network specifically called out for in 4G LTE [26].
6. **Pointing, Acquisition, and Tracking** - The pointing, acquisition, and tracking (PAT) is essential to maintain connectivity between node pairs in the backbone of a DWB network. It has provides a feedback mechanism for signal-to-noise ratios immediately available the topology control algorithms as an input. The topology

control processes in turn reply with instructions to either maintain the current link or to mechanically redirect the antenna to establish a new connection. Extensive investigation has been done in the field by J. Rzasa [18].

7. **Mobility Control Processes** - The ability to provide feedback to the platform control software (e.g. UAV flight controller) with respect to end-user coverage may be included. This four-stage process utilizes an end-user database and quality-of-service metric database as inputs to the algorithm of choice. The output of this algorithm will provide optimized waypoint/heading calculations for the selected platform.

The validation of the control architecture requires a few development procedures specific to DWB networks and the technology employed. First, a backbone node is defined to include multiple directional antennas for backbone communication and multiple Wi-Fi or WiMax radios for cross-tier links with mobile end-users as shown in fig. 3-2. The on-board routers will assume to be using standard IPv6 and OPSF protocols. A discussion on the channel propagation models, SNR, and BER calculations for directional systems is in section 3.2.1. Developments with respect directionally-aware routing using hybrid links is discussed in section 3.2.2. Section 3.2.3 and section 3.2.4 are brief overviews of the topology and mobility control processes, respectively. Lastly, section 3.2.5 assesses the dedicated-channel radio paradigm within modern DWB network research.

Figure 3-2. The AAI-RQ7 Shadow unmanned autonomous system (UAS) is the preferred platform by DARPA for current DWB network research. A notional drawing of the UAS includes four directional antennas for data relay and backhaul support and two Wi-Fi or WiMax radios for cross-tier communication. This image is provided in [5].

3.2.1 Directional Systems: Channel Models, SNR, BER Calculations

Simulation of directional wireless communication systems requires physically-accurate propagation models for modern technologies including free-space optical (FSO) and directional RF links. Often times this becomes one of the most difficult challenges facing software designers due to the complex nature and number of parameters that impact link performance. Typically, the channel model includes large-scale and small-scale variations. Large-scale propagation models predict the mean signal power for arriving at a receiver (RX) from a transmitter (TX), separated over long distances. Channel models for small-scale variations, on the other hand, include short-range effects such as wave fluctuation and multi-paths. In addition, the propagating channel model includes path loss, which is an inverse function with respect to RX-TX separation [27]. Identifying parameters in the path from TX to RX is an extensive process and may include buildings in an urban environment, interferences from other TXs, and temperature of the environment.

Typically, small-scale variations are due to multipath effects at the receiver, causing a superposition at the received signal of two or more data streams that have travelled different paths. Commonly found in terrestrial wireless communications, this effect has been broadly investigated and requires rigorous modeling of the environment to achieve reliable received power estimates [37]. However, since the directional systems investigated within this dissertation assume improved line-of-sight capabilities through narrow-beams, there are no multipath effects within the proposed propagation model [24, 62].

Shadow fading effects are an example of large-scale variations and are typically due to large obstructions between TX-RX. In directional optical systems, for example, the effects of shadowing, as seen by a signal propagating through fog and clouds can have a drastic impact on link performance. Commonly, this is caused by the optical beam breaking up into distinct paths of fluctuating illumination, an increase in the beam width over expected diffraction limit, and a wandering of the centroid of the beam [28-34]. Numerous obscuration models have been investigated by previous MOG members [17] including real-time weather databases from the National Climate Data Center (NCDC) at the National Oceanic and Atmospheric Administration (NOAA) [35]. Directional RF systems suffer a similar decrease in performance when penetrating rain and snow [33]. The end result is an exponential model with respect to distance and an obscuration coefficient and is illustrated in fig. 3-3.

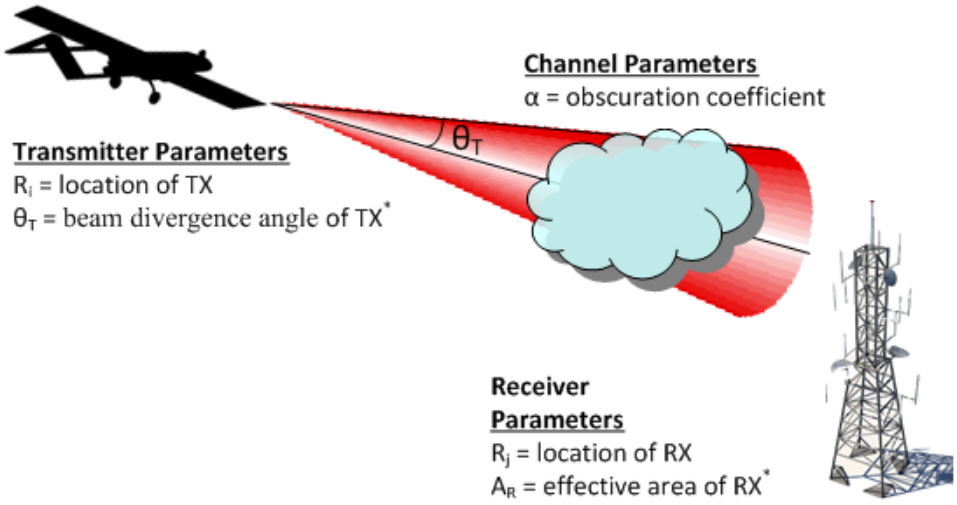

Figure 3-3. The received power of a directional wireless link is a function of the transmitter, receiver, and channel parameters. The simplest model includes node separation distance (in kilometers), transmitter beam divergence angle (in milli-radians), effective area of receiver aperture (in meters), and environmental path loss (in dB/km). An asterisk (*) denotes a technology specific parameter.

The loss of signal power across the separation between TX-RX is known as the path loss. The path loss for terrestrial wireless systems is again a difficult modeling problem as it is very sensitive to signal absorption. Materials that will absorb a wireless signal include everything from the material used to construct a building to the number of humans within the path from TX-RX. Therefore, great care is taken into consideration when developing models for wireless systems [37]. However, DWB networks benefit from having little to no materials in the sky between TX-RX and therefore, the modeling is restricted to distance, directivity of the TX antenna, and effective RX area as illustrated in fig. 3-3. The last two variables are technology specific and will change depending on the system in-use, FSO or RF.

Free-Space Optical Systems

Combining all the components together, the propagation channel for an FSO system can be modeled:

$$\tau = \underbrace{e^{-\alpha L}}_{obs.} \quad \underbrace{\frac{2A_R}{\pi\theta_T^2 L^2}}_{\substack{free-space \\ path\ loss}} \tag{16}$$

where α is the obscuration coefficient (in dB/km), L is the separation distance between TX-RX (in km), Θ_T is the beam divergence angle of the transmitter (in meters), A_R is the effective area of the receiver (in meters), and commonly, n=2. From this, the received power can be established,

$$P_R = P_T \underbrace{e^{-\alpha L} \quad \overbrace{\frac{2A_R}{\pi\theta_T^2 L^2}}^{\substack{technology \\ dependant}}}_{\tau} \tag{17}$$

where P_R and P_T are the received and transmit powers, respectively. In terms of communication performance, the received power determines the signal-to-noise ratio (SNR) and bit-error-rates (BER). SNR and BER are inversely proportional to each other. That is, as the link fluctuates due to obscuration and separation, SNR will decrease and more errors will be seen (BER goes up).

The performance of a link is a direct result of its signal-to-noise ratio (SNR). Typically, sources of noise within an electronic system include thermal and dark current shot noise [36]. The thermal noise is due to the random motions of electrons (e.g. thermal velocities) and is a factor of temperature and the components (e.g. resistors) used in the detection hardware. The dark current shot noise is associated with the randomness of the discrete quantization of the source signal and is proportional to the amount of current passing through the detection hardware and the bandwidth of the system. The total noise can be approximated,

$$\sigma_N = \underbrace{\frac{4kT\Delta f}{R}}_{thermal} + \underbrace{2qI_D\Delta f}_{shot} \tag{18}$$

where k is the Boltzmann constant, T is the effective component temperature measured in Kelvin (may be higher than ambient temperature), R is the impedance of the detection hardware measured in ohms (typically around 50Ω), q is the charge of an electron in Coulombs, I_D is the detection current, and Δf is the bandwidth of the system. Approximations can be made though, to reduce the complexity of the noise calculation. For example, in incoherent FSO systems, the thermal noise is much greater than the shot noise since,

$$\frac{4kT}{R} \gg 2qI_D \tag{19}$$

and subsequently, shot noise can be neglected.

The SNR can be found by combining all sources of noise with the received power,

$$\langle SNR_0 \rangle = \frac{\langle i_S \rangle^2}{\sigma_N} = \frac{\left(\Re \langle P_R \rangle \right)^2}{\frac{4kT\Delta f}{R}} \tag{20}$$

where i_S is the output signal current from the detection hardware and $\Re$is the responsivity of the receiver. Using the OOK-modulation scheme, as is typical for FSO systems, the bit-error-rate (BER) is defined with a threshold level of $i_{TH} = i_S/2$ and is computed using the complementary error function,

$$BER = \frac{1}{2} erfc\left(\frac{1}{2\sqrt{2}} \sqrt{SNR_0} \right). \tag{21}$$

Note to achieve BERs similar to hard-wired systems (e.g. 10^{-6}) a SNR = 19.5 dB is required for an FSO system.

Directional RF Systems

A more complex analysis for the received power of directional RF systems was recently offered by Dr. John Rzasa [18] as a function of transmitted intensity I_P, channel attenuation α, receiver aperture diameter D_R, beam divergence Θ, and angular misalignment angles β,

$$t_{path} = 2\underbrace{\left(\frac{A_R}{\lambda L}\right)^2}_{I_P}\int_0^{D_R/2} r\,\frac{J_1\left(\frac{\pi D_R}{\lambda}\sin\theta_T+\beta_T\right)^2}{\left(\frac{\pi D_R}{\lambda}\sin\theta_T+\beta_T\right)^2}dr \tag{22}$$

as shown in fig. 3-4. J_1 is the first-order Bessel function [44]. The transmit frequency is used to establish λ,

$$\lambda = \frac{c}{f} \tag{23}$$

with typical frequencies in the f= (75-85) GHz range and c being the speed of light. Since the bandwidth of directional RF systems is higher than FSO, both sources of noise are included in the SNR calculation,

$$\langle SNR_0\rangle = \frac{\langle i_S\rangle^2}{\sigma_N} = \frac{\left(\Re\,\langle P_R\rangle\right)^2}{10\left(2qI_D\Delta f+\frac{4kT\Delta f}{R}\right)} \tag{24}$$

Using the BPSK modulation scheme, the BER for the directional RF systems can be found [78]:

$$BER = \frac{1}{2}erfc\left(\sqrt{SNR_0}\right). \tag{25}$$

Directional RF system can tolerate more noise in the channel and achieve the golden BER = 10^{-6} at around SNR = 10.8 dB. However, this is at a much lower data rate than is available with FSO links.

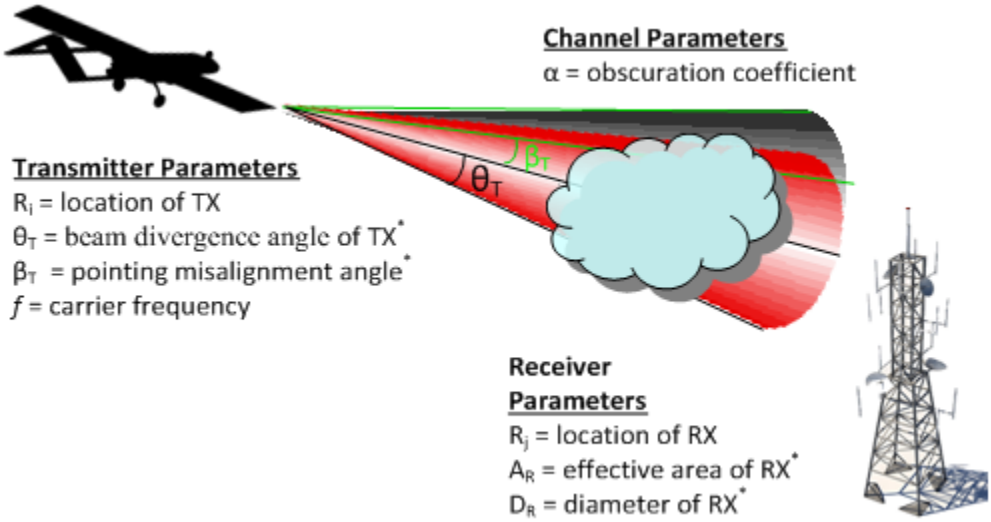

Figure 3-4. Using the most current research by J. Rzasa [18], the directional RF system can be more accurately modeled by introducing pointing misalignments in the PAT system.

3.2.2 Development of Directional Aware Routing Protocols

Directional aware routing protocols have been developed which incorporate the bandwidth and latency metrics for directional systems (see Appendix B for more information). These have been incorporated on top of the standard OSPF routing protocol. Open-Shortest-Path-First (OSPF) is a link-state routing protocol that computes the Bellman-Ford algorithm for shortest paths between all nodes in the network. The term 'open' is attached to the acronym to infer the protocol is an open-source routing protocol (versus proprietary). The standard OSPF process maintains two states that are critical for operation of directional networks – LINK_UP and LINK_DOWN. Normal operation of the OSPF protocol requires the status of a link to be checked on regular intervals (e.g. 30 seconds). However, in a directional wireless

networks, 30 seconds of downtime prior to the resolution of a down link is not practical and hence modifications were made to reduce this link status check. Most notably, the OSPF database is updated via the topology control process prior to a network reconfiguration. This ensures OSPF is properly alerted to the down link and can begin its re-routing computation immediately.

Further alterations to the OSPF database include modification of the cost metric. The cost metric in the OSPF algorithm represents the weighted-value of a link between two nodes and is usually a function of the link's bandwidth. The weight of an FSO link was set to be 1/10 the weight of an RF link. This ensured FSO links (whose bandwidth is approximately 10 x BW_{RF}) will be selected and a reduced latency is achieved.

3.2.3 Developing the Topology Control Process

The topology control algorithm is a 5-stage process that evaluates the aggregate performance of the network, computes the optimal network topology, and triggers a transition to a new topology should a reconfiguration become necessary.

1. **Link State Assessment** – Since the DWB network operates in a dynamic environment, link states are constantly monitored using metrics such as bit-error-rates and transmit power to establish a link budget.
2. **Link State Dissemination** – The link states are disseminated across the network to maintain current potential neighbor connectivity databases. LSA are also inputted into routing protocols to provide real-time routing information. This is part of the directionally aware routing protocol.
3. **Topology Computation** – A designated topology control node (DTCN) processes the LSA to determine if a network reconfiguration is necessary. This process is centralized to mitigate optimization collisions.
4. **Topology Dissemination** – New topology information is disseminated among the nodes in the network along with new routing tables since the new topology is known ahead of the reconfiguration.
5. **Physical Reconfiguration** – The radio channels are selected locally and the pointing, acquisition, and tracking (PAT) establishes the new topology.

An overview of the integration process into the modeling and simulation software is provided in fig. 3-5.

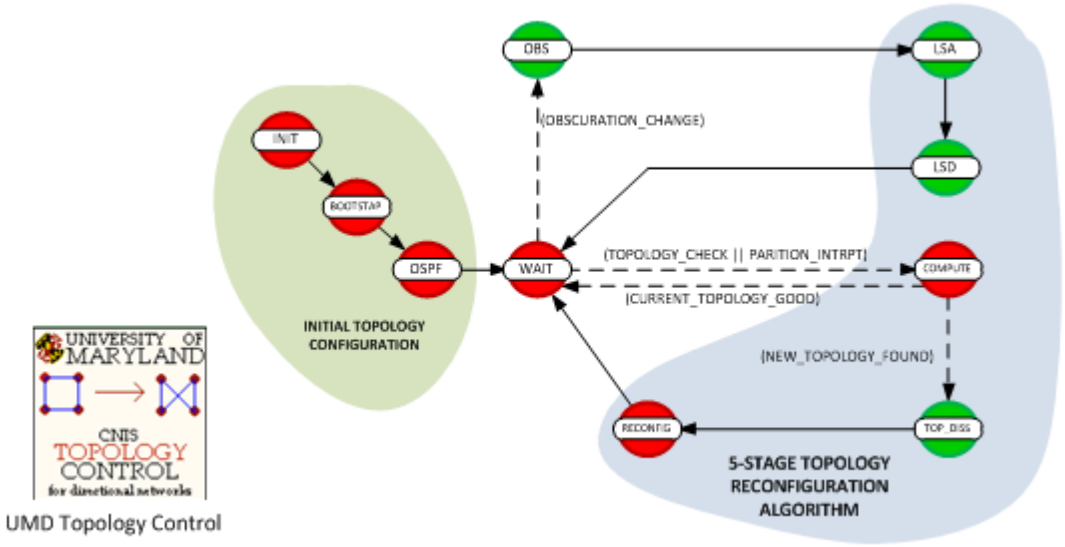

Figure 3-5. A custom process was written in OPNET for topology control using the previously investigated algorithms. The FSM includes three states which initialize the OPNET simulation kernel, two states to control simulation execution, and the 5-step topology control algorithm. This process is written in ANSI-C and uniquely integrates with IPv6 and OSPF for directional wireless backbone networks.

3.2.4 Incorporating Mobility Control Processes

The mobility control process is a four-stage procedure and is designed to integrate any mobility management algorithm throughout input files. The decision to generate a generic mobility algorithm platform on the backbone nodes is two-fold: 1) control of the UAS is not always available due to flight controller software and 2) the control architecture is a framework not tailored to one algorithm over another. The four-stages include announcement of backbone nodes, network metric computation, end-user reassignment, and mobility management algorithm execution. The FORCE [7] algorithm is inserted here since it is the preferred algorithm for this dissertation. An overview of the integration process into the modeling and simulation software is provided in fig. 3-6.

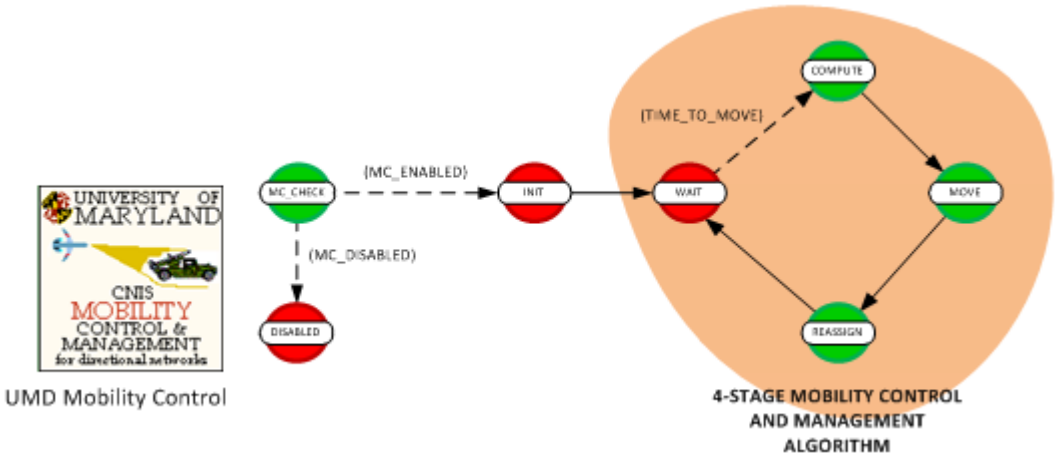

Figure 3-6. A custom process was written in OPNET for mobility management and permits importing of any algorithm. The FSM includes three states which initialize the OPNET simulation kernel, and four stages to execute the preferred scheme. This process is written in ANSI-C and attempts to reduce the complexity of trajectories assignments within OPNET.

3.2.5 Assessing Dedicated-Channel Radio Paradigm

Current DARPA sponsored research in DWB networks calls out the separation of receive/transmit channels in the 75-85GHz spectrum to permit simultaneous communication between backbone nodes with less inference. DARPA's "Mobile Hot" BAA [5], calls out two distinct radios/channels, as shown in fig. 3-7. The first radio (termed "radio A), transmits on a channel around 75GHz and receives on a channel centered at 85GHz. The second radio (termed "radio B") transmits on a channel centered at 85GHz and receives on 75GHz. This feature maintains that the two rear-facing pods may only communicate with the front-facing pods of another platform, and vice-versa.

Though simultaneous communication can be achieved in this manner, it complicates the topology control algorithms and may reduce the amount of time radios are being used (since turning, shadowing, will block certain pairings). As such, following an optimal topology has computed, the specific connections between two nodes must specify the radio channel for communication which may place limitations on available topologies. Therefore, topology configuration is now a two-step process with feedback, as shown in fig. 3-8. First, the optimal topology is computed based off distance and obscuration metrics within the environment collected during link state assessments. Next, a radio availability test is performed which includes the radio field of regard (e.g. 220°). If the available radios are able to satisfy the optimal topology, the radios are paired; otherwise, the topology computation receives this information and computes a new topology.

To reduce the amount of radio switching, a radio retention policy was developed. In other words, once a pairing is established (e.g. 1F-2R from fig. 3-9), the algorithm will maintain this pairing until either UAS is outside the assigned radio's field of regard. This is favorable to reduce frequency of change in radio pairings during a stable topology. As such, this policy is another first attempt to mitigate performance losses due to the overhead associated with local radio hand-offs (e.g. between radios on the same UAS). Expectedly, during a topology reconfiguration, radio assignments are dropped completely and optimized within current fields of regard.

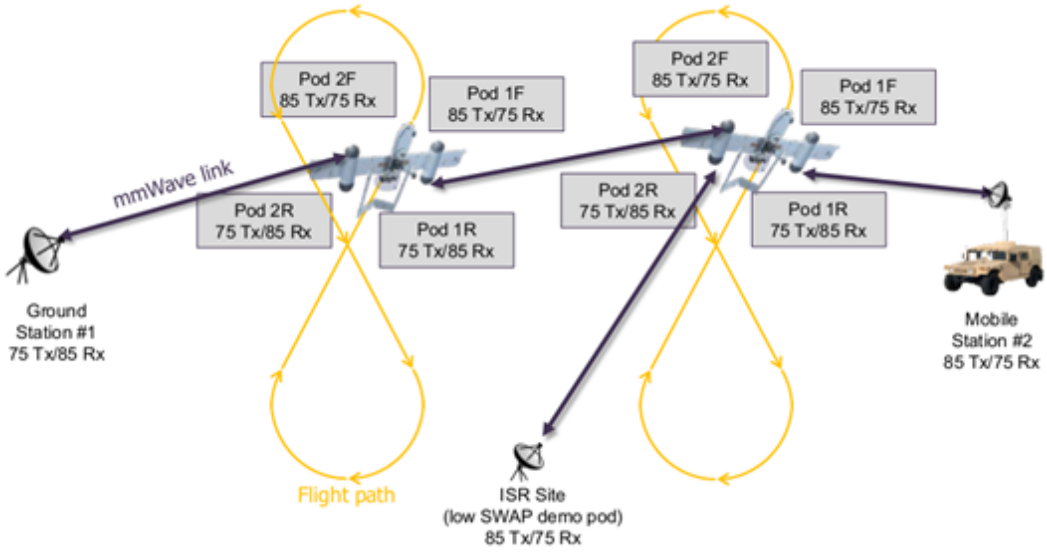

Figure 3-7. A notional network was provided in [5] and gave specific channel assignments for the radios and locations within each pod. This configuration leads to inefficiencies in the topology assignment since the radios are not frequency agile.

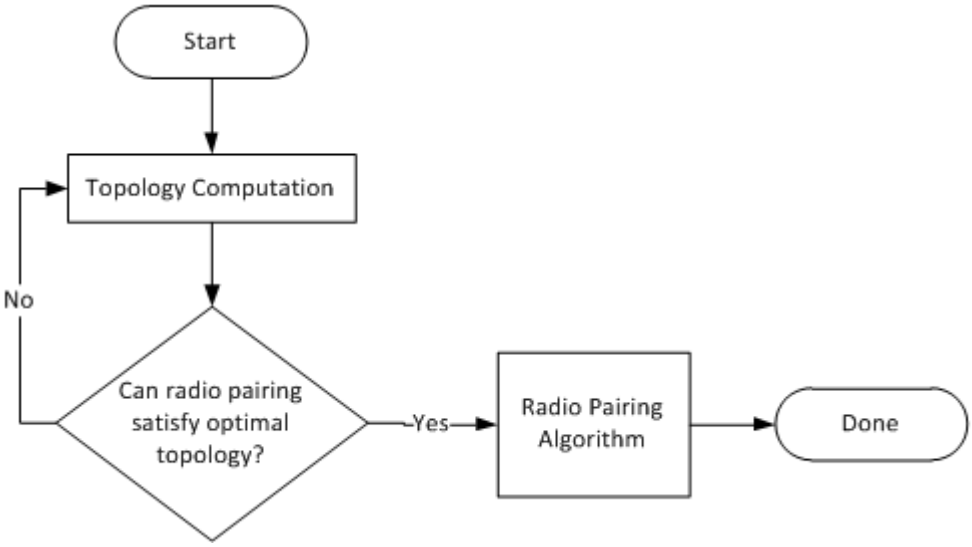

Figure 3-8. The radio assignment stage complicates the previously developed topology computation algorithm. The additional stage requires a mutual radio channel to be available before two nodes can be successfully connected. Therefore, the output of the topology control algorithm is followed by a feedback loop to ensure proper configuration. If a mutual channel is not available, the topology control algorithm executes again with this information.

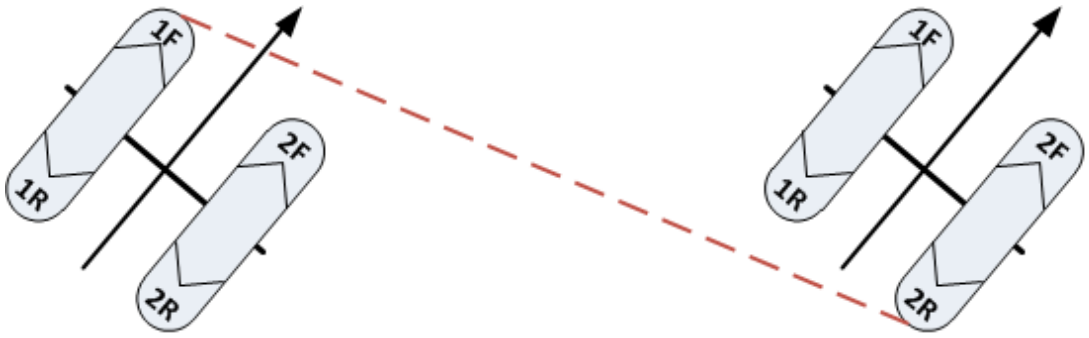

Figure 3-9. The radio assignment in MATLAB is a greedy-algorithm with respect to the radio fields-of-regard. This means the first radio which can satisfy the constraint is chosen without regard for other constraints (amount of coverage). Furthermore, the radio assignment is held until the receiver is outside the field-of-regard to reduce the frequency of radio switching within one UAS.

3.3 Validation of Proposed Control Architecture

The control architecture was validated experimentally using a MATLAB script to generate random scenarios. These scenarios were inputted into OPNET experiments for collection of network metrics. The MATLAB script was first utilized to develop and simulate twelve backbone nodes alongside 200 end-users in a region of random terrain. The end-users have full autonomy of the environment, have a velocity of 1 km/minute, and move according to the RPGM mobility model. Each end-user is assigned to the nearest backbone node. The backbone nodes have a velocity of 3 km/minute and their mobility is a combination of the reaction to the end-users' movement and the connectivity of the network.

The traffic within the network is generated using a normalized mesh-network algorithm. The algorithm first distinguishes half the end-users per backbone node as a 'transmitter' and the other half as 'receivers.' Next, the transmitting end-nodes are assigned to receivers in other subnets (i.e. attached to other backbones) in a round-robin fashion until all end-users are paired up. The amount of traffic one transmitter placed on the network (i.e. traffic demand) is randomly distributed. Each load is between 30 kbps and 80 kbps with packet sizes ranging between 1KB and 10KB[13]. An example traffic pattern for four backbone nodes is shown in fig. 3-10.

[13] The specific traffic demands and link data rates are scaled to accommodate existing procedures within OPNET.

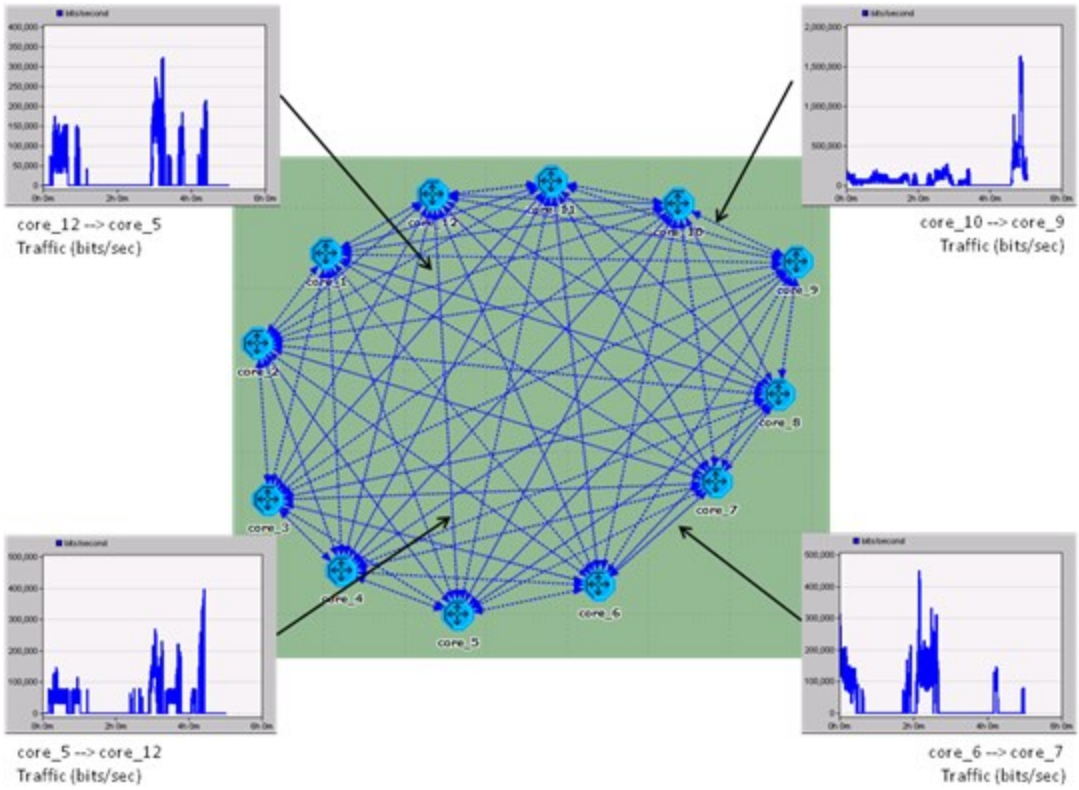

Figure 3-10. The traffic is abstracted to reduce simulation complexity and traffic demand profiles are used to introduce traffic loads in the network. These demands are shown as blue lines and are generated in MATLAB as a function of end-user mobility/priority.

The output of each MATLAB scenario includes text files with backbone positions, end-user positions, terrain profile, and traffic demands at regular intervals. These files are the input to OPNET which now offers a processes specific to mobile DWB networks.

Two experiments have been developed to validate the procedures in OPNET along with the effectiveness of our algorithms: 1) network degradation due to one link disruption event (LDE); and 2) network partition due to multiple LDEs. Within each experiment, the network is able to respond through adjustment of link parameters (e.g. frequency, data rate) and redirection of links (e.g. topology control). Furthermore, the

traffic has been design to highlight average and worst case performance of the network. An average case traffic load is normally distributed across the network and as such, the traffic flow over an individual link is not sustained in excess of the link bandwidth. The worst-case, on the other hand, is designed to constantly exceed the link bandwidth and is placed within the network across the link which will experience the LDE. This would represent the case where traffic is being shared among two high-priority users and a direct high-capacity link is established on their behalf.

The first response of the network in the experiments is referred to as the "baseline" and no adjustments in link parameters or topology is permitted; re-routing is the only solution available to increase performance. This is the case with no control architecture integration. The second response is referred to as "link adaptation" since the system is able to autonomous adjust link parameters when the LDE(s) occur(s). For example, this adaptation may include adjusting the frequency band used by an RF system (e.g. switching from 70 GHz to 80 GHz) to reduce interference or penetrate weather more efficiently. Lastly, the third response permits link adjustments and topology reconfigurations to mitigate performance loss from single and multiple LDEs. This provides the most robust tactics and maintains network performance during long-term LDEs. This response is referred to as "full topology control."

3.3.1 Network Degradation Due to One Link Disruption Event

In the first scenario, a link disruption event (i.e. link failure) occurs in the network. This failure occurs multiple times over a 3.5 hour period (for statistical collection) and the results are shown in table 3-1 (averaged together for reliability). Figure 3-11 focuses on one worst-case LDE as a sample to illustrate the difference between the three simulation setups (baseline, link adaptation, and full topology control) before and after the LDE as a function of latency. At first, all three networks are identical with traffic flowing between the source and destination nodes across a high-data rate link. At the time of the LDE (time = t_e), a the direct link between S-D is severed and the network responds accordingly. The baseline network is able to maintain traffic flow through re-routing, yet at a steep increase (11.3X) in latency since the traffic must be routed around the entire network (now 11-hops versus 1-hop). The network response with link adaptation experiences a similar phenomenon resulting in a 4.05X increase in latency. Though the traffic is still routing in a one-hop fashion, the drop in link data-rate negatively impacts the performance of the network. The best performer is the full topology control case which is able to respond to the LDE by forming a new network and routing traffic on a two-hop path from source to destination, resulting in a 2X increase in latency.

The average-case experienced similar outcomes with each case illustrated in Fig. 3-12. However, since the traffic flows were more evenly distributed, the latency increase was not as substantial as the worst-case. On the other hand, topology control was still the best performer and provided latencies 4.14X (12.01μs vs 49.8μs) better

than the baseline scenario and 1.83 X (12.01µs vs 22.08µs) better than the link adaptation.

Notably, the use of a recovery period, t_r, was used in fig. 3-11 and fig. 3-12 to designate a reasonable amount of time necessary to facilitate response by the topology control process and subsequent new link creation. This includes such processes as the mechanical swing time of gimbals, acquisition period to establish new links, and routing convergence times. Previous work has shown the PAT period to be on the order of single-digit seconds [21].

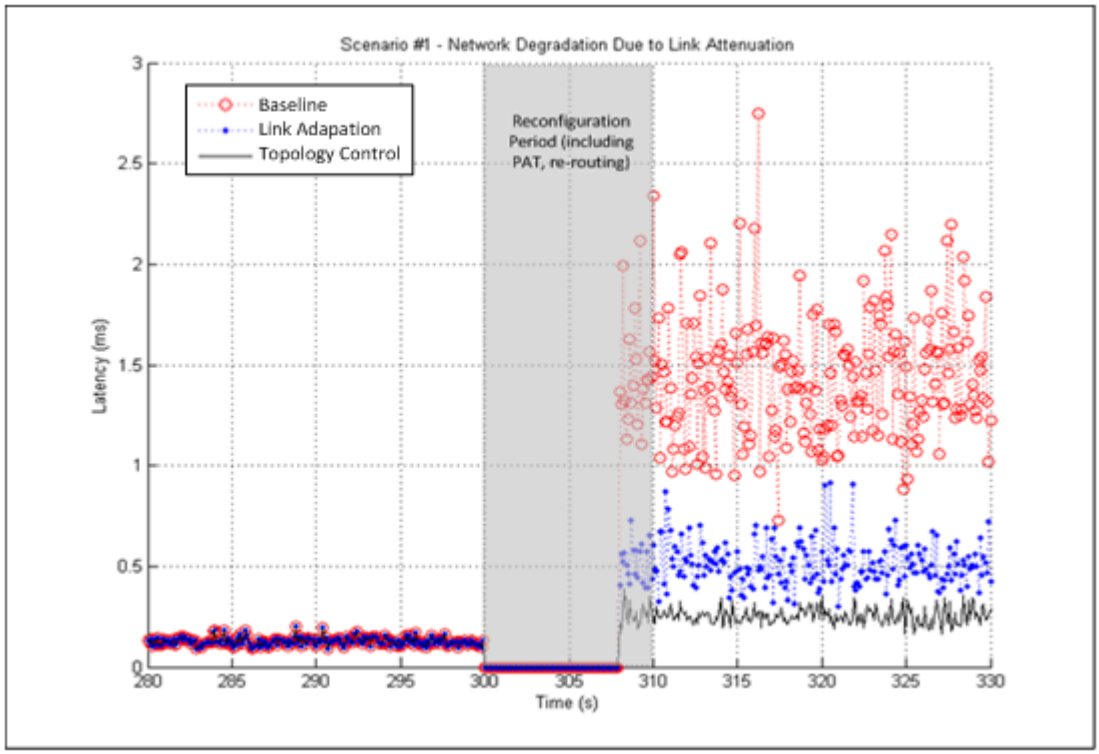

Figure 3-11. In the first scenario, one link is partially obscured and the network is able to respond in three ways: 1) re-route traffic along stable links, 2) adjust transmit frequency to increase link performance, or 3) redirect the point-to-point links to reconfigure the network topology. These schemes are referred to as baseline, link adaptation, and topology control, respectively. After the link becomes partially obscured, the topology control provides the minimum latency by offering a 2-hop route. This data highlights the worst-case traffic loss wherein the network traffic is isolated on the partially obscured link.

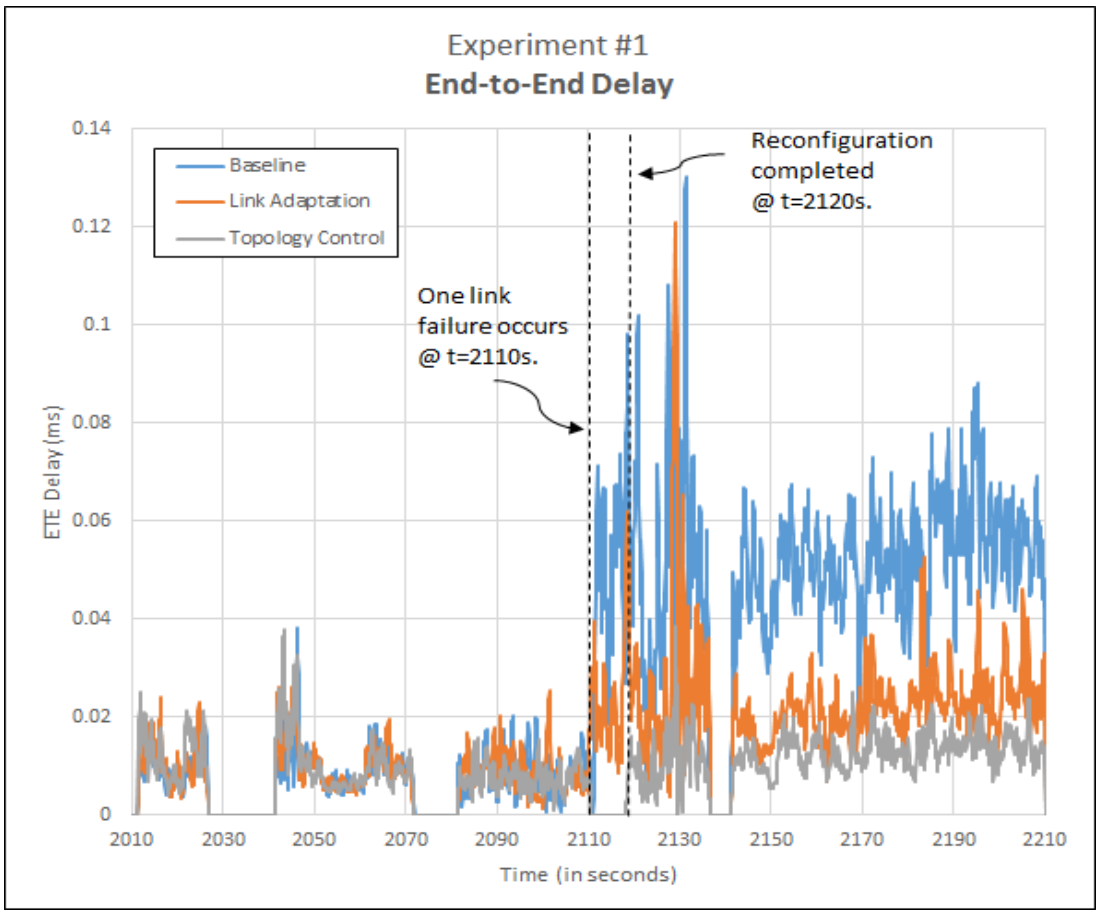

Figure 3-12. In the first scenario, one link is partially obscured and the network is able to respond in three ways: 1) re-route traffic along stable links, 2) adjust transmit frequency to increase link performance, or 3) redirect the point-to-point links to reconfigure the network topology. These schemes are referred to as baseline, link adaptation, and topology control, respectively. This data highlights the average-case traffic loss where the traffic in the network is evenly distributed and therefore, less of a penalty is seen on within the other schemes. The topology control is still the best approach to reduce latency and maintain a more stable throughput.

Table 3-1. A decrease in network performance is seen after a link disruption event. In the baseline control scheme, throughput can be maintained by re-routing traffic on stable links at the cost of a latency increase. The link adaptation technique permits a slight increase in performance compared to the baseline. The best solution is the topology control process which redirects the point-to-point links maintaining throughput and a minimum latency.

	Average-case Scenario		*Worst-case Scenario*	
Strategy	Latency	Throughput	Latency	Throughput
Baseline	7.04 X	<1% of traffic is lost	11.48 X	<1% of traffic is lost
Link Adaptation	3.01 X	<1% of traffic is lost	4.01 X	<1% of traffic is lost
Topology Control	1.51 X	<1% of traffic is lost	1.96 X	<1% of traffic is lost

3.3.2 Network Partition Due to Multiple Link Disruption Events

In the second scenario, the network experiences two LDEs in the existing eleven links within the network as shown in fig. 3-13. The failures will occur (and subsequently reset) multiple times over a 3.5 hour period and the results are shown in Table 3-2 (averaged together for reliability). Note the failure of two links in a bi-connected network results in two disjoint networks and, as expected traffic is unable to flow between the two halves. This catastrophic event is also known as a network partition. Similar to scenario #1, fig. 3-13 and fig. 3-14 are offered as samples of the network performance in both the average and worst-cases, before and after the LDEs occur. Again, at first all three networks are identical with traffic flowing between the source and destination nodes across a high-data rate link. At the time of the LDEs (time = t_e), two links are severed and the network responds accordingly. As expected, the baseline network is unable to maintain traffic flow between the two disjoint halves of the network – regardless of average and worst case traffic flows. The network response with link adaptation is able to maintain connectivity but at a severe penalty in latency – 400X in the worst-case – and >60% dropped packet ratio; the average case showed only a 2.15X increase in latency with <1% of packets being dropped. Once again, the full topology control case is the best performer with only a 2.37X increase in latency across both traffic demands and maintained <1% packet loss after reconfiguration. By far, this shows the validity and necessity of LDE mitigation techniques to be present in mobile DWB networks.

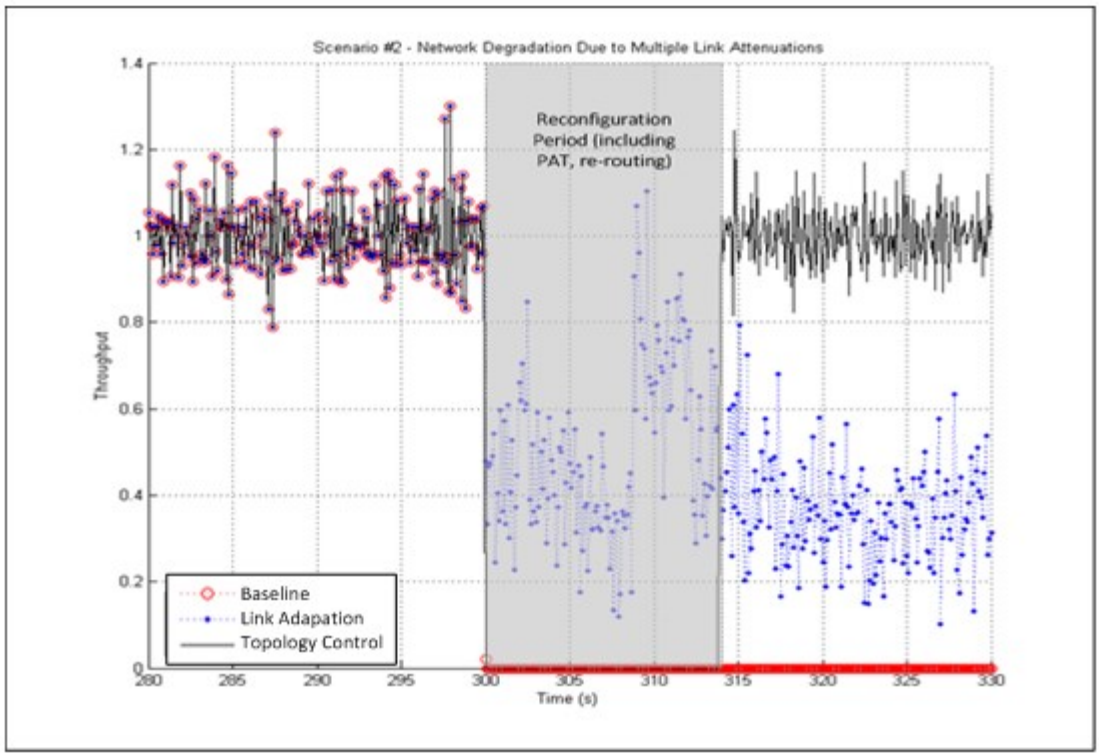

Figure 3-13. In the second scenario, two links are obscured and this defines a network partition in a bi-connected network. The network is able to respond in three ways: 1) re-route traffic along stable links, 2) adjust transmit frequency to increase link performance, or 3) redirect the point-to-point links to reconfigure the network topology. These schemes are referred to as baseline, link adaptation, and topology control, respectively. After a partition, the topology control is the only scheme able to maintain traffic throughput. Notice the baseline scheme drops all of its traffic. This data highlights the worst-case traffic loss wherein the network traffic is isolated on the partition.

Table 1-2. A decrease in network performance is seen after multiple link disruption events creating a partition in the network. The baseline control process cannot re-route traffic to mitigate the partition and all traffic is lost. The link adaptation and topology control processes are able to maintain the network at either a significant impact or no impact at all, respectively.

	Average-case Scenario		*Worst-case Scenario*	
Strategy	Latency	Throughput	Latency	Throughput
Baseline	N/A	All traffic is lost	N/A	All traffic is lost
Link Adaptation	2.15 X	<1% of traffic is lost	400 X	60% of traffic is lost
Topology Control	2.75 X	<1% of traffic is lost	1.99 X	<1% of traffic is lost

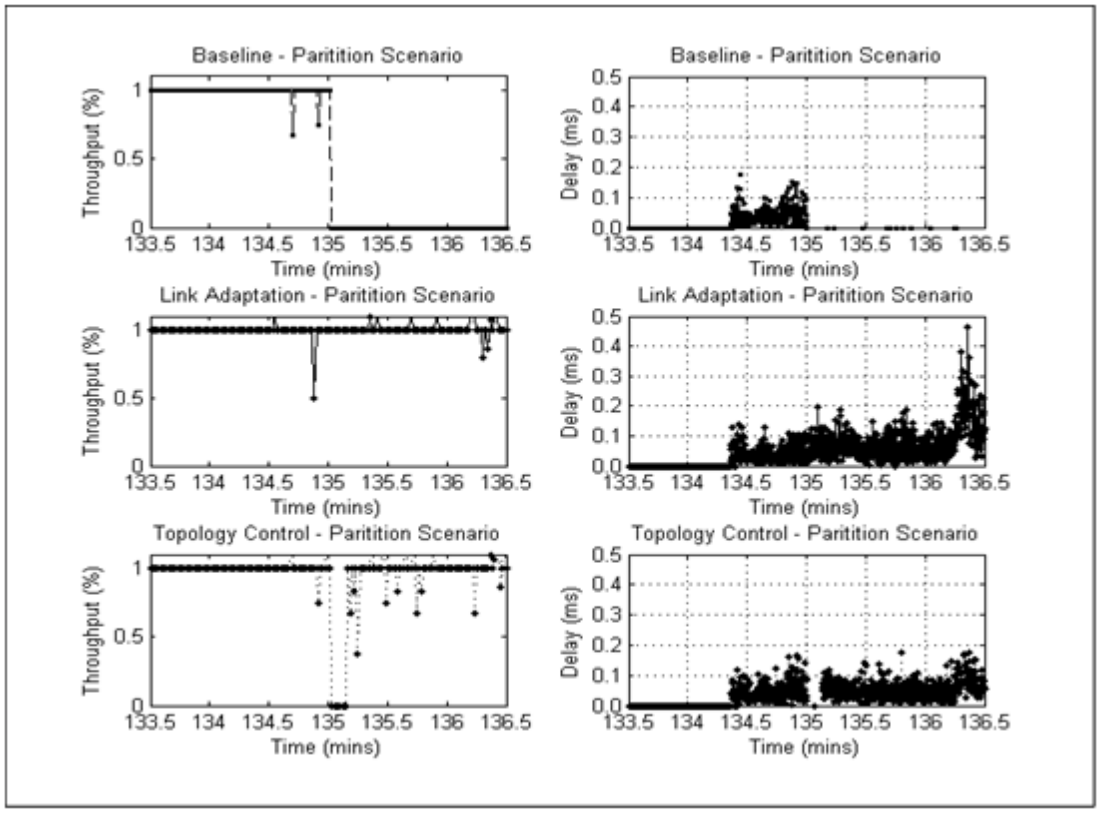

Figure 3-14. In the second scenario, two links are obscured and this defines a network partition in a bi-connected network. The network is able to respond in three ways: 1) re-route traffic along stable links, 2) adjust transmit frequency to increase link performance, or 3) redirect the point-to-point links to reconfigure the network topology. These schemes are referred to as baseline, link adaptation, and topology control, respectively. This data highlights the average-case traffic loss where the traffic in the network is evenly distributed and therefore, less of a penalty is seen on within the other schemes. On the other hand, the baseline case is still not able to transport traffic from one partition to the other and therefore, classical routing techniques alone do not provide a solution during a network partition.

3.3.3 Assessing Dedicated-Channel Radio Paradigm

A number of experimental setups were investigated and the radio pairing mechanism (i.e. connectivity) was examined to highlight the effectiveness of multiple exclusive channels on-board the UAS platforms. A similar application was written in MATLAB using six mobile base stations providing the backbone layer at an altitude of 2 kilometers with constant obscuration. One-hundred end users are distributed in a 50km x 50km plane and they move according to the RPGM model [43]. The previously developed force-driven model is used to make backbone nodes adjust their locations until convergence to the optimal backbone configuration [64]. At the same time, radio are assigned using a greedy algorithm and monitored for blockages. The radio assignments will be updated throughout the simulation relative to UAS movement.

A sample scenario is shown in fig. 3-15 in which the end-users are scattered throughout the environment (shown as red dots). Over time, the backbone UASs move to satisfy mobile end-user coverage and connectivity. As a function of this movement, radio assignments must adapt and may become blocked or unavailable due to channel pairings. The radios are illustrated by either a colored tip on the pod to represent "in-use" or an outline to represent "available" states. In fig. 3-15, the UAS use an A/B configuration where the (1F/2R) pods are channel A and (1R/2F) are channel B. This configuration is referred to as an alternating configuration and provides a better opportunity to make connections between radios. However, as illustrated in fig. 3-15, situations still arise in which the radios are not able to be paired. On average, this situation accounted for an efficiency rating of only 74% - in other words, 26% of the time, the UAS platform was not bi-connected. This can be improved with more stable

flight patterns exhibited by the UASs; however connectivity and coverage metrics will suffer. This instance was not examined due to the adherence of the force-algorithm.

A similar scenario was investigated where the A/B radio configuration is assigned to the front and back radios, respectively. That is, {1F, 2F} use channel A and {1R, 2R} use channel B, as illustrated in fig. 3-16. Notice in this scenario the network starts out bi-connected. Due to orbital patterns exhibited by the UASs once their individual demand is satisfied, links break more often. This is more in line with the figure-eight patterns proposed by DARPA [5].

Providing capabilities for frequency agility in the radios can increase the efficiency of the system by over three-fold. As shown in fig. 3-17, the efficiency of the radios is at 93% when channel selection is not a prohibiting factor. The percentage of time each UAV is 'k-connected' (in this case k=2) is shown per UAS. Though this requires a more detailed radio design, functionality and network availability are paramount for DWB networks.

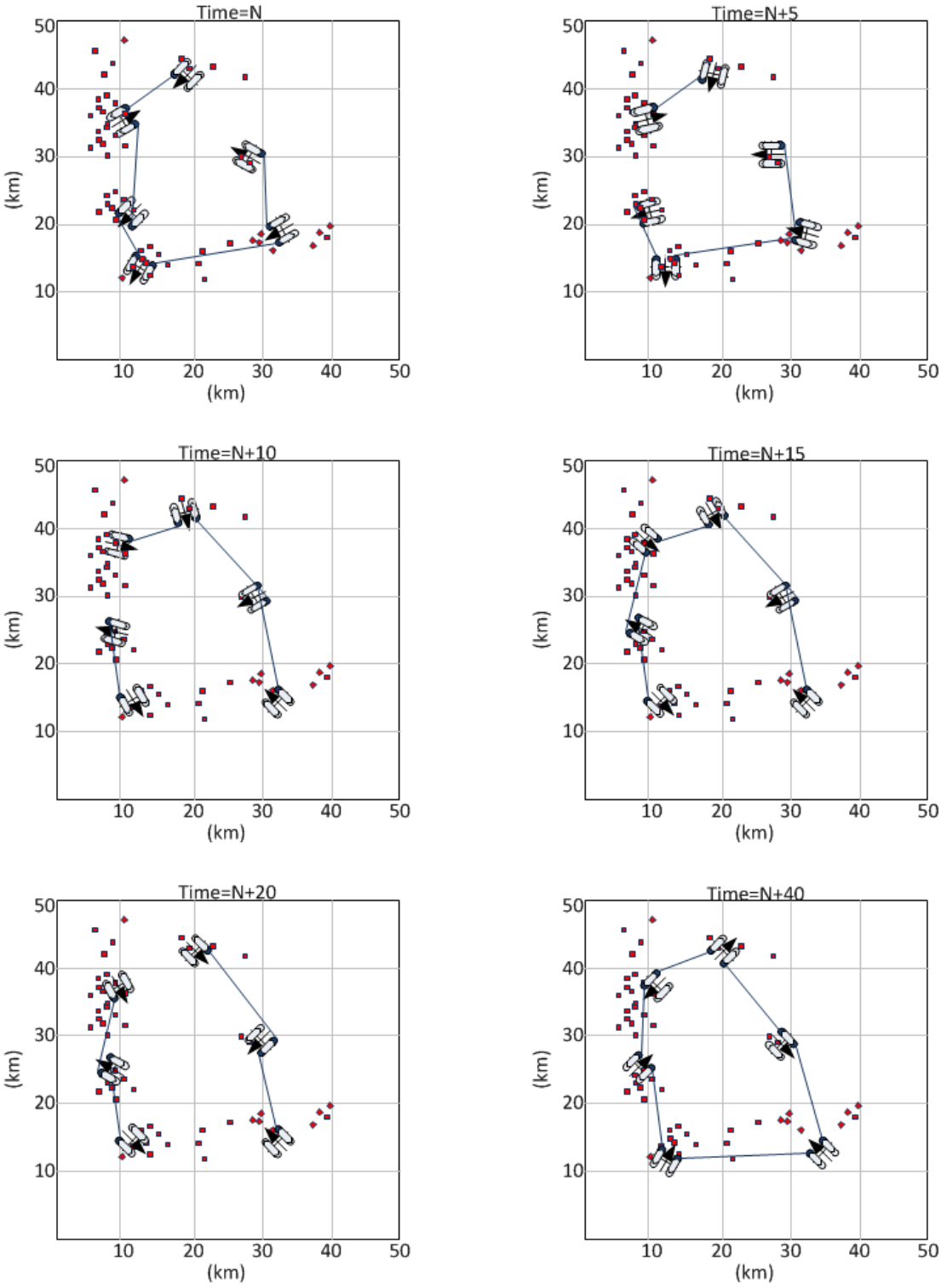

Figure 3-15. The evolution of radio assignments is a function of the morphing behavior of the network in an attempt to satisfy mobile end-user coverage. The radio assignments are in an A/B fashion (i.e. {1F, 2R} use channel A and {1R, 2F} use channel B).

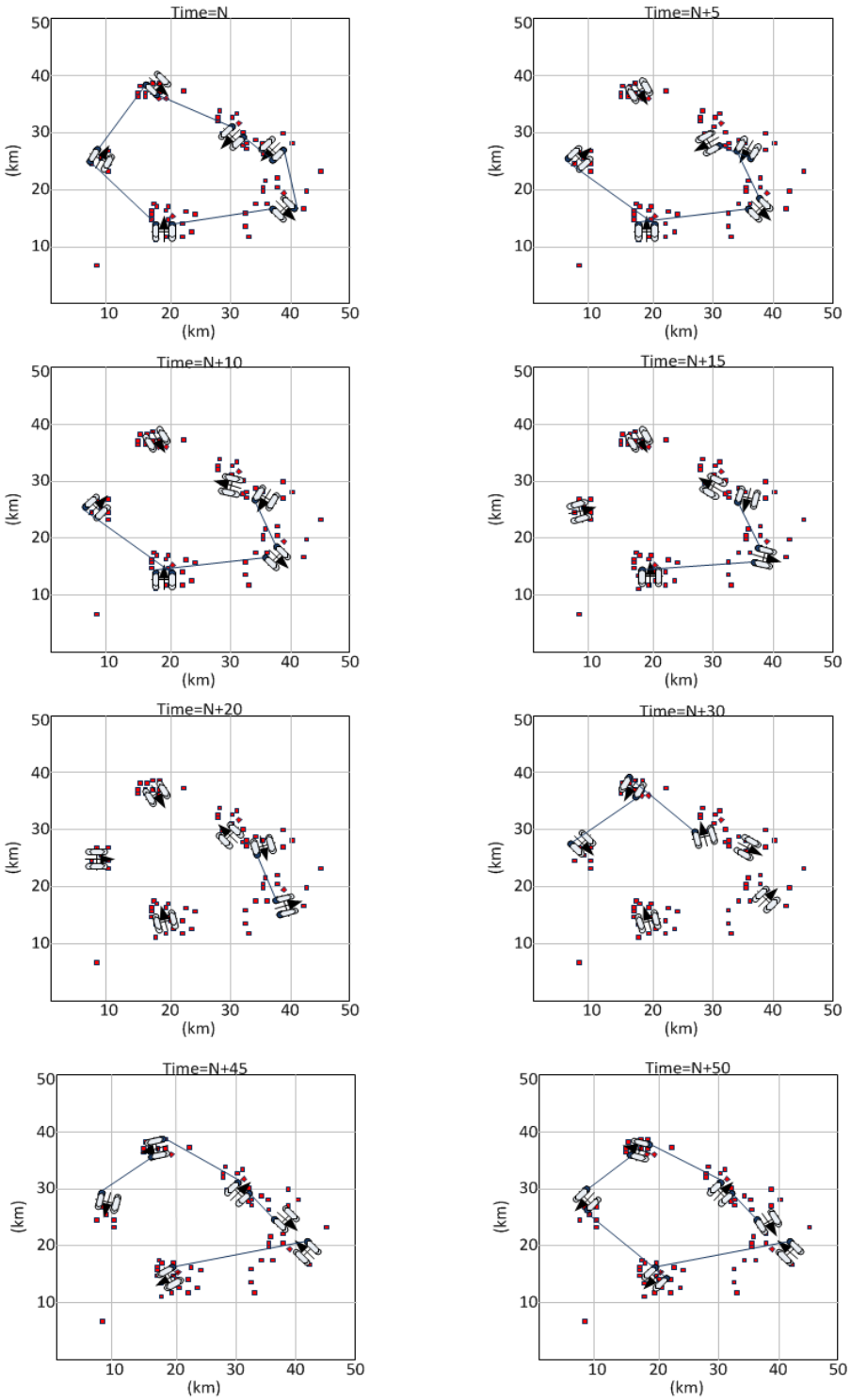

Figure 3-16. The evolution of radio assignments is a function of the morphing behavior of the network in an attempt to satisfy mobile end-user coverage. The radio configuration is a front/back assignment (i.e. {1F, 2F} use channel A and {1R, 2R} use channel B).

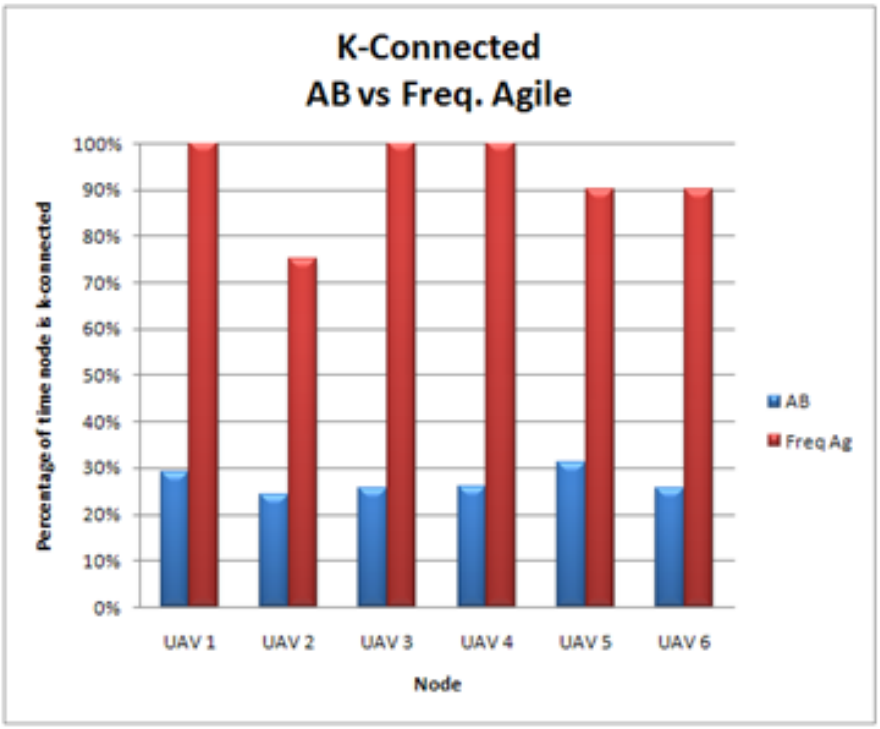

Figure 3-17. As previously eluded, the efficiency of the radio assignment is improved when the radios can be frequency agile. In this scenario, the efficiency as measured through "k-connectedness" is a function of the amount of time a UAS is bi-connected (k=2). At times, the UAS may only be 1-connected if channel assignments restrict connectivity as is the case in the A/B scenario. Even frequency-agile radios may not be able to satisfy all constraints due to shadowing and turning/banking of the platform.

3.4 Summary

In this section, a control framework for DWB network was proposed and validated which included traditional networking aspects such as routing, addressing, and quality-of-service metrics with that of platform specific constraints such as navigation/dynamics (e.g. turbulence, turning radius, banking), technology availability (e.g. radio channel assignments), and network topology reconfigurations. It was first shown that the control architecture properly executes using IPv6 processes and further shown that it continues to provide solutions to mitigate network partitions through the topology control process with <1% of traffic lost when multiple links fail. A hybrid routing scheme was developed using an upgraded version of the OSPF routing protocol to achieve directionally-aware routing that increases bandwidth and reduces latency as a function of environmental parameters. Propagation models for modern directional systems were incorporated into the modeling and simulation software to validate the control architecture using this technology with recent work from J. Rzasa with respect to the PAT process. And finally, an assessment of the dedicated channel radio methodology proposed in current DWB network research was analyzed to only be 35% effective in random scenarios.

Chapter 4: Future Work

This dissertation investigates a novel molecular-inspired framework for directional wireless backbone network wherein the links of the network are able to grow/retract in a similar manner as the bonds that hold molecules together in order to explain network reconfigurations with respect to configurations and node dynamics. In this work, the potential energy of the network has been extended to include both joint and disjoint nodal interactions in the formation of the potential energy surface. This surface is used to identify the transition points (i.e. point at which the current topology is sub-optimal and the network will trigger a reconfiguration process) between network topologies in an effort to predict reconfiguration. A normal mode analysis was also performed on the same network which highlights the second-order dynamics inherent to a connected entity. In a similar manner as the PES, the NMA calculations can lead to predicting instabilities within a DWB network.

Further work will include validation of the effectiveness of the molecular model for more DWB networks with other objectives beyond connectivity and coverage. The molecular model for DWB networks will also be integrated more closely with network science and link quality metrics. A correlation and analysis of the molecular model as it relates to reconfiguration prediction in in real-world networks to assess the impact the proactive process has on mitigating traffic loss will also be performed.

The incorporation of new directional systems into OPNET for application on higher data rate links and DARPA projects (e.g. 100G) will be conducted. Terrain models and weather models can be incorporated into OPNET to further validate the implementation and shared with DWB designers. The MATLAB test bed will be

enhanced with further node dynamics with a reduced emphasis on power optimization but more-so on network-centric metrics such as bit-error-rate. Other work will include incorporating the controls developed herein into existing routers to deploy a hardware test-bench for this application in the near future.

Appendix A: Analogous Models for Reconfigurable DWB Networks

Nature-inspired algorithms have been investigated at the University of Maryland that provides robust strategies that are scalable and power efficient. Each design proposes analogous behavior of DWB networks and attempts to mimic the natural reaction behavior to increase the aggregate network performance. The two analogous models included in this appendix draw conclusions from biological and physical systems and seek to optimize mobility and transmission power. In a similar manner, a novel molecular-inspired model is developed in Chapter 2.2 to serve as the theoretical methodology for predicting reconfigurations.

A.1 Biological Model

H. Zhang [13] investigated two biology-inspired strategies: a Flocking Algorithm (FA) and a Particle Swarm Optimizer (PSO). Each of these approaches seeks to optimize the DWB network in a self-organizing manner using global information. In addition, these techniques are scalable because they mimic nature-inspired process and are able to adapt to the ever-changing environment. This was also the first attempt at including geographical obscuration, undesired weather events, and security areas. Collectively, these are referred to as "taboo areas."

In the FA approach, an analogy is drawn between the airborne backbone of the DWB network and the dynamic movement of birds. The flocking behaviour of birds is a simple yet powerful analogy to draw and provides a framework to control the DWB network. Three simple rules govern all flocking outcomes: alignment, separation, and

cohesion - alignment moves an individual node towards the average heading of neighbouring nodes; separation avoids local collision of nodes; and cohesion maintains the clustering of the flock [38, 39]. It is evident from these three rules that the backbone tier can maintain objectives of coverage and connectivity through a distributed manner using only local information in a force-driven heuristic way. Further adaptation of the model includes classifying the end-users are "leaders" and the airborne backbone as "followers." In effect, coverage is maximized by the end-users (i.e. leaders) influencing the mobility of the backbone nodes (i.e. followers). Results from this approach are shown at 31.62% improvement over the early joint-optimization approaches [11].

The PSO investigation explored the duality between a DWB network and a school of fish [40]. The methods in which fish adapt to a changing environment is through the use of local and global information – a stochastic global optimization approach. Each particle (e.g. node, fish) in the group possess its own position and velocity parameters and adjusts each gradually according to its interaction locally with the environment and globally with the entire swarm. This method yields a reduction in complexity compared to previous efforts because the parameters are locally tuned, is easier to implement (vs. a centralized optimization algorithm), and has a fast convergence rate. Again, improvements were shown at 35.11% over previous efforts.

A.2 Physical Model

The framework provided by J. Llorca in numerous publications [7, 10-12], uses a physical approach to model the DWB network. In this context, the properties of physical configuration occurring in nature are investigated to best characterize, control,

and optimize the behavior of DWB networks, and ultimately to improve aggregate network performance. The first approach uses a network of convex springs that has a potential energy relative to the stretching/retracting of the interconnections between nodes. The weighted-effort of each node in the network contributes to the system's potential energy and movements (and reconfigurations) are performed to in an effort to minimize the potential energy, similar to a spring network achieving equilibrium. The second approach utilizes an exponential Morse Potential to either "release" or "retain" a node within the network at distances greater than 10km.

The first approach [7] examines the analogous potential energies of spring and a DWB networks. Physical systems (e.g. springs) naturally react to parameters in the environment in an effort to minimize their potential energy. Similarly, a DWB network can react to changes in the environment such as obscuration changes, end-user mobility, terrain, and power constraints. These reactions are done through either physical position changes or network topology reconfigurations. Collectively, the decisions are based on the backbone connectivity and the demand for communication energies between end-user and backbone nodes. This can be expressed as

$$U = \underbrace{\sum_{i=1}^{N}\sum_{j=1}^{M} b_{ij}u\left(R_i, R_j\right)}_{F} + \underbrace{\sum_{k=1}^{M} u\left(R_{h(k)}, r_k\right)}_{G} \tag{1}$$

where R_i is the location of backbone node i, r_k the location of terminal node k, N the number of backbone nodes, M the number of terminal nodes, $h(k)$ the index of the backbone node covering terminal node k, and b_{ij} the integer variable that determine the backbone topology, T

$$b_{ij} = \begin{cases} 1 & if\,(i,j) \in T \\ 0 & o.w. \end{cases} \tag{2}$$

Subsequently, this integer program will optimize the connectivity of all the nodes in the network. The next step provides the mechanism for a distributed algorithm satisfying end-user coverage: the first-derivative of the potential energy is the force function. Applying unique forces in a distributed manner permits the backbone nodes a reactive step with respect to the random trajectories displayed by the end-users. This can be expressed as

$$f_{ij} = -\nabla^{\mathrm{i}}\mathbf{u}_{\mathrm{ij}} = \begin{bmatrix} -\frac{\partial \mathrm{u_{ij}}}{\partial \mathrm{X_i}} \\ -\frac{\partial \mathrm{u_{ij}}}{\partial \mathrm{Y_i}} \\ -\frac{\partial \mathrm{u_{ij}}}{\partial \mathrm{Z_i}} \end{bmatrix} \tag{3}$$

where f_{ij} is the gradient of the potential energy stored in the link (i,j), $\boldsymbol{u}_{ij}$ with respect to location R_i. By following the gradient of the potential energy, the individual backbone nodes move in a heuristic manner towards the equilibrium location with respect to the end-users it is currently covering. The work in this dissertation uses this framework and extends it to investigate second-order principles with respect to topology reconfigurations.

The second approach [12] extended the distributed force-driven heuristic to provide more intelligent decisions and included power constraints. The previous spring model used a harmonic approach to quantify the potential energy of the system. As such, the force increases quadratically with respect to distance and exponentially with respect to obscuration. Though this is mathematically consistent with a spring network, a real-world application of DWB networks may be power limiting and interconnections between distance (or higher obscured) nodes is not possible. Therefore, the Morse potential was introduced to model the potential energy with power limitations,

$$u_{ij} = D_{ij}\left(1 - e^{-\beta_{ij}L_{ij}}\right)^2. \quad (4)$$

This non-convex extension includes D_{ij} as the "dissociation energy." In other words, this is the point where the link between nodes (i,j) separated by distance L_{ij} is "released." The term β_{ij} is a tuned force constant [14]. At relative distance (e.g. $L_{ij}<$ 10km) the Morse potential acts similarly to the harmonic function and thus the link is said to be "retained."

Appendix B: Modeling and Simulation of Reconfigurable Beam-Steered DWB Networks in OPNET

A plurality of custom processes, node models, finite state machines, and code modifications were made to OPNETv17 to accurately model and simulate reconfigurable beam-steered directional wireless backbone networks. These include:

- **Base-station node definition** – a custom node model was developed to support multiples radios (three in this case), custom MAC layer for narrow point-to-point links, and enhancements to the routing protocols.
- **Dynamic receiver groupings** – the DRG utility permitted radio pairings to restrict entries in the potential connectivity matrix used in the topology control processes.
- **Physically-accurate propagation models for FSO/RF** – modern propagation, signal-to-noise ratios, and bit-error rate modulation curves were used for free-space optical and directional RF links.
- **MAC layer in DWB networks using narrow beam point-to-point links** – Due to the narrowness of the directional beam, collisions and interferences are minimized and therefore, a simplified MAC layer is used for DWB networks.
- **Modifying routing protocols to support the hybrid link scheme** – Information is passed between the control processes and the routing algorithms to ensure optimal routing for traffic.
- **Topology control FSM** – An abstracted control process is used to optimize the connections in the network. This is a 5-stage process and includes parameter exchanges with the OPNET kernel to control simulation events.

- **Mobility control FSM** – The mobility of the base-station nodes is controlled through input files with designated time signatures. In this manner, any mobility control scheme can be simulated.
- **Packet definition** – control parameters in the packet headers are necessary to establish the link type (FSO or RF) and associated attributes.
- **Traffic demands and end-user abstractions** – The end-users are abstracted to reduce simulation complexity. Their demands are generated externally and inputted via XML files.

B.1 Base-Station Definition

The backbone nodes are modeled using the default mobile wireless LAN routers – though they are subsequently modified as shown in fig. B-1. This model was chosen because it provides the necessary IP stack, wireless antennas, and mobility. Three transmitter/receiver pairs were added to the model – two radios (*wlan_1_0* and *wlan_2_0*) for bi-connectivity at the backbone tier and one radio (*wlan_0_0*) acting as an access point for terrestrial end-users. Loop-back interfaces were additionally appended to facilitate the transfer from adjacent radios within each node (not shown). Additional modifications were made to each element within the model and are discussed in the next sections.

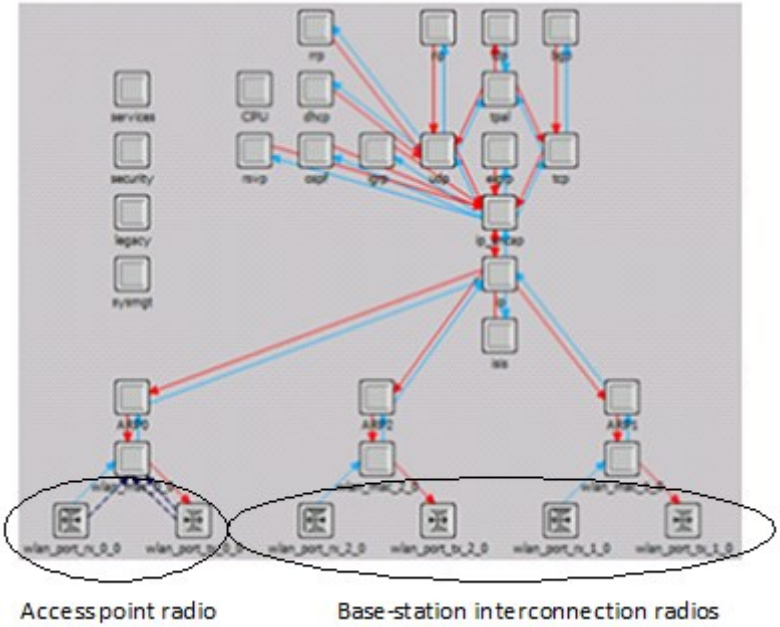

Figure B-1. The directional antenna for the backbone nodes utilize a modified WLAN transmitter/receiver pair provided in the default model in OPNET. The modifications are made to correctly simulate the narrow FSO and directional RF links as described in section 3.3.

B.2 Packet Definition

A custom packet was defined to include two headers (source/destination addresses), a data field, and two control flags as shown in fig. B-2. The first control flag is set high if the number of errors in the received packet is below a set threshold and is used discard packets. In the OPNET procedures, a packet passes through the entire pipeline stack regardless of the accept field in order to collect statistics at the final stage. However, packets marked as unacceptable are not unpackaged for processing. The second control flag is used to accommodate the hybrid link scheme. For example, if the link between two nodes is set to type = FSO, then the TX_Data_Rate field will have a value to reflect this situation (i.e. 11 Mbps for FSO, 1Mbps for RF). This field is necessary to ensure proper SNR/BER curves are used and the field is modified as the packet is transmitted between nodes between source-destination. Each of these fields has a size of 0 bits because they are not attached to the packet and are used locally at each node for control decisions.

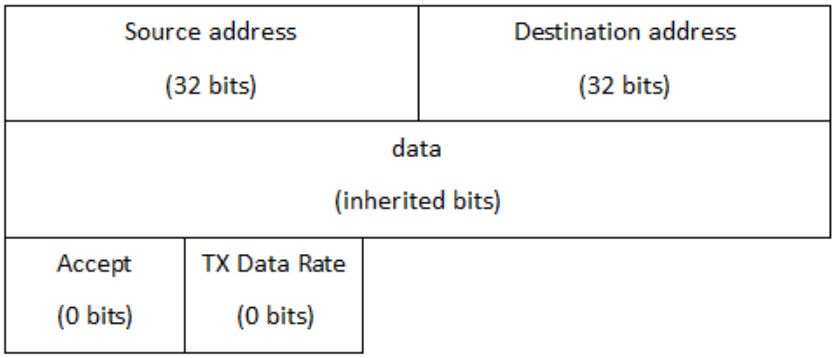

Figure B-2. Only three data fields and two control fields were needed to define a packet in the directional wireless implementation. The 'accept' field designated if the number of errors in the packet was below a threshold and the 'TX Data Rate' field controlled the link type definition (FSO/RF) for the hybrid link scheme.

B.3 Propagation Models for FSO/RF

A full discussion of the physical propagation models including SNR/BER modulation curves is offered in Chapter 3. This section will detail the implementation of the work.

B.3.1 Transmitter

Only one part of the transmitter was adjusted and was done to accommodate the new packet definition. This work is located in the *umd_wlan_txdel* file as shown in fig. B-3. The objective of the transmitter is to send the packet to a receiver and to model the delay correctly. To accomplish this goal, the transmitter delay was set to be

$$TX\_DELAY = \frac{PACKET\_LENGTH}{TX\_DATA\_RATE}.$$

The TX data rate and packet length parameters are obtained on lines 53 and 56, respectively as shown in fig. B-4. The delay is set on line 64 and the OPNET kernel transmission data attribute (TDA) for the packet's data rate is updated on line 69.

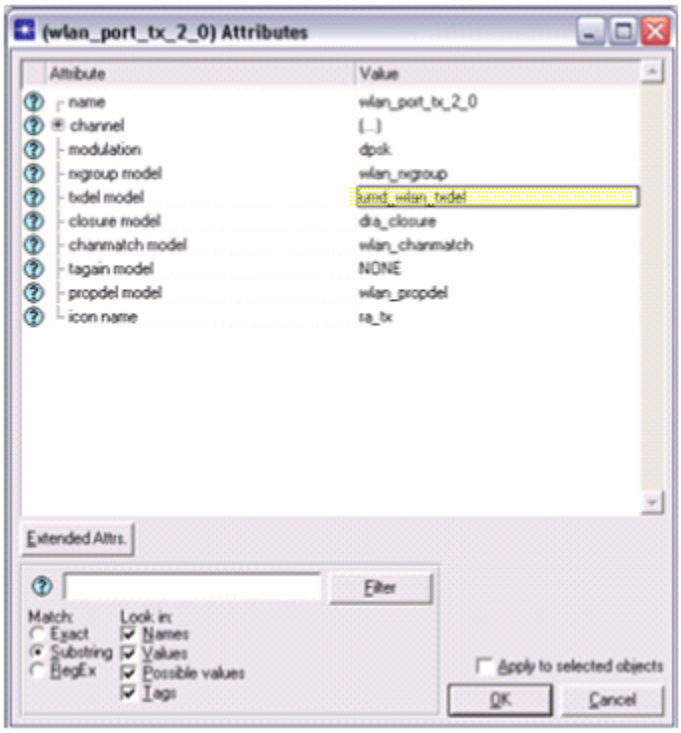

Figure B-3. The 'txdel model' file controls the delay between packets for the transmitter. To enable unique data rates, this file needed to be modified for the hybrid linking scheme.

```
#if defined (__cplusplus)
extern "C"
#endif
void
umd_wlan_txdel_mt (OP_SIM_CONTEXT_ARG_OPT_COMMA Packet * pkptr)
    {
    OpT_Packet_Size pklen;
    double          tx_drate, tx_delay;

    /** Compute the transmission delay associated with the  **/
    /** transmission of a packet over a radio link.         **/
    FIN_MT (umd_wlan_txdel (pkptr));

    /* Obtain the transmission rate from the packet.        */
    op_pk_nfd_get_dbl (pkptr, "Tx Data Rate", &tx_drate);

    /* Obtain length of packet.                             */
    pklen = op_pk_total_size_get (pkptr);

    /* Compute time required to complete transmission of    */
    /* packet.                                              */
    tx_delay = pklen / tx_drate;

    /* Place transmission delay result in packet's          */
    /* reserved transmission data attribute.                */
    op_td_set_dbl (pkptr, OPC_TDA_RA_TX_DELAY, tx_delay);

    /* Also update the transmitter's data rate TDA with the */
    /* information retrieved from the packet to be used in  */
    /* the following pipeline stages.                       */
    op_td_set_dbl (pkptr, OPC_TDA_RA_TX_DRATE, tx_drate);

    FOUT
    }
```

Figure B-4. The associated code modifications within the txdel model file include calculating the packet size and delay and setting internal parameters correctly.

B.3.2 Receiver

The modifications to the two receivers were accomplished by editing the six files highlighted in fig. B-5 to include models for power, background noise, signal-to-noise ratios, bit-error-rates, error distributions, and error-correction.

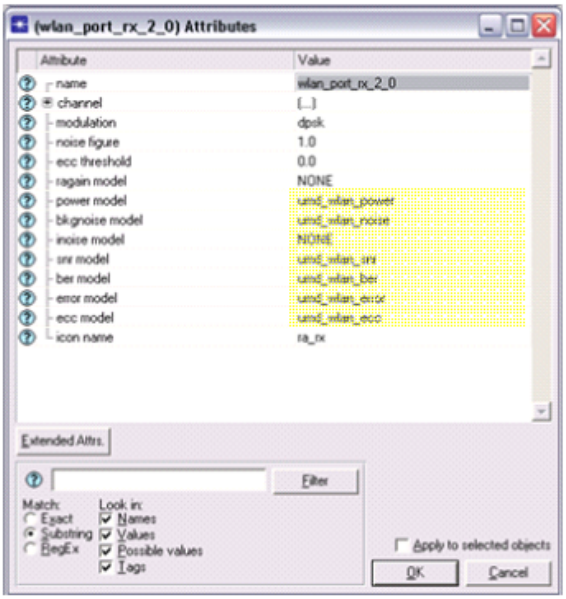

Figure B-5. To incorporate the hybrid linking scheme, along with the correct modulation curves for FSO/RF systems, numerous files had to be adapted on the receiver.

Power Model

First, the type of link must be distinguished in order to select the correct propagation model. This is done in line 95 of fig. B-6, where *pkptr* is the incoming packet and the second parameter is an OPNET kernel TDA constant. Next, the path loss variable is calculated based off the distance and converted obscuration value. The RF link required additional processing since its path loss integral is harder to compute for each packet. For this reason, a look up table was generated as a function of distance (with constant obscuration) and read for each packet. The received power is set using the TDA again, on line 124. This transmission data attribute will be used in subsequent stages of the pipeline.

```
75  #if defined (__cplusplus)
76  extern "C"
77  #endif
78  void
79  umd_wlan_power_mt (OP_SIM_CONTEXT_ARG_OPT_COMMA Packet* pkptr)
80      {
81      double      prop_distance_m, prop_distance_km, rcvd_power, path_loss;
82      double      tx_power;
83      double      data_rate;
84      //double        obs_per_km, obs_loss;
85
86      /** Compute the average received power in Watts of the      **/
87      /** signal associated with a transmitted packet.            **/
88      FIN_MT (umd_wlan_power (pkptr));
89
90      /* Get distance between transmitter and receiver (in meters)*/
91      prop_distance_m = op_td_get_dbl (pkptr, OPC_TDA_RA_START_DIST);
92      prop_distance_km = prop_distance_m / 1000;
93
94      /* Get the data_rate which is used to select RF/FSO eq'ns   */
95      data_rate = op_td_get_dbl (pkptr, OPC_TDA_RA_TX_DRATE);
96
97      /* We can determine if link is FSO/RF based upon the       */
98      /* data_rate in the packet                                 */
99      if(data_rate == FSO_DATA_RATE)
100     {
101         /* Compute the path loss for this distance             */
102         if (prop_distance_m > 0.0)
103             path_loss = FSO_PATH / (prop_distance_m*prop_distance_m)
104                                  * exp(-1*CONVERTED_OBSCURATION*prop_distance_m);
105         else
106             path_loss = 1.0;
107
108         rcvd_power = tx_power * path_loss;
109     }
110     else    //RF_LINK_TYPE
111     {
112         /* Compute the path loss for this distance             */
113         if (prop_distance_m > 0.0)
114         {
115             path_loss = do_rf_lookup(prop_distance_m);
116         }
117         else
118             path_loss = 1.0;
119
120         rcvd_power = tx_power * path_loss;
121
122     }
123
124     op_td_set_dbl (pkptr, OPC_TDA_RA_RCVD_POWER, rcvd_power);
125
126     FOUT;
127     }
128
```

Figure B-6. The received power equation is dependent the present link type (FSO/RF). This calculation is stored internally for the next stage.

Noise Models

The thermal and shot noise values are established in either one of the *bkgnoise* or *inoise* model files. In this case, the values were set in the *bkgnoise* file and thus, *inoise* is set to NONE. A full discussion of noise elements in FSO and RF systems was provided in chapter 3. Following the calculations (as a function of received power and link type), the noise TDA variable can be set using the OPNET kernel procedure,

```
op_td_set_dbl (pkptr, OPC_TDA_RA_BKGNOISE, <value>);
```

where pkptr is the current packet and <value> is the noise value. This will be used in the signal-to-noise calculation seen in the next file.

SNR Model

Now that the receiver power and noise values have been established (as a function of link type), the signal-to-noise ratio can be calculated as a function of the receiver responsivity $\Re$,

$$\langle SNR_0 \rangle = \frac{\left(\Re \langle P_R \rangle\right)^2}{\sigma_N}.$$

This is done on line 49 of fig. B-7. Once again, the link type determines the format for which the SNR is saved. The OOK modulation bit-error-rate curves for the FSO link were tabulated in raw form whereas, the RF modulation curves is in decibels. This conversion is shown on lines 51-61. Finally, the time at which the SNR measurement was obtained is saved for statistical collection.

```
#if defined (__cplusplus)
extern "C"
#endif
void
umd_wlan_snr_mt (OP_SIM_CONTEXT_ARG_OPT_COMMA Packet * pkptr)
    {
    double      noise, rcvd_power, sig_power, data_rate;

    /** Compute the signal-to-noise ratio for the given packet. **/
    FIN_MT (umd_wlan_snr (pkptr));

    /* Get the packet's received power level. */
    rcvd_power = op_td_get_dbl (pkptr, OPC_TDA_RA_RCVD_POWER);

    /* Get the packet's accumulated noise levels calculated by the */
    /* noise stages.                                               */
    noise = op_td_get_dbl (pkptr, OPC_TDA_RA_BKGNOISE);

    /* Get the link type */
    data_rate = op_td_get_dbl (pkptr, OPC_TDA_RA_TX_DRATE);

    /* Factor in the responsivity of the receiver */
    sig_power = rcvd_power*rcvd_power*RESPONSIVITY_SQ;

    if(data_rate == FSO_DATA_RATE)
    {

        /* Assign the SNR in raw form. */
        op_td_set_dbl (pkptr, OPC_TDA_RA_SNR, (sig_power / noise));
    }
    else
    {
        /* Assign the SNR in dB. */
        op_td_set_dbl (pkptr, OPC_TDA_RA_SNR, 10.0 * log10 (rcvd_power / noise));
    }

    /* Set field indicating the time at which SNR was calculated. */
    op_td_set_dbl (pkptr, OPC_TDA_RA_SNR_CALC_TIME, op_sim_time ());

    FOUT
    }
```

Figure B-7. The SNR is a straight-forward calculation based on previously calculated received power and noise levels. The internal parameter is set for use in the next stage.

BER Model

To obtain the bit-error-rate from the SNR, a look-up table was created in OPNET. This table is automatically generated by the import of a modulation curve as discussed in lab session 1580 [76]. Once imported, the look up table is accesses using the SNR value from the previous file in conjunction with the correct modulation table as specified by the link type once again. For example, if the link type = FSO, then <selected modulation table> would have a value of the OOK modulation curve.

```
snr = op_td_get_dbl (pkptr, OPC_TDA_RA_SNR);
ber = op_tbl_mod_ber (<selected modulation table>, snr);
```

Finally, the TDA for the BER should be set for use in the error file.

```
op_td_set_dbl (pkptr, OPC_TDA_RA_BER, ber);
```

Error Model

No changes were made to the error file since it already had in place a decent probability distribution function. To accommodate existing code, the TDAs used previously were necessary and had to be implemented as such.

ECC Model

Unlike the error model, a simplified error correction model was used for this work. Specifically, the decision to accept or drop a packet was simplified to compare the number of errors below or above a prescribe amount, respectively. The specific value of the threshold is set on the receiver parameters and is read on like 43 of fig. B-8. The decision to accept or drop the packet is made on line 55 as a function of the

percentage of bits in error over the length of the packet. The decision is saved on line 57 and is used by the MAC layer next.

```
31
32  void
33  umd_wlan_ecc_mt (OP_SIM_CONTEXT_ARG_OPT_COMMA Packet* pkptr)
34  {
35      OpT_Packet_Size         pklen;
36      int                     num_errs, accept;
37      double                  ecc_thresh;
38
39      /** Determine acceptability of given packet at receiver.        **/
40      FIN_MT (umd_wlan_ecc (pkptr));
41
42      /* Obtain the error correction threshold of the receiver.   */
43      ecc_thresh = op_td_get_dbl (pkptr, OPC_TDA_RA_ECC_THRESH);
44
45      /* Obtain length of packet.                                 */
46      pklen = op_pk_total_size_get (pkptr);
47
48      /* Obtain number of errors in packet.                       */
49      num_errs = op_td_get_int (pkptr, OPC_TDA_RA_NUM_ERRORS);
50
51      /* Test if bit errors exceed threshold.                     */
52      if (pklen == 0)
53          accept = OPC_TRUE;
54      else
55          accept = ((((double) num_errs) / pklen) <= ecc_thresh) ? OPC_TRUE : OPC_FALSE;
56
57      op_td_set_int (pkptr, OPC_TDA_RA_PK_ACCEPT, accept);
58
59      FOUT
60  }
61
```

Figure B-8. The number of errors in the packet is compared to a preset threshold and the packet's accept field is set accordingly. This is a simplified process compared to the default WLAN module.

B.4 The Role of the MAC Layer in DWB Networks Using Narrow Beam Point-To-Point Links

The responsibility for the medium access control (MAC) layer in the traditional Internet protocol includes collision avoidance, retransmission requests, back-off requests, and other signal processing. This is necessary since multiple transmissions can overlap a receiver and the information must be distinguished between senders. Moreover, in beam-formed DWB networks, the MAC layer handles the DSP necessary to facilitate channel designations including power management schemes.

On the other hand, in beam-steered DWB networks, the MAC layer's responsibilities are diminished since the narrowness of the link between two nodes assumes no overlap and minimal interference is present. Power management can be abstracted from the protocol stack since additional work is necessary to maintain alignment such as pointing, acquisition, and tracking. The majority of this work is outlined in Chapter 3.

With that said, OPNET assumes a protocol stack with a MAC layer and therefore, it is utilized in this framework as a packet forwarding mechanism. Figure B-9 outlines the finite state machine for the MAC layer process. The first few states are used in the initialization period of the OPNET simulation kernel and register the process for access by other control processes (e.g. topology control). The bulk of the work resides in the WAIT and BUSY states. During the WAIT state, a packet can arrive at the MAC layer either from a receiver (i.e. from the network) or a higher layer at the current node to be sent out (i.e. from IP). If it is received from a receiver the NETWORK state simply forwards the packet for address resolution (e.g ARP layer).

Care is taken, however, if the packet needs to be transmitted to another node within the network. By introducing a BUSY state, the packets that need to be transmitted can be buffered to ensure proper handling by the radios. By default, OPNET does not have a mechanism to prevent packet overflows; thus, if a BUSY state and buffer mechanism are not introduced packets will unintentionally be sent out by the transmitters at an instantaneous rate (with no delay). The two additional states ADVANCE and IP are responsible for popping the next packet from the buffer and sending it out after a delay period, respectively.

The code is not provided in this dissertation for proprietary reasons. However, for comparison, the simplicity of the directional MAC layer over the default MAC layer provided in OPNET for Wi-Fi can be seen by the lines of code associated with each. The default MAC layer for Wi-Fi 802.11 has over 6500 lines of C code (with comments) whereas the MAC layer produced herein contains less than 500. Evidently, this is due to the limited responsibilities placed on the MAC layer for reconfigurable beam-steered links. The bulk of the control process resides in the abstracted framework within the topology control process which includes a few thousands lines of C code.

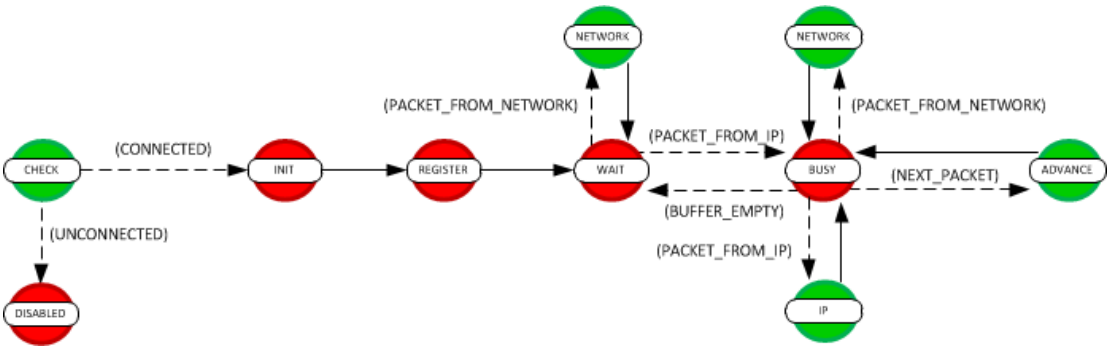

Figure B-9. The MAC layer for narrow-beam directional systems mimics a point-to-point link with minimal simultaneous contentions. Therefore, the MAC layer work is simplified to a store-forward mechanism.

B.5 Modifying Routing Protocols to Support the Hybrid Link Scheme

Three major changes were made to the OSPF protocol to support DWB networks. First, the link state advertisement (LSA) interval was set aggressively low to maintain up-to-date changes within the network as shown in fig. B-10. This is accessed through the model parameters of each node. Values of one second and four seconds were sued for the hello and dead intervals, respectively. The hello timer is the interval for which hello packets are sent throughout the network to check for alive neighbor connectivity. The dead interval is the amount of time to wait for a response from a hello packet. Therefore, if a node does not response within four seconds, it is considered “dead” and no longer an immediate neighbor for packet forwarding.

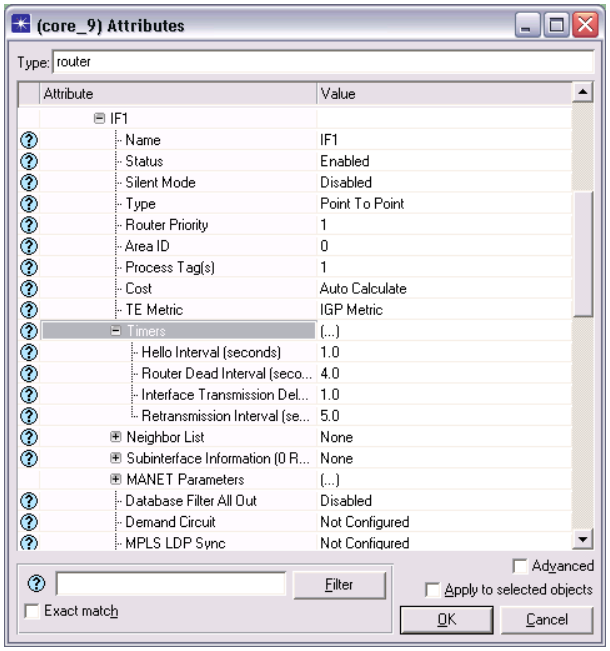

Figure B-10. The two primary OSPF timers are the Hello and Dead intervals. These intervals define the time span between LSA disseminations and updates in the network reflected within the routing table.

The second modification was a further effort to diminish the time between reconfiguration and updating of the routing tables. Without this inter-process communication, the only mechanism for OSPF to discover a new network topology is through the hello packets which require four seconds to determine connectivity. As such, during a topology reconfiguration, the OSPF process is sent an interrupt with an associated code indicating the status (UP/DOWN) of the individual links,

```
op_intrpt_schedule_process(<opsf_process_handler>,
                           op_sim_time(),<status_code>);
```

Additionally, interrupt handlers have been introduced within the OSPF protocol files.

The final modification pertains to the "cost" of a link for the routing algorithm. By default, OPNET uses a cost metric which is relative to the capacity of a link. Once again, however, the capacity (i.e. 10 Mbps) is only acknowledged during LSA

exchanges and will not be updated between dead intervals. Thus, the inter-process communication (i.e. interrupt schedulers) is used to alert the OSPF process of the link capacity change. The code within the topology control process is the same as give above with different associated interrupt codes. The additional work done within the ospf_interface_v2.c file is shown in fig. B-11. The correct link metric is adjusted in lines 545-550 and a new LSA is distributed in the network on lines 559-561. By sending out a new LSA immediately, the routing table can update without having to wait to discover the change in the links.

```
330  /* UMD edit BEGIN */
331  /* Added ospf_interface_cost_change()   */
332  static void
333  ospf_interface_cost_change()
334      {
335      int     code;
336
337      FIN(ospf_interface_cost_change());
338
339      /* Code should have a value of 1 for RF, 10 for FSO */
340      code = op_intrpt_code();
341
342      /* Default RF cost = 20 */
343      /* Set FSO = 20/10 = 2  */
344
345      if( (ospf_interface_self_ptr->cost != UMD_RF_COST) && (code==1) )
346          ospf_interface_self_ptr->cost = UMD_RF_COST;
347      else if ( (ospf_interface_self_ptr->cost != UMD_FSO_COST) && (code==10) )
348          ospf_interface_self_ptr->cost = UMD_FSO_COST;
349      else if ( (ospf_interface_self_ptr->cost != UMD_DOWN_COST) && (code==911) )
350          ospf_interface_self_ptr->cost = UMD_DOWN_COST;
351
352      printf("Cost is now %d\n", ospf_interface_self_ptr->cost);
353      /* If the lsa generation event is already active, cancel it first.              */
354      /* start the timer and originate the flood LSA                                  */
355      op_ev_cancel_if_pending (ospf_interface_self_ptr->LSA_generation_event);
356
357
358      /* Store the event handle and schedule the event                                */
359      ospf_interface_self_ptr->LSA_generation_event =
360              op_intrpt_schedule_call (op_sim_time (), OSPFC_INTF_LSA_ORIGINATE_CODE,
361                  ospf_v3_lsa_lazy_generate, ospf_interface_self_ptr);
362
363      FOUT;
364      }
```

Figure B-11. The routing algorithm was slightly modified to incorporate the different bandwidths of the hybrid linking scheme. Additionally, the events for LSA disseminations were toggled to ensure immediate identification of network reconfigurations.

B.6 Dynamic Receiver Groupings

To limit the potential neighbor connectivity of the nodes without producing new antenna diagrams (i.e. restricting the directionality), a utility is used to restrict which nodes can communicate. This utility is known as dynamic receiver groups (DRG). By using the DRG, the radios will maintain their omni-directional antenna patterns, yet the radios who can receive the information are restricted through software. Furthermore, by restricting each transmitter to only communicate with one receiver, a faux-directional point-to-point link is produced. As shown in fig. B-12, the TX/RX pairings are done on lines 2214 and 2218. The first call pairs the transmitter on node A to the receiver on node B and the second call pairs the transmitter on node B with the receiver on node A. This pairing is done each time the topology is changed. A similar procedure is done to remove a receiver from a transmitter's group which is necessary during a reconfiguration or to simulate the loss of a node.

```
2210                    if((mutual_link_type==LINK_TYPE_FSO) || (mutual_link_type==LINK_TYPE_RF))
2211                    {
2212                        txch = current_node->tx_info_ptr->wlan_port_txch_arr[channel_selection];
2213                        rxch =  next_node->rx_info_ptr->wlan_port_rxch_arr[channel_selection];
2214                        op_radio_txch_rxgroup_set (txch, 1, &rxch);
2215
2216                        txch = next_node->tx_info_ptr->wlan_port_txch_arr[channel_selection];
2217                        rxch =  current_node->rx_info_ptr->wlan_port_rxch_arr[channel_selection];
2218                        op_radio_txch_rxgroup_set (txch, 1, &rxch);
2219                    }
```

Figure B-12. The dynamic receiver group utility permits exclusive pairings between transmitters and receivers within the network to establish point-to-point directional links. Two sets of commands were used to pair TX-A to RX-B and TX-B to RX-A.

B.7 Topology Control FSM

The topology control algorithm is a 5-stage process that evaluates the aggregate performance of the network, computes the optimal network topology, and triggers a transition to a new topology should a reconfiguration become necessary.

1. **Link State Assessment** – Since the DWB network operates in a dynamic environment, link states are constantly monitored using metrics such as bit-error-rates and transmit power to establish a link budget.
2. **Link State Dissemination** – The link states are disseminated across the network to maintain current potential neighbor connectivity databases. LSA are also inputted into routing protocols to provide real-time routing information. This is part of the directionally aware routing protocol.
3. **Topology Computation** – A designated topology control node (DTCN) processes the LSA to determine if a network reconfiguration is necessary. This process is centralized to mitigate optimization collisions.
4. **Topology Dissemination** – New topology information is disseminated among the nodes in the network along with new routing tables since the new topology is known ahead of the reconfiguration.
5. **Physical Reconfiguration** – The radio channels are selected locally and the pointing, acquisition, and tracking (PAT) establishes the new topology.

An overview of the integration process into the modeling and simulation software was previously provided in fig. 3-6.

B.7.1 Timing Constraints

Since OPNET is event-driven, timing constraints need to be observed to ensure proper operation. The most notable is the priority handling of OPNET's kernel processes and the control presented to the user (i.e. the topology control process initialization code). These priorities are equivalent, however, they cannot co-exist since the 'UMD topology control' process obtains identification numbers during the initialization stage. The strategy employed in the 'UMD topology control' process is to delay the initialization stage for one-half second period. This provides enough time for the kernel to assign unique identification numbers to the processes.

After this delay, transceiver binding and OSPF parameters such as data rates and channel frequency should be defined. Constraining this stage is the beginning of the OSPF routing process that utilizes these parameters. As such, any parameters required for routing should be established now in the simulation; this is the start time for the OSPF routing process. Further access to OSPF parameters that are declared after the first route (link cost metrics) is available after 10 seconds.

The only other timing constraints that a user should be aware include the timing of the updates in obscuration variables and the frequency of the topology control algorithm. These are both set in the attributes panel of the topology control process discussed in the next section.

B.7.2 Specialized Inputs/Outputs

Parameters available on the 'UMD Topology Control' process include environmental features such as obscuration values, enabled/disabling of scenario adjustments like network partitions/link adaptation, output file creation, and timing of obscuration/topology control events, as shown in fig. B-13. Controlling events such as one and two link disruption events is done through toggling the parameters 'link adaptation' and 'network partitions.' The environmental parameters are adjustable by varying the frequency of updates and the maximum/minimum settings. Enabling the topology control algorithm and its frequency of execution is done in the last two variables. The frequency of the topology control algorithm can either be equivalent to the obscuration change (if mobility is disabled) or be more often to account for terrain and node mobility.

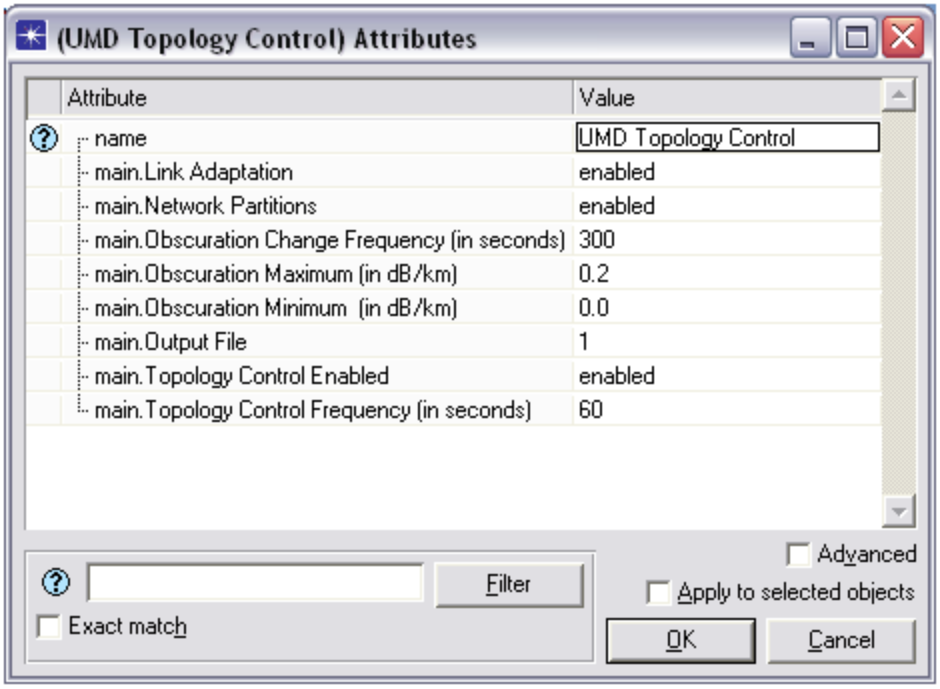

Figure B-13. The parameters of the UMD topology control process are adjustable at the user-level within OPNET. These attributes control which processes are active, statistics available for collection, and environmental effects on the links.

B.8 Mobility Control FSM

The mobility control process is a four-stage algorithm and is designed to incorporate any mobility management algorithm. The decision to generate a generic mobility algorithm platform on the backbone nodes is two-fold: 1) control of the UAS is not always available due to flight controller software and 2) the control architecture is a framework not tailored to one algorithm over another. The four-stages include announcement of backbone nodes, network metric computation, end-user reassignment, and mobility management algorithm execution. The FORCE [17] algorithm is inserted here since it is the preferred algorithm for this dissertation. An overview of the integration process into the modeling and simulation software was previously provided in fig. 3-6.

B.9 Integration of MATLAB with OPNET for Traffic Demands and End-User Abstractions

A four-step approach that integrates work done in MATLAB and OPNET is illustrated in fig. B-14 and described below.

1. MATLAB generates an initial scenarios with outputs for obscuration, mobility of the base-stations (as waypoints), and representative traffic. Obscuration models can include random terrains and cloud models extensively explored in previous work [17]. The mobility of the base-stations can follow any model (or none at all) in order to achieve networks that provide maximum coverage, higher connectivity, or a blend of the two. The traffic is generated as a function of end-user classification; each end-user is classified as either a receiver (of information) or a sender at the beginning of the scenario. Each sender places a random load onto the base-station with a receipt end-user. This load is representative of two end-users communicating through the backbone of the network and is sized appropriately (with a Gaussian distribution). The final output is an XML file.
2. The OPNET modeling has been customized for mobile directional wireless antennas of both types: FSO and mmW RF. These changes are further documented in section 3.3. The traffic demand generated in MATLAB is now converted from arbitrary units to bits-per-second and packets-per-second traffic demands. During the simulation, this traffic will follow standard IP model/routing protocols to validate our design.

3. The output of an OPNET simulation is an extensive library of metrics that include received/sent packets (and bits), obscuration levels, received power, aggregate signal-to-noise (SNR) ratios, and aggregate bit-error rates (BER), among many more default metrics. The physical topology information over time is output via text file for regeneration in MATLAB.
4. The collective information from OPNET is imported back into MATLAB for a final recreation of the entire simulation. This approach has proven more efficient since the rendering of graphics in OPNET is computationally intensive and the mathematics within the results browser is limited. The final scenario is saved as an AVI file for future analysis/presentations.

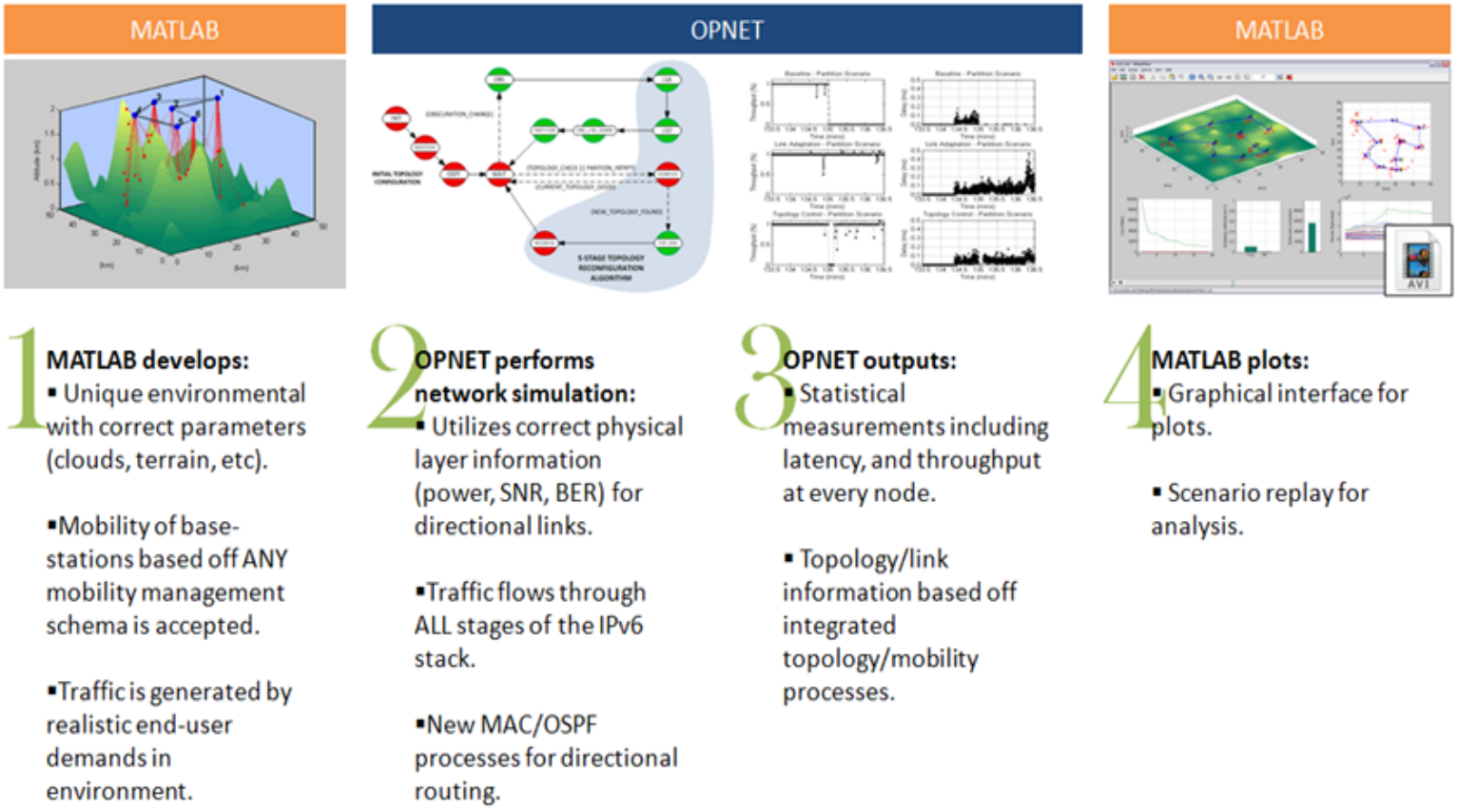

Figure B-14. A novel 4-step integration of MATLAB and OPNET was developed to simulate DWB networks. MATLAB first generates the unique environmental parameters, mobility, and traffic patterns; this becomes the input to OPNET for network simulation, second. OPNET is able to generate network-centric outputs such as routing efficiencies, latencies, dropped packets, etc., in addition to topological information regarding the SNR/BER characteristics of each link. Lastly, MATLAB combines all the available information to produce graphs and video for further analysis.

B.9.1 End-Users Abstraction

To minimize computation complexity with OPNET, the end-users were omitted from the design. Since MATLAB outputs the location of backbone nodes throughout the simulation and the relative traffic demands, the impact end-users have on the simulation outcome is maintained. The final stage of the four-stage integration of MATLAB/OPNET re-introduces the end-users for analysis.

B.9.2 Traffic Generation

The end-users in MATLAB are classified as either a recipient or a sender of information. Throughout the MATLAB simulations, each sender places a Gaussian distributed load onto the network with a designated recipient. This is simulated in OPNET by a fully-connected network with unbalance loads as illustrated by the example previously provided in fig. 3-11. This technique provides a realistic network pattern where end-user demands are busty – versus a sustained request for a large number of packets [20]. It has provides opportunities where demand exceeds the bandwidth of the links which is typical within a network.

Bibliography

[1] Welles, C.G. et al. “HAVE LACE – Final Report for Period January 1984-March 1986”, AFWAL-TR-86-1102

[2] Feldmann, R.J. and Gill, R.A., “Development of laser crosslink for airborne operations”, Military Communications Conference, 1998 MILCOM 98 Proceedings, Volume 2 Pages: 633-637, 18-21 Oct 1998.

[3] Gangle, Michael; Fisher, Donald; et. al. “Airborne Laser Communication Terminal for Intelligence, Surveillance, and Reconnaissance”, Free Space Laser Communications IV, Edited by Ricklin, Jennifer c. Voelz, David G. Proceedings of the SPIE, Volume 55 50, pp. 92-103, (2004)

[4] Larry B. Stotts ; Brian Stadler ; Gary Lee; Free space optical communications: coming of age. Proc. SPIE 6951, Atmospheric Propagation V, 69510W (April 18, 2008); doi:10.1117/12.783798.

[5] DARPA-BAA -12-23, Mobile Hotspots. Available online: https://www.fbo.gov/

[6] 100 Gb/s RF Backbone (100G). Available online: https://www.fbo.gov/

[7] Milner, S.D., Llorca, J., and Davis, C.C., “Autonomous reconfiguration and control in directional mobile ad hoc networks,” IEEE Circuits and Systems Magazine, vol. 9, no. 2, 10–26(2009).

[8] Llorca, J.,Desai, A.,Baskaran, E., Milner, S.D., and Davis, C.C., “Optimizing performance of hybrid FSO/RF networks in realistic dynamic scenarios,” Free Space Laser Communications V,vol.5892 of Proceedings of SPIE,52–60,(2005).

[9] Milner, S.D., Desai, A., Ho, T-H., Llorca, J., Trisno, S., and Davis, C.C., "Self-organizing broadband hybrid wireless networks," Journal of Optical Networking,vol.4,no.7, 446–459 (2005).

[10] Llorca, J., Kalantari, M., Milner, S.D., and Davis, C.C., "A quadratic optimization method for connectivity and coverage control in backbone-based wireless networks," Ad Hoc Networks,vol.7,no.3,614–621 (2009).

[11] Llorca, J., Milner, S.D., and Davis, C.C., "A convex optimization method for autonomous self-organization in dynamic wireless networks," Proceedings of the IEEE Military Communications Conference (2008).

[12] Llorca, J., Milner, S.D., and Davis, C.C., "Molecular system dynamics for self-organization in heterogeneous wireless networks." EURASIP Journal on Wireless Communications and Networking (2010).

[13] Zhang, H., Llorca, J., Davis, C.C., and Milner, S.D., "Nature-inspired self-organization, control, and optimization in heterogeneous wireless networks," IEEE Transactions on Mobile Computing, (6) 1536-1233 (2011).

[14] Wilson, E.B., Decius, J.C., and Cross, P.C., [Molecular vibrations: the theory of infrared and Raman vibrational spectra], McGraw-Hill, New York, NY (1955).

[15] Smith, P.J., Hurst, M.J., Watt, D.G., and Pulsipher, D.C. (2012) US Patent No. 8,194,573. Washington, DC: U.S. Patent and Trademark Office.

[16] J. Llorca, A. Desai and S.D. Milner. *Obscuration Minimization In Dynamic Free Space Optical Networks Through Topology Control*. Proc. IEEE MILCOM, November, 2004.

[17] Llorca, J., Self-Organizing Directional Wireless Backbone Networks, *University of Maryland Doctorate of Philosophy Dissertation*, 2008.

[18] Rzasa, J., Pointing, Acquisition, and Tracking for Directional Wireless Communications Networks, *University of Maryland Doctorate of Philosophy Dissertation*, 2013.

[19] S. D. Milner, et al., "Wireless Warfighter's Internet," Proc. MILCOM '97, Nov. 1997.

[20] Thompson, K.; Miller, G.J.; Wilder, R.;, "Wide-area Internet traffic patterns and characteristics," *Network, IEEE* , vol.11, no.6, pp.10-23, Nov/Dec 1997

[21] Ho, T., Trisno, S., Smolyaninov, I.I., Milner, S.D., Davis, C.C., "Studies of pointing, acquisition, and tracking of agile optical wireless transceivers for free-space optical communication networks," Proc. SPIE 5237, Optics in Atmospheric Propagation and Adaptive Systems VI, 147(2004).

[22] P. Gupta and P. R. Kumar, "The capacity of wireless networks," *IEEE Trans. Inform. Theory*, vol. 46, no. 2, pp. 388–404, Mar. 2000.

[23] Davis, C., Z. Haas, and S. Milner. (2006). "On How To Circumvent The Manet Scalability Curse." *Proceedings of IEEE MILCOM*, Washington, DC.

[24] C.C. Davis, I.I. Smolyaninov, and S.D. Milner, "Flexible Optical Wireless Links and Networks", *IEEE Comm. Mag.*, 41, 51-57, 2003.

[25] Kennedy, R. A., Cain, J.B. (2003) US Patent No. 7,382,765. Washington, DC: U.S. Patent and Trademark Office.

[26] R.Schiphorst, F.W. Hoeksema, and C. H. Slump, "A Real-Time GPP Software-Defined Radio Testbed for the Physical Layer of Wireless Standards," EURASIP Journal on Applied Signal Processing:16, 2664–267, 2005.

[27] T. S. Rappaport, *Wireless Communications: Principles and Practice,* Englewood Cliffs, NJ: Prentice-Hall, 1996.

[28] Steven F. Clifford and John W. Strohbehn, "The Theory of Microwave Line-of-Sight Propagation Through a Turbulent Atmosphere", IEE Trans., AP-18, pp. 264-274, 1970.

[29] A. Gurvich, M. Kallistrova, and N. Time, "Fluctuations in the parameters of a light wave from a laser during propagation in the atmosphere", *Radiophys. Quant. Electron.*, 11, 771-776, 1968.

[30] C.C. Davis and I.I. Smolyaninov, "Effect of Atmospheric Turbulence on Bit-Error-Rate in an On-Off-Keyed Optical Wireless System," Proc. SPIE Vol. 4489, 126-137, 2002.

[31] Christopher C. Davis, "Correlation Functions, Aperture Averaging, And Related Issues For Line-Of-Sight Optical Links Through Weak and Strong Scattering," A Tutorial Discussion, Not Published to date.

[32] X. Zhu and J.M. Kahn, "Free-Space Optical Communication through Atmospheric Turbulence Channels", *IEEE Trans. Comm.*, 50, 1293-1300, 2002.

[33] Brian R. Strickland, Michael J. Lavan, Eric Woodbridge, and Victor Chan, "Effects of fog on the bit-error-rate of a free space laser communication system", Applied Optics, Vol. 38, No. 3, January 1999.

[34] Achour, M. (2002). "Simulating atmospheric free-space optical propagation, part II: haze, fog, and low clouds attenuations." *SPIE Proceedings* 4873, 1-12.

[35] "Upper air digital data sets," National Climate Data Center (NCDC), NOAA.

[36] Davis, C.C., Lasers and Electro-optics: Fundamentals and Engineering. Cambridge University Press (1996)

[37] Taylor, K. Using Commercial Ray Tracing Software to Drive an Attenuator-Based Mobile Wireless Testbed. *University of Maryland Master's Thesis,* Nov. 2012.

[38] C. Reynolds, "Flocks, Herds, and Schools: A Distributed Behavioral Model," Computer Graphics, vol. 21, no. 4, pp. 25-34, 1987.

[39] C. Reynolds, "Steering Behaviors for Autonomous Characters, "Proc. Game Developers Conf., pp. 763-782, 1999.

[40] J. Kennedy and R.C. Eberhart, "Particle Swarm Optimization, "Proc. IEEE Int'l Conf. Neural Networks (ICNN '95), pp. 1942-1948, Nov./Dec. 1995.

[41] Cramer, C. J., [Essentials of Computational Chemistry, Theories and Models], J. Wiley & Sons Ltd, West Sussex, England (2004).

[42] Leach, A. R., [Molecular Modeling, Principles and Applications], Pearson Education Limited, Essex, England (2001).

[43] X. Hong, M. Gerla, G. Pei, and C.-C. Chiang, "A group mobility model for ad hoc wireless networks," in Proceedings of the 2nd ACM International Workshop on Modeling, Analysis and Simulation of Wireless and Mobile Systems, pp. 53–60, 1999.

[44] Arfken, G. "Bessel Functions of the First Kind, $J_\nu(x)$" and "Orthogonality." §11.1 and 11.2 in *Mathematical Methods for Physicists, 3rd ed.* Orlando, FL: Academic Press, pp. 573-591 and 591-596, 1985.

[45] Röhrig, U. F.; Frank, I., "First-principles molecular dynamics study of a polymer under tensile stress," J. Chem. Phys. vol. 115, 8670 (2001)

[46] Rohrig, U. F.; Troppmann, U.; Frank, I. "Organic chromophores under tensile stress," Chem. Phys., 289, 381– 388 (2003)

[47] D. Aktah, I. Frank, "Breaking bonds by mechanical stress: when do electrons decide for the other side?" J. Am. Chem. Soc., 124, 3402 (2002)

[48] Milner, S.D., Davis, C.C., Llora, J., "Control and prediction in hierarchical wireless networks," Mobility Management in the Networks of the Future World (MobiWorld) Workshop (2011)

[49] Ma, J., "Usefulness and limitations of normal mode analysis in modeling dynamics of biomolecular complexes," Structure 13:373–380 (2005)

[50] Bradley, G., Weaire, D., "Instabilities of two liquid drops in contact," *Computing in Science & Engineering*, vol.3, no.5, pp.16-21, (2001)

[51] Cui, Q., Bahar, I., Normal Mode Analysis: Theory and Applications to Biological and Chemical Systems. Chapman and Hall/CRC (2005)

[52] Tama, F., et. al., "Symmetry, form, and shape: guiding principles for robustness in macromolecular machines," Annual Review Biophysical Bimolecular Structure, (35) 115-33, (2006).

[53] Vadim, A., et. al., "Normal modes for predicting protein motions: a comprehensive database assessment and associated Web tool", *Protein Science*, vol. 13, no 3, 633-643 (2005).

[54] Bahar, I., et.al., "Collective motions in HIV-1 reverse transcriptase: examination of flexibility and enzyme function," Journal of Molecular Biology, 285 , 1023-1037 (1999).

[55] Zheng, W., et. al., "Normal-modes-based prediction of protein conformational changes guided by distance constraints," Biophysical Journal, Vol. 88, 3109–3117 (2005).

[56] Eyster, J.M. and Prohofsky, E.W., "On the B to A conformation change of the double helix," *Biopolymers* 16, 965-982 (1977).

[57] Petrone, P. and Pande, V., "Can conformational change be described by only a few normal modes?," *Biophysical Journal*, Vol. 90, 1583-1593 (2006).

[58] Llorca, J., Milner, S.D., and Davis, C.C., "Molecular inspired models for prediction and control of directional fso/rf wireless networks," SPIE Proceedings Vol 7814, Free-Space Laser Communications X, (2010).

[59] Hoshino, K., Shimojo, F., and Nishida, T., "The photo-induced structural change in a Se chain and a Se8 ring: an ad initio molecular-dynamics simulation," Journal of the Physical Society of Japan, Vol. 68, No. 6, 1907-1911 (1999).

[60] Acevedo, O. and K. Armacost, "Claisen Rearrangements: Insight into Solvent Effects and 'on Water' Reactivity from QM/MM Simulations." Journal of the American Chemical Society. vol. 132, no 6, pp. 1966-1975 (2010).

[61] Lim, T.C., “The relationship between Lennard-Jones (12-6) and Morse potential functions,” Z. Naturforsch. Vol. 58a**,** 615 – 617 (2003).

[62] Liu X., Sheth, A., Kaminsky, et. al., “DIRC: increasing indoor wireless capacity using directional antennas,” ACM Sigcomm, Barcelona, Spain (2009).

[63] Hamzeh, B., Kavehrad, M., “Characterization of cloud obscured free space optical channels,” Proceedings of WMSCI’05, Orlando, Florida, (2005).

[64] S. Bloom, E. Korevaar, J. Schuster, and H. Willebrand, "Understanding the performance of free-space optics (Invited)," J. Opt. Netw. 2, 178-200 (2003).

[65] Zhu, X. and Kahn, J.M., "Free-space optical communication through atmospheric turbulence channels," Trans. on Comm., IEEE, Vol. 50, No. 8, 1293-1300 (2002).

[66] Prokes. A, "Atmospheric effects on availability of free space optics systems," Opt. Eng., Vol. 48, Is. 6 (2009).

[67] Ellinas, G. and Stem, T.E., "Automatic protection switching for link failures in optical networks with bi-directional links," IEEE GLOBECOM '96, vol. 1, 152-156, (1996).

[68] Xue, G.,Chen, L. and Thulasiraman, K., "Quality-of-service and quality-of-protection issues in preplanned recovery schemes using redundant trees," IEEE Journal on Selected Areas in Communications, vol. 21, no. 8, 1332-1345, (2003).

[69] D. Weaire, M. F. Vaz, P. I. C. Teixeira and M. A. Fortes, *Soft Matter*, vol. 3, pg. 47-57 (2007)

[70] Brooks BR, Karplus M, “Normal modes for specific motions of macromolecules: application to the hinge-bending mode of lysozyme,” ProcNatlAcadSci USA 82:4995–4999 (1985)

[71] Tirion, M.M., “Large amplitude elastic motions in proteins from a single-parameter atomic analysis,” Phys. Rev. Lett, vol. 77, pp. 1905–1908 (1996)

[72] J. Kovecses, J.M. Font-Llagunes, “An Eigenvalue Problem for the Analysis of Variable Topology Mechanical Systems,” J. Comput. Nonlinear Dynam. 4, 031006 (2009)

[73] Sedeh, R.S., Bathe, M. Bathe, K.L., “The subspace iteration method in protein normal mode analysis,” J. Chem. Phys. vol. 31, pg. 66-74 (2010)

[74] Beyer, M.K., “The mechanical strength of a covalent bond calculated by density functional theory,” American Institute of Physics (2000)

[75] Ramanathan, Ram; Redi, J.; Santivanez, Cesar; Wiggins, D.; Polit, S., "Ad hoc networking with directional antennas: a complete system solution," *Selected Areas in Communications, IEEE Journal on* , vol.23, no.3, pp.496,506, (2005)

[76] OPNET Technical Lab Manual, “Modeling Custom Wireless Effects—Advanced” available online: http://www.opnet.com

[77] Stotts, L.B., Andrews, L.C., et. al., "Hybrid Optical RF Airborne Communications," Proceedings of the IEEE, vol.97, no.6, 1109-1127 (2009).

[78] H. Stern & S. Mahmoud, [Communications Systems], Pearson Prentice Hall, (2004).